Investigating the use of connectivity mapping to manipulate MGMT protein levels in T98G glioblastoma multiforme cells

Thesis submitted for the degree of
Doctor of Philosophy
At the University of Sussex

By Sarah Smalley BSc Hons (UEA)
School of Life Sciences
University of Sussex

July 2013

Declaration

I hereby declare that this thesis has not been submitted, either in the same or different form, to this or any other university for a degree.

Sarah Smalley

Acknowledgements

My biggest thank you goes to Simon Morley, for giving me the opportunity to do some really amazing and enjoyable work, and for having the faith in me to be able to spend four years working with him in the lab and to remain (relatively) sane throughout! His help and expertise during my PhD have been invaluable, and as well as being an extremely helpful and professional mentor, Simon has also been an ear to bend in trying times, and someone to celebrate with in happy times, and for that I am extremely grateful.

My time at Sussex was definitely made more memorable by lab members, both past and present. I owe an especially huge thank you to Michele Brocard for taking time out of her work schedule to teach me new experimental techniques. I also want to thank both Julie Aspden and Michele for our weekly galette eating ritual, which during my final year was not only a brilliant distraction, but a chance to get some much needed advice and reassurance.

I was really lucky to have Mark O'Driscoll as a second supervisor, I'm sure I've taken up far too much of his time talking about work, but I am sure that without his advice and encouragement, I'd still be writing now!

I want to say a big thank you to David Whitehouse, who provided me with teaching opportunities throughout the years, which were very fun and greatly rewarding.

Of course none of this could have been achieved without the unwavering support of my friends and family. I was extremely fortunate to be able to carry out some of my research with a fellow biochemist in the form of my brother Joshua Smalley. It was extremely enjoyable and I'm sure we will collaborate again in the future. I also want to thank my mum and dad for all of their help, encouragement and interest in my work. I also want to thank them for ideas and advice that they've shared with me to help with my research.

An extra special thank you goes to Ben Andrews, who managed to make me smile, even after a long day in the lab!

UNIVERSITY OF SUSSEX

Submitted for the degree of doctor of Philosophy

Investigating the use of connectivity mapping to manipulate MGMT protein levels in T98G Glioblastoma multiforme cells

Summary

Glioblastoma multiforme (GBM) is the most common and most aggressive type of primary brain tumour. It is currently treated by a mixture of ionising radiation and Temozolomide (TMZ) chemotherapy, however virtually all patients experience disease recurrence and 75% die within two years of diagnosis.

Tumours which express elevated levels of the DNA repair protein O^6-methylguanine DNA methyltransferase (MGMT) have a particularly poor prognosis, suggesting that levels of MGMT and the inefficacy of treatment are linked.

MGMT is a “suicide” repair protein that binds irreversibly to a DNA adduct (such as those caused by TMZ) and is destroyed by the proteasome once repair has taken place. Therefore the ability of the cell to repair DNA damage relies on the rate at which it can resynthesise MGMT. Previous research has shown that reducing MGMT levels via promoter silencing increases the effectiveness of treatment, however this causes toxicity in bone marrow stem cells and is therefore unable to be used as a possible treatment option.

My preliminary data suggests that inhibition of mTOR signalling reduces the steady state levels of MGMT without affecting mRNA levels, potentially making them more sensitive to TMZ treatment. I am therefore using inhibitors of the mTOR pathway and associated proteins, which have been selected via a novel bioinformatic technique, to ascertain how these affect MGMT protein levels and to determine whether a mixture of these inhibitors with DNA damaging agents could be used to increase the efficacy of TMZ treatment.

Table of Contents

List of figures

List of Tables

Abbreviations

4E-BP – eIF4E binding protein
ADP – Adenosine diphosphate
AMPK – AMP activated protein kinase
APS – Ammonium persulphate
ASK – Apoptosis stimulating kinase
ATM – Ataxia telangiectasia mutated protein
ATP – Adenosine triphosphate
ATR – Ataxia telangiectasia and Rad 3 related protein
DAPH – 4,5-dianilinophthalimide
DMSO – Dimethyl Sulfoxide
DNA – Deoxyribonucleic acid
DNAPK – DNA dependent protein kinase
DNAPKcs – DNA dependent protein kinase catalytic subunit
DOC – Deoxycholate
Dsh – Dishevelled
EDTA – Ethylenediaminetetraacetic acid
EGFR – Epidermal growth factor receptor
eIF – Eukaryotic initiation factor
ERK – Extracellular signal-regulated kinase
FCS – Foetal calf serum
FGFR – Fibroblast growth factor receptor
GAP – GTPase activating protein
GBM – Glioblastoma Multiforme
GDI – GDP dissociation inhibitor
GDP – Guanosine diphosphate
Grb2 – Growth factor receptor-bound protein 2
GTP – Guanosine triphosphate
HGFR – Hepatocyte growth factor receptor
HR – Homologous recombination

IR – Ionising radiation

IRES – Internal ribosomal entry site

kDa – Kilodalton

M^7GTP – 7-methyl guanosine triphosphate

MAPK – Mitogen activated protein kinase

MEK – Mitogen activated protein kinase kinase

MGMT – 0-6-methylguanine-DNA methyltransferase

MLK – Mixed lineage kinase

mTOR – Mechanistic target of rapamycin

MMR – Mismatch repair

NHEJ – Non-homologous end joining

p70S6K – 70 kDa ribosomal protein S6 kinase

PABP – Poly (A) binding protein

PAGE – Polyacrylamide gel electrophoresis

PDK1 – phosphoinositide dependent kinase 1

PH – Pleckstrin homology

PI3k – Phosphatidylinositide-3-kinase

PIP_2 – Phosphatidylinositol 4,5-bisphosphate

PIP_3 – Phosphatidylinositol (3,4,5)-triphosphate

PTEN – Phosphatase and tensin homolog

PVDF – Polyvinylidine difluoride

REDD1 – regulation of DNA damage response

RNA – Ribonucleic acid

RPA – Replication protein A

RTK – receptor tyrosine kinase

SDS – Sodium dodecyl sulphate

SH2 – Src homology 2

SH3 – Src homology 3

SOS – Son of sevenless

ssDNA – Single stranded DNA

SDSA – synthesis dependent strand annealing

TAK – Transforming growth factor kinase

TBS – Tris buffered saline

TCA – Trichloroacetic acid

TMZ – Temozolomide

Tween 20 – Polyoxyethylene sorbitan monolaurate

UTR – Untranslated region

WHO – World health organisation

Chapter I

Introduction

1 Introduction

The term ‘cancer’ encompasses a broad range of diseases caused by the uncontrolled proliferation of cells. There are currently over 200 distinct types of cancer, each with different causes and symptoms, therefore requiring different treatments. Cancers arising from cells in the brain are among the 20 most commonly diagnosed types of cancer and yet have a very low survival rate, with only 14.5% of men and 16.1% of women in the UK surviving 5 years or more after diagnosis [1]. With over 3500 people dying of brain tumours in the UK every year, new approaches are needed to increase the efficacy of treatment.

1.1 Glioblastoma multiforme

Glioblastoma multiforme (GBM) is a world health organisation (WHO) classified grade IV astrocytoma. The WHO grading system describes how fast the tumour is actively growing on a scale from 1 to 4; 1 being the slowest growing tumours and 4 being the fastest growing. An astrocytoma is a type of cancer that arises from glial cells, which are the star shaped cells that form a supportive network for neurons. GBM is one of the most aggressive types of primary brain tumour, and it is also the most common [2]. GBM occurs most frequently in adults, with less than 9% occurring in children [3]. The tumours are especially hard to treat, as they display extensive heterogeneity, both at the cellular and molecular levels [4]. It is this heterogeneity that earned the tumour its name ‘multiforme’.

There are two main types of glioblastoma; primary glioblastoma and secondary glioblastoma. Here I will focus on primary glioblastoma, as secondary glioblastomas are the result of metastasis of cancerous cells from a pre-existing tumour and have different underlying mutations than the primary form. Primary glioblastomas arise *de novo* in older patients with no prior history of glioma and have a particularly poor prognosis. As with most brain tumours, the specific causes are unknown, yet GBM tumours are characterized by oncogene amplification of EGFR, CDKN2A deletions and *PTEN* mutations. These mutations will be discussed in greater depth later in the chapter. Recent work by

the Cancer Genome Atlas Research Network has begun to reveal the extent of the genetic and chromosomal abnormalities that contribute to the aggressive and treatment resistant nature of this tumour [5].

1.2 Signs and symptoms

Common symptoms of brain tumours include, but are not restricted to, headaches, seizures and nausea. However, depending on the site of the tumour, changes in behaviour and mood can also be experienced. Headaches can be an early sign of brain tumours, especially if the headache fits the pattern for raised intracranial pressure, is unremitting, arises in unexpected circumstances or is accompanied by vomiting or neurological deficit [6].

The symptoms caused by GBM can be due to the increased pressure in the brain caused by the tumour, but can also be caused by haemorrhage or the development of oedema around the tumour. Oedema around the tumour is caused by the aberrant and un-regulated formation of blood vessels during tumour formation, which does not form a functioning blood brain barrier and allows cerebrospinal fluid to leak in to the brain cavity [7]. Symptoms occurring from physical pressure in the brain can sometimes, but not always, be reversed by surgical removal [8]. Nausea can be an unpleasant symptom of GBM and may have a variety of causes. It may arise as part of posterior fossa syndrome (an unexplained neurological condition that arises after tumour removal surgery, which can present itself with stroke-like symptoms) [9] but may also be caused by raised intracranial pressure, yet it is also associated with seizures and chemotherapy side effects. Anti-emetics can be used to treat nausea, and in some more extreme cases tranquilizers may be used [2,9].

1.3 Diagnosis and tumour progression

Diagnosis of GBM is usually achieved through imaging using computerised tomography (CT) or magnetic resonance imaging (MRI). The tumours will appear during such scans as grey masses with areas of necrosis and sometimes cysts at the centre. They may appear to have a capsule, but this is

always an artefact of rapidly growing tumour cells and compressed brain. As mentioned previously, adjacent brain can be swollen with peri-tumoral oedema, which tends to spread along the white-matter tracts and can form a conduit for the migratory tumour cells, which can be found many centimetres from the main tumour mass. These migratory cells may form secondary masses. Therefore, although glioblastomas may appear to arise in multiple locations, this usually represents spread from a single tumour [10]. Spread in this way does not respect boundaries between the lobes of the brain and spread across the corpus callosum (the large area of white matter that links the left and right cerebral hemispheres) is common. This pattern is common in malignant glioma and the term ‘butterfly tumour’ is frequently used to describe a tumour that spans both lobes in this fashion [10]. Although rare, GBM can also arise in the cerebellum, brain stem and spinal cord. The tumours are highly heterogeneous at a cellular level, with almost any size and shape of cell being seen, including multi-nucleated giant cells, which are characteristic of glioblastoma. Although spread of the tumour within the brain is common, systemic metastasis is rare [11]. Diagnosis can be confirmed by biopsy of the tumour, but it is generally good practice to resect as much of the tumour as possible during biopsy retrieval, so as to assist with treatment and delay progression.

1.4 Current treatments

At present GBM is generally treated by surgical removal (where possible) followed by two types of therapy: Ionizing radiation (IR) and chemotherapy [12]. The combination treatment is rigorous, yet prognosis is often poor and although chemotherapy improves survival in a subset of patients, 75% die within 2 years and the majority of patients experience disease recurrence [13].

Surgery has three main roles in brain tumour management: to obtain a diagnosis, to contribute to survival and to relieve symptoms. For the resection of a tumour, access is gained by craniotomy. A scalp incision is made and a flap of skin and peri-cranial tissue lifted. The site of the craniotomy will depend on the position of the tumour. Most surgeons prefer a free bone flap, which is created

first by making burr-holes (small holes drilled in to the scull), freeing the dura mater and then cutting the flap using a high-speed craniotome. The dura mater is then opened only by an amount that will give adequate exposure of the tumour-bearing brain. The size of the opening of the dura mater is restricted to reduce possibility of infection. It is common practice to confirm the diagnosis with an intra-operative frozen section or cytological smear, prior to performing the full resection. The resection itself is normally performed by using a mixture of sharp dissection, cauterisation and ultrasonic aspiration [14]. The aim is always to remove as much of the tumour as is safely possible. The operation is then completed with dural closure, replacement of the bone flap and skin closure. This procedure can be performed while the patient is awake to allow for 'cortical mapping' of neurological function. Cortical mapping during the operation can be used to avoid resection of brain tissue needed for important functions such as speech, walking, movement, and memory [15].

Most radiotherapy is delivered using post-operative external beam X-rays. However, various other techniques are possible, including intra-operative radiotherapy and particle radiotherapy. In all situations the aim is to deliver a maximal (or curative) dose to the entire tumour, whilst minimizing the normal-tissue dose and volume [10].

For a chemotherapeutic drug to be effective it must be detrimental to tumour growth and maintenance and be able to access to the tumour site. In the brain, the intact blood-brain barrier generally inhibits the passage of molecules with molecular weights greater than 200 Daltons. Drugs with a high partition coefficient (nitrosoureas) or that are small (TMZ) can circumvent this barrier [10]. Although in the vicinity of tumour the barrier is partially defective [9], large hydrophilic molecules remain largely excluded from the tumour structures and are not useful for therapy.

A standard chemotherapeutic agent used to treat GBM is TMZ. TMZ is used as it is readily absorbed by the digestive tract due to its small size (194 daltons), and also benefits from being acid stable, allowing oral administration [16]. The

lipophilic character of TMZ allows it to cross the blood brain barrier, an important factor for potential GBM chemotherapeutic compounds.

Once TMZ is absorbed in to the blood and exposed to a pH exceeding 7, it is spontaneously broken down in to 5-(3-methyltriazen-1-yl)-imidazole-4-carboxamide (MTIC). The dependence on pH makes TMZ an appealing treatment for GBM, as brain tumors, in contrast to surrounding healthy tissue often have an alkaline pH [17]. MTIC reacts with water and is then broken down in to 4-amino-5-imidazole-carboxamide (AIC) and a methyldiazonium cation. It is the latter that creates lesions at the N^7 and O^6 positions of guanine and the N^3 position of adenine in DNA, the most lethal of these lesions is O^6-methylguanine [18].

Another chemotherapeutic that is commonly used to treat GBM is procarbazine. It is also an alkylating agent, but unlike temozolomide, procarbazine is metabolically activated in the liver. Although procarbazine is used as a treatment option, its mechanism of action is not fully understood [19]. Procarbazine is usually administered in combination with vincristine. Vincristine depolymerises tubulin polymers such as microtubules, which prevents mitosis from taking place, promoting the process of apoptosis [20]. Countless other chemotherapeutic options have been trialled, but none have been successful enough to replace the current alkylating agents as a “gold standard” for treatment.

An alternative treatment option is the use of the Gliadel® system. This comprises a biodegradable polymer in wafer form that is impregnated with carmustine. The mechanism of action of carmustine is discussed later in the chapter. A number of these wafers are used to line the cavity left after resecting a brain tumour. After wound closure the polymer slowly breaks down, delivering the carmustine in a more concentrated fashion than is possible to achieve by systemic delivery[21]. Although Gliadel® has been shown in prospective randomized clinical trials to improve survival in patients undergoing surgery for newly diagnosed and recurrent high-grade glioma, it is little used in the UK [21].

As the effectiveness of the chemotherapeutic agents and their delivery are problems which need to be resolved, new techniques are being developed to try and address these issues. Convection-enhanced delivery (CED) is a new surgical technique in which a thin catheter is placed into the brain and connected to an extracranial, pump-driven syringe containing a chemotherapeutic agent. By selecting an appropriate delivery rate, the chemotherapeutic can be made to 'flow' directly into the tumour. This technique can be used to deliver a variety of cytotoxic agents, including large molecules, to regions in the brain remote from the catheter tip. This technique is currently under investigation in large randomized clinical trials [22].

1.5 DNA damage and repair

The O^6-methylguanine lesion is particularly cytotoxic if left unrepaired as it results in a mispairing of guanine and thymine. This mispairing then activates the mismatch repair (MMR) pathway [23,24], through recognition from hMutSα, a DNA mismatch recognition protein. Upon recognition the daughter strand opposite the lesion is then excised by hMutLα and EXO1. Replication protein A (RPA) then binds the single- stranded DNA to prevent it from folding back on itself, while the X family DNA polymerase members, lambda and mu, resynthesise the daughter strand [25]. However, because the MMR pathway solely excises and inserts nucleotides in the daughter strand, the O^6-methylguanine on the template strand is left intact. This leads to a futile MMR cycle of reinserting thymine, causing replication fork stalling, ATM/ATR activation, and DNA double-strand breaks, eventually forcing the cell in to apoptosis [18,26].

Radiotherapy utilises γ rays to cause double-strand breaks in DNA. Double-strand breaks in humans activates both the non-homologous end joining (NHEJ) and the homologous recombination (HR) DNA repair pathways [27].

NHEJ repairs the double strand breaks by direct ligation of the broken strands. The double-strand break sites are held in close proximity by the end binding complex heterodimer, Ku (Ku70-Ku80), which forms part of the DNA

dependent protein kinase (DNAPK). The end joining complex then recruits the catalytic subunit of DNAPK (DNAPKcs) which then forms a complex with Artemis and DNA ligase IV [28], which reattaches the broken ends. NHEJ is often error prone, due to small insertions, deletions or substitutions at the break site, or possibly translocations if two strands from different parts of the genome are accidentally joined [28].

HR is initiated when the DSBs are recognised and then resected by nucleases and helicases, generating a single-stranded DNA (ssDNA) overhang onto which the RAD51 recombinase assembles as a nucleoprotein filament (Fig.1.1). RAD51 then directs the strand to similar or identical sequences to use as a template for repair. As HR generally only occurs in cells after DNA replication there should be a sister chromatid to use as a template strand, minimising the opportunity for error. In cells that favour non-crossover HR and require only short inserts of DNA sequence, the RTEL helicase can be expressed, inhibiting D-loop formation and encouraging synthesis-dependent strand annealing (SDSA) [27]. If the RTEL helicase is not expressed, D-loop formation occurs. This D-loop can then be cleaved which results in resolution. If the D-loop is not cleaved a double Holliday junction can form (dHJ). Once formed, the double holiday junctions can either be ‘migrated’ by topoisomerase III, resulting in dissolution [29], or cleaved by endonucleases (resolvases), which, depending on the cleavage site, can result in crossover or non-crossover products.

1.6 ATM and ATR

Phosphatidylinositol-3-kinase related kinases (PIKKs) comprise a family of serine/threonine protein kinases that show sequence similarity to the phosphoinositide 3-kinase family. They contain the DNA damage repair proteins ataxia telangiectasia mutated protein (ATM), ataxia telangiectasia and Rad 3 related protein (ATR) and DNAPK, as well as the mechanistic target of rapamycin (mTOR). ATM regulates cell cycle checkpoints and DNA repair [30]. Activation of ATM by autophosphorylation on Ser1981 occurs as a response to

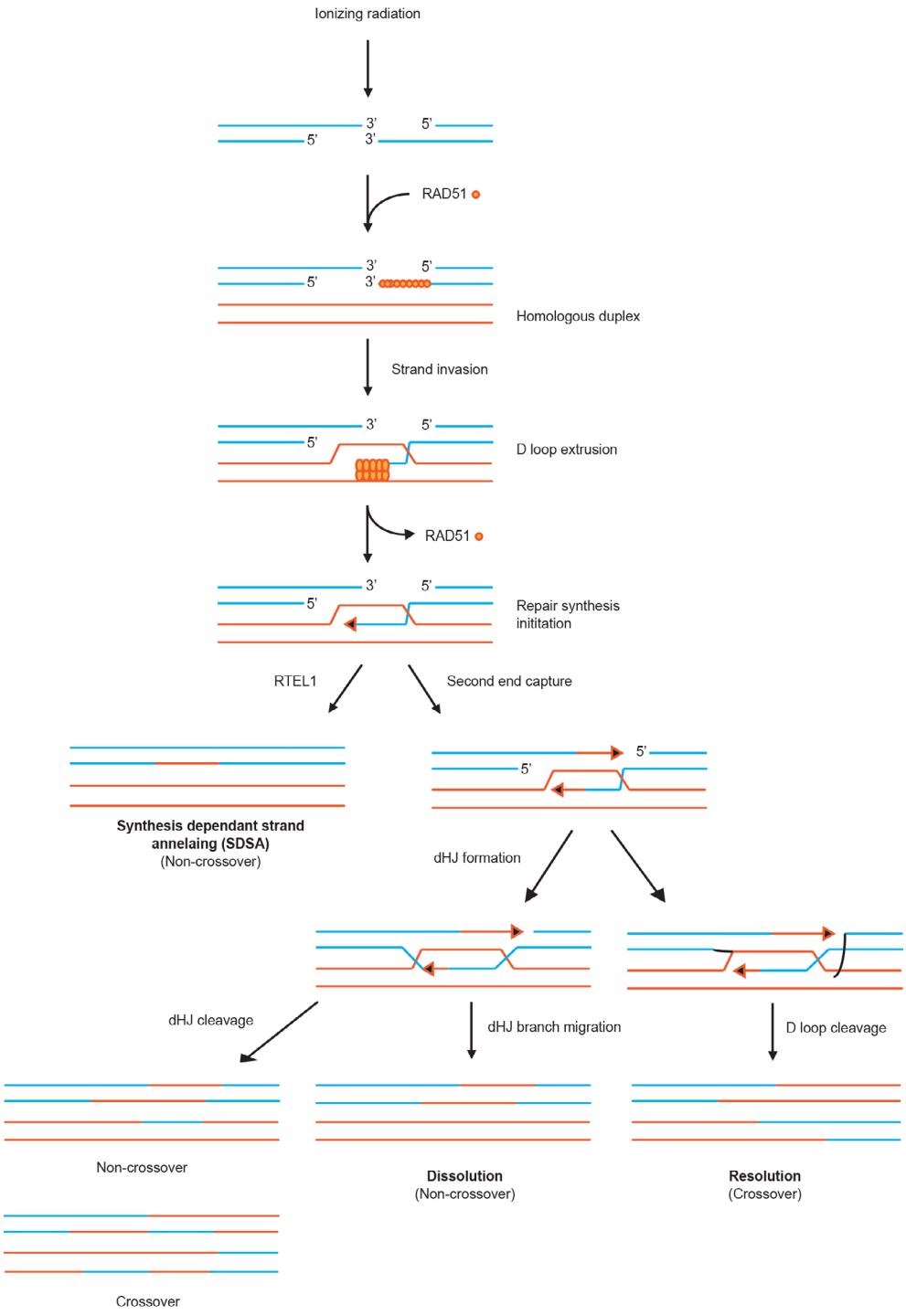

Figure 1.1 Schematic representation of homologous recombination pathway choices

The initial stages of HR are similar in all cells during all phases of the cell cycle. The double strand break is recognised, and the RAD51 recombinase accumulates on the 3' overhang of the broken DNA. RAD51 then directs the strand to similar or identical sequences to use as a template for repair. In cells/phases where non-crossover HR that only inserts short sequences of DNA are favourable, the RTEL helicase can be expressed, inhibiting D-loop formation and encouraging SDSA. If this does not occur a D-loop forms. This D-loop can then be cleaved and result in resolution, or a double Holliday junction can form (dHJ). Once formed, the double holiday junctions can either be 'migrated' by topoisomerase III, resulting on dissolution, or cleaved by endonucleases (resolvases), which, depending on the cleavage site, can result ion crossover or non-crossover products. Adapted from Chapman *et al*. 2012.

exposed DNA double stranded breaks [31]. However, it has also been recently suggested that ATM may also play a part in translational control and signalling upstream of mTOR [30]. ATM has not only been implicated in inhibiting 4E-BP1 in response to insulin signalling, but also in activating Akt, thereby increasing signalling through mTORC1. The increased signalling through mTORC1 can result in increased rates of protein translation (see section on mTOR signalling for further details).

During DNA replication and cellular stress, ssDNA often arises. This can be caused by replication fork stalling, futile MMR cycles (as mentioned previously) or lesions such as DNA crosslinks. ssDNA is bound by the ssDNA-binding protein RPA, which in the canonical ATR signalling pathway, is the ligand that recruits ATR and other ATR signalling components to sites of replication stress [32].

As mentioned above, DNAPK comprises the Ku heterodimer, Ku70/80, and the catalytic subunit DNAPKcs. Both the Ku heterodimer [33] and DNA-PKcs [34] can bind directly to DNA, but, in the absence of Ku the affinity of DNA-PKcs for DNA is greatly reduced [35]. As well as playing a role in actively repairing double-strand breaks via NHEJ, DNAPK also phosphorylates p53 in response to double strand breaks.

p53 has two known negative regulators, MDM2 and MDM4 (sometimes known as MDMX). MDM2 acts by binding to the N-terminal end of p53 and inhibiting the transcriptional activation function of p53 [36,37] (Fig.1.2). MDM2 also possesses E3 ubiquitin ligase activity that targets p53 for modification and subsequent degradation through the 26S proteasome [38–40].

Ubiquitination is the reversible process of ‘tagging’ a substrate with ubiquitin. This process guides proteins to different compartments of the cell, including the proteasome, where proteins are broken down in to constituent amino acids. The Ubiquitin system was discovered in 2004 by Aaron Ciechanover, Avram Hershko and Irwin Rose [41], and consists of a three-step process whereby an E1 ubiquitin-activating enzyme ‘charges’ an E2 ubiquitin-conjugating enzyme with ubiquitin. An E3 ligase then binds both the E2 ligase and the substrate, an

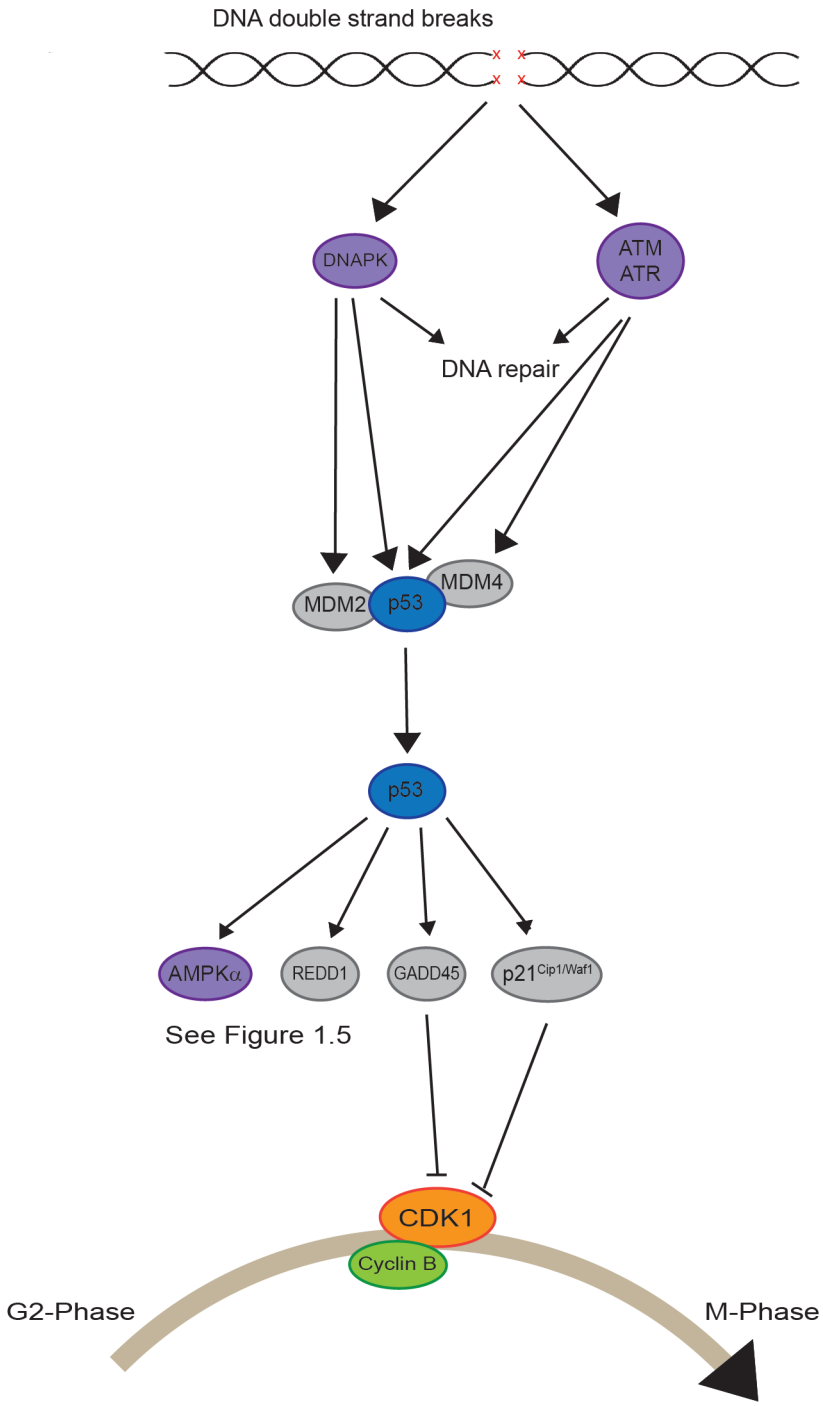

Figure 1.2 Schematic representation of cell cycle arrest following DNA damage

Double strand breaks in DNA activate the PIKKs DNAPK, ATM and ATR. The activation of these proteins results in both the activation of DNA repair pathways and the activation of p53. p53 has two negative regulators; MDM2 and MDM4. DNAPK inhibits MDM2 whilst activating p53, and ATM/ATR inhibit MDM4 whilst simultaneously activating p53. The proteins activated by p53 then lead to mTOR signalling inhibition (Figure 1.5) and cell cycle arrest at the G2/M checkpoint via the activation of GADD45 and p21 cip1/waf1, which then inhibit CDK1.

isoppeptide bond is then formed between the two [42,43]. The result of protein ubiquitination can be degradation of the target by the proteasome, but can also play a part in protein-protein interactions [44], depending on the amount of ubiquitin added and where it is attached to the substrate. In humans, there are currently 2 known genes that encode E1 ligases, 37 genes that encode E2 ligases, and over 600 genes that encode E3 ligases [45].

MDM4 binds p53 in a similar manner to MDM2, inhibiting the transcriptional activity of p53. In response to DNA double-strand breaks and ssDNA, ATM, ATR and DNAPK all phosphorylate p53. The phosphorylation of p53 impairs the ubiquitin degradation ability of MDM2, allowing p53 stabilisation and activation [46]. In addition to this DNAPK also phosphorylates MDM2, and ATM/ATR phosphorylates MDM4, both events result in inhibition of the regulatory effects of the proteins. The following activation/lack of inhibition of p53 can result in the increased transcription of p21 cip1/waf1, which ultimately leads to inhibition of the CDK1/cyclin b complex formation, resulting in G2/M cell cycle arrest [47], allowing the cell time to repair DNA damage (Fig.1.2).

1.7 O^6-methylguanine DNA methyltransferase

The DNA repair protein that is responsible for repairing the O^6-methylguanine lesion in DNA is O^6-methylguanine DNA methyltransferase (MGMT). MGMT repairs the cytotoxic lesion created by methylating agents such as TMZ (but also environmental pollutants such as tobacco-specific carcinogens) [48] by transferring the methyl group on the DNA to a cysteine acceptor site in the MGMT protein itself (Fig.1.3). This reaction is irreversible and once bound to the alkyl group, the MGMT protein is ubiquitinated and destroyed by the proteasome [49]. The success of TMZ chemotherapy therefore relies, in part, on the ability of the tumour to re-synthesise MGMT and maintain steady state levels of the protein.

Genetic profiling of GBM in some patients is currently used to predict the outcome of TMZ chemotherapy. It has been shown that if a tumour contains cells with a methylated MGMT promoter (and therefore lacking MGMT protein),

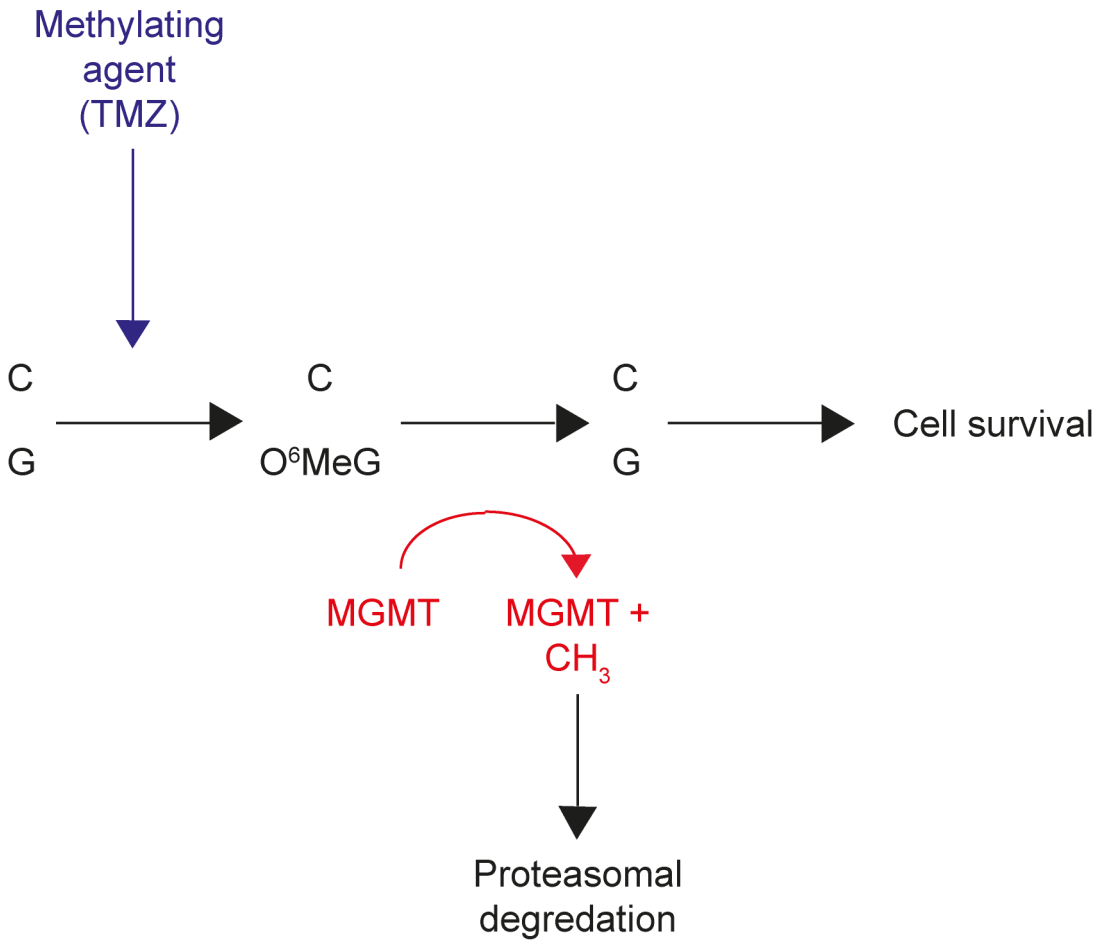

Figure 1.3 Schematic representation of the DNA repair function of MGMT

MGMT removes methyl adducts in DNA by transferring the methyl group on the DNA to a cysteine acceptor site in the MGMT protein itself in a stoichiometric reaction. Once the MGMT protein has undergone this reaction, it is unbiquitinated and degraded by the proteasome. MGMT is known as a suicide repair protein, as it can only repair one methyl adduct before being degraded.

this can be correlated to enhanced survival of patients treated with TMZ [50]. However, only around half of GBM tumours exhibit MGMT promoter methylation, and prognosis is still poor for those with an unfavourable genetic status [51,52].

1.8 MGMT protein expression

MGMT protein expression is controlled by both transcriptional and post-transcriptional mechanisms. MGMT is known to be positively controlled by the transcription factors, SIP1 and NFκB [53]. It has been suggested that SIP1 can be sequestered by p53 during DNA damage, preventing the transcription of MGMT, which could aid in the efficacy of DNA methylating agents. However, this may not occur in cancerous cells as p53 is often poorly expressed [54]. The methylation of the MGMT promoter can also inhibit its transcription, leading to reduced amounts of MGMT protein expression [55,56].

Alternative splicing of genes is an important mechanism of post-transcriptional regulation which can generate different transcripts from a single pre-mRNA. MGMT has multiple predicted splice variants, yet these have limited support in the scientific community [57], and further work will need to be carried out to explore these possibilities. The expression of MGMT protein varies across tissues in the body, with tissues that are exposed to a higher degree of carcinogens and environmental damage such as the digestive tract, liver, skin and lungs showing moderate amounts of the protein expressed. On the other hand, cardiac tissues and the central nervous system (which should be exposed to environmental damage at a lower frequency) show much lower levels of MGMT protein expression [48]. Although increased methylation of the promoter region of DNA encoding MGMT is strongly correlated with decreased MGMT protein levels [55], MGMT levels in cells lacking a methylated promoter show varying degrees of MGMT protein expression. These data suggest that MGMT protein may also be regulated in a post-transcriptional fashion. Coupled with this, research has suggested possible miRNA binding sites in the MGMT mRNAs 3'UTR, again suggesting an additional regulatory mechanism [58]. It is

clear that the mechanisms underlying MGMT expression are not fully understood, and this should be of upmost importance, as MGMT is undoubtedly a hurdle in successful cancer treatment.

1.9 Modulating levels of MGMT in GBM

Attempts have been made at modulating levels of MGMT protein in GBM cells. Adenovirus based gene therapy directed at methylating the MGMT promoter in GBM cells resulted in a positive outcome in mice xenographs [59]. In spite of this success adenoviral gene therapies in GBM patients are difficult to administer, and often fall short of expectations during clinical trials [60].

Before TMZ became widely available as a treatment in the late nineties, carmustine, a nitrosourea that is both an alkylating agent and causes DNA crosslinks was used as a chemotherapeutic treatment. Carmustine only increased survival by approximately 2 months when used alone [61], however, when used in conjunction with direct MGMT protein inhibitors such as O^6-benzylguanine, which binds to the active site of MGMT, this combination sensitised tumours to alkylating agents. However, this combination was also cytotoxic to cells with a long self-renewal period (such as haematopoietic stem cells which replicate approximately every 40 weeks [62]), in a dose limiting manner [63]. To avoid cytotoxicity when combining TMZ and O^6-benzylguanine in GBM, O^6-benzylguanine has been administered directly to surgical cavities after tumour resection. However, as surgery is not always possible, alternative therapies need to be developed to reduce levels of MGMT protein in GBM tumour cells [64].

1.10 Common mutations in GBM cells

Common mutations in GBM cells include mutations in the tumour suppressor protein p53 [65], amplification of epidermal growth factor receptor (EGFR) [66] and loss of phosphatase and tensin homolog (PTEN) function [67,68] (Fig.1.4). The amplification of EGFR and the loss of PTEN can result in the hyperactivity of PI3K/mTOR signalling (Fig.1.5). Another common mutation in GBM is an

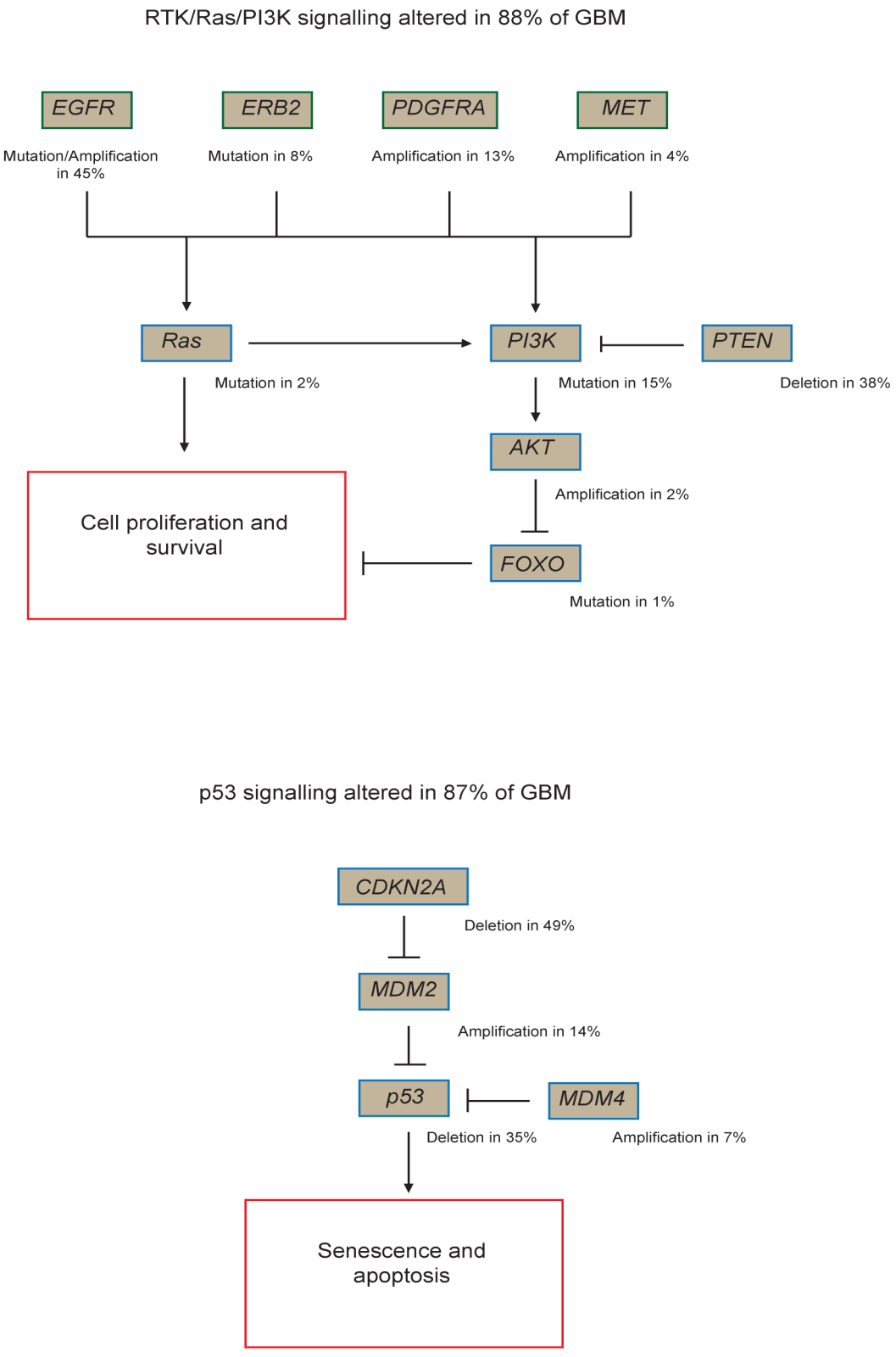

Figure 1.4 Diagram representing common mutations found in GBM

Many genetic mutations arise in cancer cells, these can often result in amplifications of pro-proliferation genes, and deletions of pro-apoptotic genes. This is an example of some of the most commonly mutated genes in GBM tumours, that can directly influence mTOR signalling and therfore growth and proliferation. Adapted from Shinji & Tanaka, 2013.

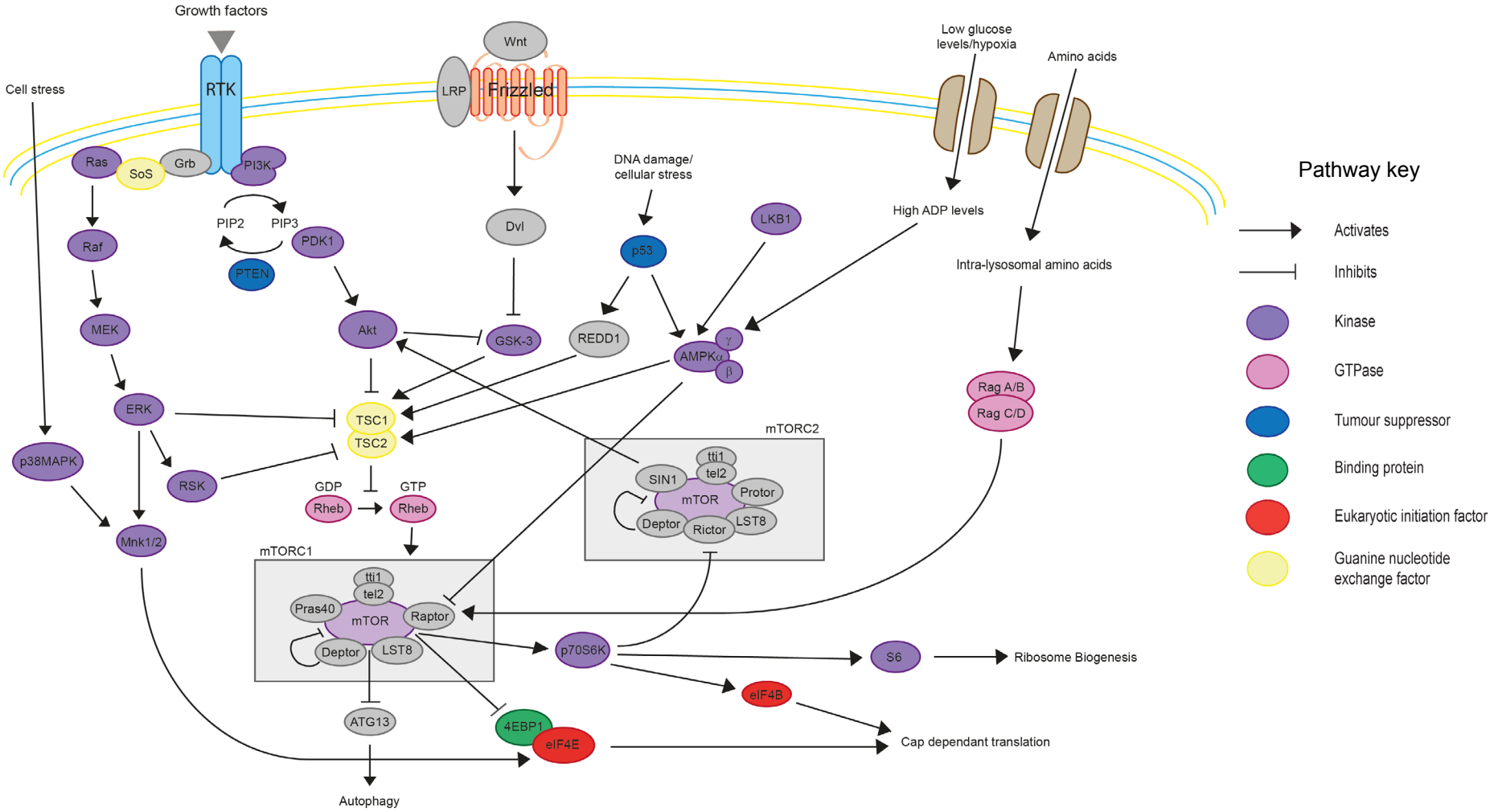

Figure 1.5 Schematic representation of the mTOR signalling pathway and associated proteins

The mTOR signalling pathway integrates signals from extracellular signalling molecules, hypoxia, glucose signalling and amino acid sensing.

amplification of *Met*, which encodes the hepatocyte growth factor receptor (HGFR), an RTK that is usually only expressed in epithelial cells [69]. This amplification not only causes hyperactive signalling through ERK and PI3K pathways, but also drives angiogenesis. In addition to the amplification of numerous signalling proteins, GBM exhibits a mutation of *FOXO* in 1% of cases (Fig.1.4). The FOXO proteins are a family of transcription factors that are known to promote expression of pro-apoptotic proteins, but have also been observed to mediate some protein-protein interactions [70].

As cancerous cells can become reliant on hyperactive pathways driven by mutations, in a process known as oncogenic addiction [71], they offer a possible target for cancer treatments. The concept of oncogenic addiction is appealing not only because it provides a rationale for directly targeting hyperactive pathways in cancerous cells, leading to cell growth inhibition and possibly apoptosis, but also selectively targeting cancerous cells, as healthy cells would be able to overcome pathway inhibition by using an alternative mechanism.

1.11 mTOR signalling

Schreiber *et al*. first identified the mTOR protein in 1994 [72] as the target of the macrolytic fermentation product of the bacterium *Streptomyces hygroscopicus,* rapamycin. Rapamycin gained its name from the island from which it was first obtained in a soil sample in 1975 (Rapa Nui [73,74]) and it sparked considerable interest due to its antiproliferative effects.

mTOR belongs to the PI3K-related kinase family of proteins and is involved in the regulation of the phosphorylation of downstream targets such as p70S6K and 4E-BP1 by: mitogens; extracellular signalling molecules; glucose availability; hypoxia; and amino acid availability. The mTOR pathway responds to these signals by regulating essential cellular functions, such as protein synthesis, lipid synthesis, autophagy, lysosome biogenesis, energy metabolism, cell survival and cytoskeletal reorganisation [75] (Fig.1.5).

The mTOR protein is currently known to interact with several proteins to form two distinct complexes, mTOR complex 1 (mTORC1) and 2 (mTORC2) [75].

mTORC1 contains six know proteins, and mTORC2 contains seven. Both mTOR complexes share the mTOR protein, mammalian lethal with sec-13 protein 8 (mLST8) [76,77], DEP domain containing mTOR-interacting protein (DEPTOR) [78] and the Tti1/Tel2 scaffold protein complex [79]. The two remaining proteins that participate in mTORC1 are the regulatory-associated protein of mammalian target of rapamycin (raptor) [80,81], which is responsible for the sensitivity of mTORC1 to rapamycin, and the proline-rich Akt substrate 40 kDa (PRAS40) [82]. In addition to the four proteins that mTORC2 shares with mTORC1, it also contains the rapamycin-insensitive companion of mTOR (rictor), the mammalian stress-activated map kinase-interacting protein 1 (mSin1) and the protein observed with rictor 1 and 2 (protor1/2) (Fig.1.5). The regulation of mTORC1/2 signalling is described below.

1.12 ERK1/2 signalling cascade

The extracellular signal-regulated kinase 1 and 2 (ERK1/ 2) signalling pathway can be activated by G-protein coupled receptors (GPCRs), integrin receptors and most commonly, receptor tyrosine kinases (RTKs) [83]. Growth factors are extracellular signalling molecules such as cytokines, mitogens and hormones. The 44-kDa ERK1 and 42-kDa ERK2 proteins were the first MAPKs to be discovered to take part in a MAPK cascade [84].

In general, growth factor binding activates RTKs by inducing receptor dimerisation [85]. The dimerisation of the extracellular RTK domain then causes the phosphorylation of a tyrosine residue on the cytoplasmic portion of the receptor [86]. The phosphorylated tyrosine residue activates the Src homology 2 (SH2) domain on the growth factor receptor-bound protein 2 (Grb2), this in turn causes a conformational change in the Src homology 3 (SH3) domain of Grb2, increasing its binding affinity and allowing it to bind to the guanine nucleotide exchange factor, son of sevenless (SOS). The interaction of Grb2 with SOS then causes the membrane recruitment of this complex bringing the guanine nucleotide exchange factor in close proximity to Ras, resulting in GTP exchange on Ras and hence its activation (reviewed in [87]). Ras then transmits the signal

by activating the protein kinases Raf-1, B-Raf, and A-Raf (Rafs). Once activated, the Raf family of MAPKKKs specifically activates two MAPKKs, MAP/Erk kinase 1 (Mek1) and Mek2, which in turn selectively activate Erk1 and Erk2. Erk1 and Erk2 are nearly 85% identical overall, with much greater identity in the core regions mediating the binding of substrates [88].

The activated ERK1/2 inhibits tuberous sclerosis protein 1 and 2 (TSC1/2). TSC1/2 are GTPase-activating proteins that act on Ras Homolog Enriched in Brain (Rheb). As Rheb directly activates mTORC1 when GTP bound, TSC1/2 is a negative regulator of mTORC1, meaning that TSC1/2 inhibitors are activators of mTORC1 [89](Fig.1.5). As well as its direct influence on the mTORC1 signalling pathway, ERK1/2 also targets transcription factors such as, Elk1 [90], c-Fos [91] and c-Jun [92]. ERK1/2 signalling can also be extended by the phosphorylation of MAPK-activated protein kinases (MAPKAPKs). The first MAPKAPK to be discovered was p90RSK, which is phosphorylated and activated by ERK1/2 and PDK1 at multiple sites, encouraging further inhibition of TSC1/2, and therefore mTOR activation [93]. MAPK-interacting protein kinase (Mnk) [94,95] and mitogen and stress-activated protein kinase (MSK) were also identified as MAPKAPKs of the cascade [96]. However, the activation of these kinases is not restricted to the ERK1/2 cascade, as they are also activated by the p38 cascade, mainly under stress conditions [97].

Ras and Raf are commonly mutated in cancerous cells, propagating signalling even in the absence of growth factors, suggesting the ERK1/2 signalling cascade could be important in cancer development [98,99].

1.13 p38 MAPK signalling

The p38 MAP kinases are a family of stress-activated MAP kinases that contribute to the regulation of cell proliferation and autophagy. Although the p38 MAPK cascade is similar in organisation to the ERK1/2 signalling pathway (as it is a MAPK signalling cascade), it is less well characterised. The signalling cascade can be triggered by stress, DNA damage and growth factor binding.

The signal is propagated by many upstream MAPKKKs responding to distinct stimuli which include: mixed lineage kinases (MLKs); transforming growth factor activated kinases (TAKS); and apoptosis stimulating kinases (ASKs) [83].

These proteins then phosphorylate and activate three MAPKKs (MAPKK3, MAPKK4 and MAPKK6) that phosphorylate and activate p38 MAPKs [100,101]. Four p38 MAPK isoforms have been identified (α, β, γ, δ) that differ between organisms and tissues [102]. p38 MAPK is important in respect to translation initiation, as it has been shown to phosphorylate and activate the MAPK interacting proteins Mnk1/2. This will be explored further on in this chapter in respect to eIF4E phosphorylation and translation.

1.14 PI3K signalling

Phosphatidylinositol-3-kinases (PI3Ks) are a group of lipid kinases that can be split in to 3 classes. The class I PI3Ks can then be further subdivided in to class IA and class IB. Class IA, encompassing the catalytic subunit isoforms p110α, p110β and p110δ, associate with the regulatory subunits p85α, p85β, p55α, p55γ and p50α whereas the class IB PI3Ks, consisting only of the p110γ catalytic subunit, binds the regulatory subunits p101, p84 and p87PIKAP [103]. The class II PI3Ks do not contain regulatory subunits, and purely consist of the catalytic subunits C2α, C2β and C2γ [104]. The class III PI3Ks contain only one protein, PIK3C3, whose function in mammals is still unclear but are known to have a role in nutrient regulation of mTORC1 and autophagy [105]. I shall refer to the class IA PI3Ks as the representative isoforms of PI3K in this instance.

The PI3K signalling pathway is primarily activated through growth factor binding to RTKs, but can also be activated via GPCRs [106]. Growth factor binding results in autophosphorylation of the RTK on its intracellular tyrosine residues, providing a sequence-specific binding site for the p85 regulatory subunit of PI3K via its SH2 domain, which sequesters the p85 subunit from the p110 catalytic subunit. In the absence of upstream signals, the regulatory subunit stabilises the p110 subunit and suppress its catalytic activities. If the p85 subunit is docked to phosphotyrosine, a conformational change allows for

p110 to phosphorylate phosphatidylinositol 4,5-bisphosphate (PIP_2) to produce phosphatidylinositol (3,4,5)-triphosphate (PIP_3) which functions as a second messenger. This process can be reversed by the tumour suppressor protein PTEN, which is often mutated in GBM [107]. PDK1 is a serine/threonine kinase containing a C-terminal pleckstrin homology (PH) domain [108], which binds to PIP_3 with high affinity, thereby recruiting PDK1 to the inner plasma membrane. Upon membrane recruitment, PDK1 phosphorylates Akt at its Thr308 site, stimulating its kinase activity [109,110]. Activated PDK1 is also required for the activation of p90RSK. Akt possesses an N-terminal PH domain which recruits the kinase to PIP3, a central kinase domain, and a carboxy-terminal hydrophobic regulatory domain. To be fully activated, Akt also needs to be phosphorylated on its Ser473 site, which can be phosphorylated by the mTORC2 complex [111,112]. Once activated, Akt phosphorylates (therefore inhibits) TSC1 and TSC2 which allows activation of mTORC1 and its downstream effectors. Akt activation also phosphorylates and inhibits GSK3 [113], which is important in a translational context, as GSK3 (when active), phosphorylates eIF2Bε, inhibiting its GEF activity. The inhibition of GSK3 therefore stimulates guanine nucleotide exchange on eIF2 and thus the process of translation initiation (see further on in the chapter for details).

1.15 Wnt signalling and mTOR

The Wnt signalling pathway also interacts with the mTOR pathway (Fig.1.5). This interaction is primarily through glycogen synthase kinase 3 (GSK3), which has been suggested to be inhibited following phosphorylation by Akt when the PI3K pathway is active [114,115]. The Wnt signalling pathway is activated by binding of a Wnt protein to a 7 transmembrane receptor in the frizzled family of proteins [116]. Upon ligand binding, frizzled phosphorylates dishevelled (Dsh) which in turn inactivates GSK3. The inactivation of GSK3 prevents phosphorylation of TSC2, an event that also requires priming from AMP-activated protein kinase (AMPK) [117]. Active Wnt signalling therefore promotes mTORC1 signalling.

1.16 Glucose regulation and hypoxia

AMPK is composed of three subunits, regulatory γ and β subunits, and a catalytic α subunit. During reduced cellular ATP levels, ADP or AMP binds the γ subunit of AMPK, promoting phosphorylation at Thr172 on the α subunit by the upstream kinase LKB1 and protecting the protein from dephosphorylation [118,119]. Reduced glucose [120] and oxygen [121] levels can result in an increase cellular AMP levels. The activation of AMPK both phosphorylates TSC1/2 and inhibits the raptor component of the mTORC1 complex, therefore inhibiting mTORC1 signalling [122] (Fig.1.5).

1.17 DNA damage

Although the effect of DNA double-strand breaks in cell stress and cancer has already been discussed, it is important to note that as well as possessing the ability to halt the cell cycle, p53 also directly influences proteins in the mTOR signalling pathway (Fig.1.5). In response to DNA damage or acute cellular stress such as hypoxia, transcriptional expression of regulation of DNA damage response 1 (REDD1) is induced by p53. The REDD1 protein then interacts with TSC1/2 in a poorly understood mechanism [123], leading to inhibition of mTORC1 signalling. As well as the expression of REDD1, upon activation, p53 also induces the expression of sestrin1/2 which directly activates AMPKα [124]; this in turn activates TSC1/2, therefore inhibiting mTOR signalling.

1.18 Amino acid sensing

The availability of amino acids also affects mTOR signalling and downstream events. mTORC1 activation requires the presence of amino acids to be activated by any upstream signals [125]. Until recently, the molecular mechanism through which mTORC1 senses intracellular amino acids remained a mystery, but what has become clear is that amino acid dependent activation of mTORC1 is TSC1/2 independent [126], and requires a group of GTPases known as the Rag GTPases [127,128], functioning in a complex known as the

“ragulator”. Humans have four Rag proteins that form heterodimers as either RagA/B or RagC/D. The two members of the heterodimer have opposite nucleotide loading states, so that when Rag A/B is bound to GTP, Rag C/D is bound to GDP and vice versa [75]. Amino acids promote the loading of the Rag heterodimers with GTP, which then directly interacts with the raptor protein within the mTORC1 complex, promoting eukaryotic translation [128]. Little is known about the exact mechanism by which mTORC1 senses amino acid sufficiency, but evidence suggesting that mTORC1 is recruited to the surface of the lysosome by the Rag GTPases, where it is then activated by membrane localised Rheb [127,129].

1.19 Downstream targets of mTORC1

Many pathways converge at the activation of the mTORC1 complex, it is therefore unsurprising that the regulation of mTORC1 is not only important in relation to cap dependent translation (as discussed below), but that the complex is also involved in regulating other processes such as ribosomal subunit synthesis [130] and autophagy [131,132]. The activation of mTORC1 directly results in phosphorylation of p70 S6K at its Thr389 site. P70 S6K is a serine threonine kinase that, when active, phosphorylates multiple residues in the carboxyl terminal region of the ribosomal S6 protein (Ser235, Ser236, Ser240, and Ser244). These phosphorylation events have previously been thought to positively control the translation of mRNAs containing 5’ terminal oligopyrimidine tracts (TOPs), yet contradictory evidence dismissing this theory has also been found [133].

mTORC1 activation has also been shown to play a role in the regulation of autophagy. When mTORC1 is active, it phosphorylates ATG13, which inhibits autophagy. However, during reduced signalling through mTORC1, ATG13 is not phosphorylated, and this thereby triggers autophagy [134]. Autophagy is also regulated by a plethora of signalling proteins under different conditions (Fig.1.6), for example, during reduced ATP levels, autophagy is both induced by reduced mTORC1 signalling, and through the activation of p27 by AMPKα [135,136].

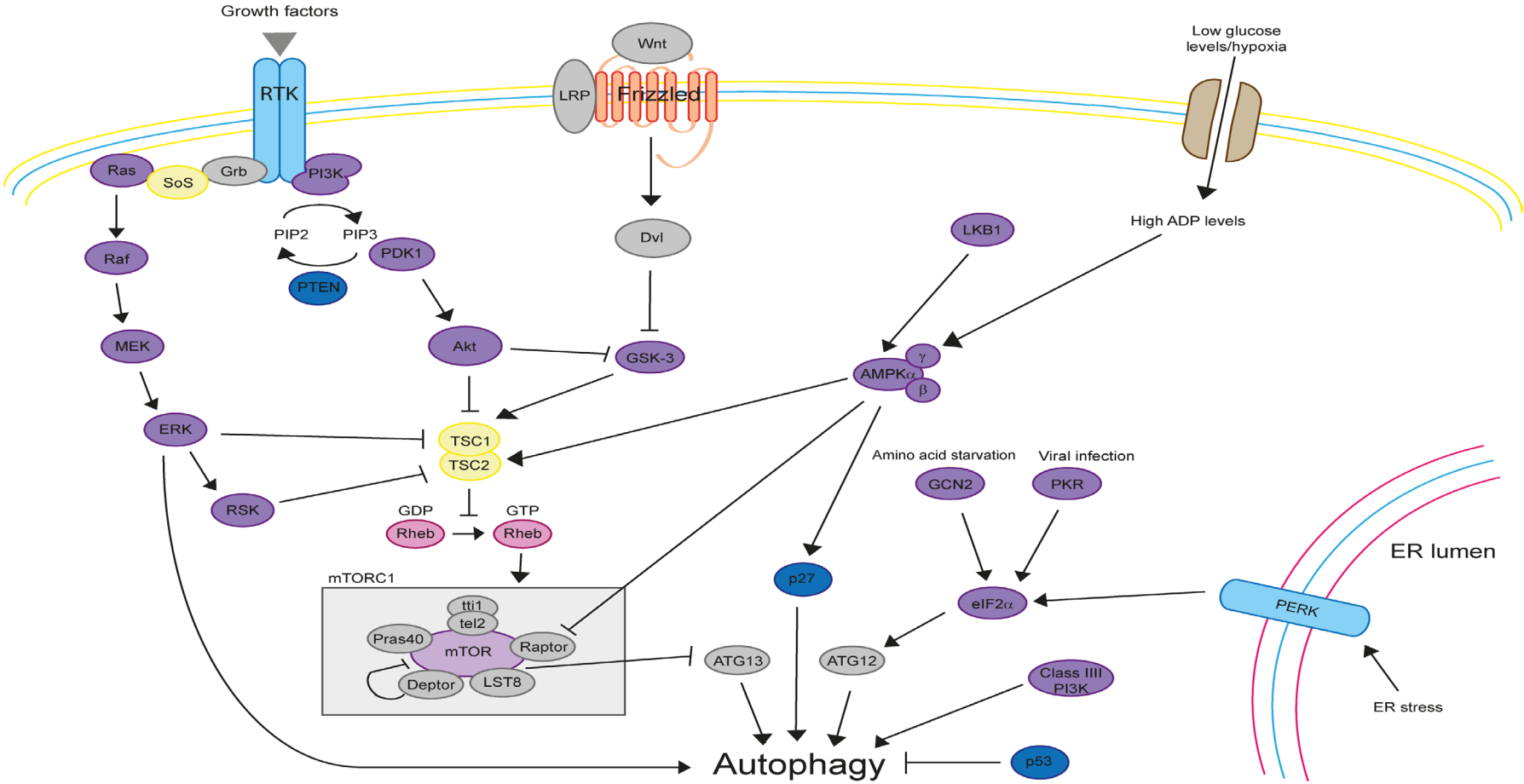

Figure 1.6 Schematic representation of the regulation of autophagy

Autophagy in mammalian cells is regulated by a variety of signalling proteins. In nutrient rich conditions, mTORC1 phosphorylates ATG13, directly inhibiting autophagy. Autophagy can also be activated by low ATP levels, amino acid deprivation, viral infection and ER stress.

Autophagy is also induced by the phosphorylation of eIF2α and the resulting activation of ATG12 (Fig.1.6), which can occur by activation of one or more of its kinases; these kinases are discussed in detail later in the chapter. The tumour suppressor, p53 plays a dual role in autophagy regulation. During cellular stress p53 is stabilised and congregates in the nucleus where it acts as a transcription factor, increasing the expression of pro-autophagic proteins such as DRAM1 [137]. However, when present in the cytoplasm, basal levels of p53 negatively regulate autophagy [138]. The class III PI3K have also been implicated in the induction of autophagy, but this link still needs to be researched in greater depth [139].

1.20 Cap dependent initiation of translation

Eukaryotic protein translation is carried out in three main stages; initiation, elongation and termination, with the initiation stage generally accepted as a major site of regulation of gene expression [140–143]. During the initiation phase the ribosome binds to the mRNA and forms an 80S initiation complex at the initiation codon. The elongation stage involves the ribosome catalysing the synthesis of a polypeptide chain by the sequential addition of one amino acid after the other as encoded by the mRNA until the termination codon is reached. The termination stage includes the steps that are needed to release the completed polypeptide chain and dissociate the mRNA from the ribosome.

The initiation stage of protein translation is an intricate process mediated by a group of proteins known as eukaryotic initiation factors (eIFs) [144–147]. The processes involved in initiation can be sub-divided in to four individual events: recruitment of Met-tRNA to the 40S ribosomal subunit, recruitment of the 43S pre-initiation complex to the mRNA, scanning of the mRNA by the ribosome and 60S ribosomal subunit joining (Fig.1.7).

1.21 Recruitment of Met-tRNA to the 40S subunit

The first stage of the initiation process is mediated by eIF2, a G-protein that comprises three subunits (α,β and γ). The γ subunit of eIF2 mediates Met-tRNA

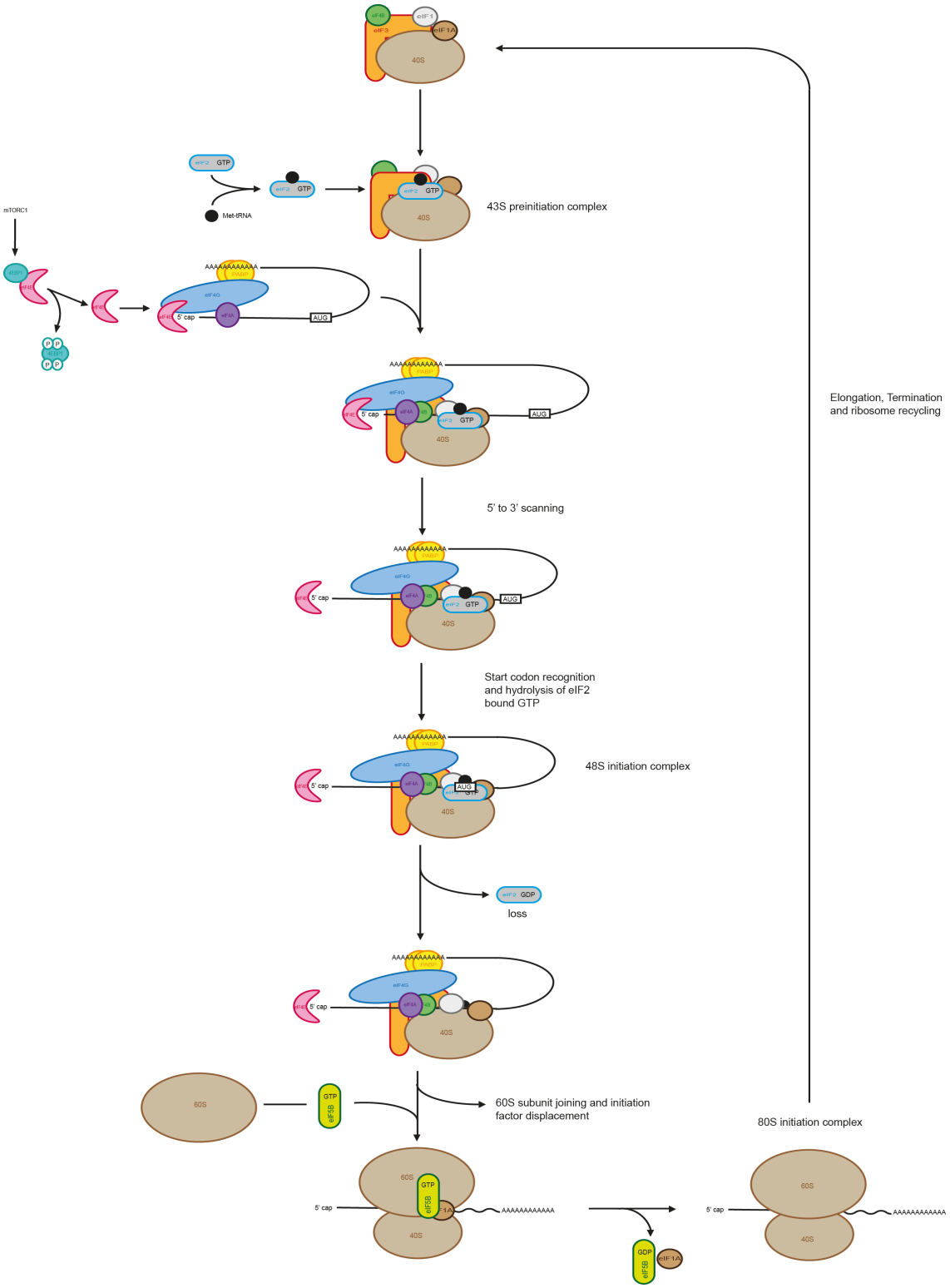

Figure 1.7 Schematic representation of eukaryotic translation initiation and ribosome binding

The binding of mRNA to the ribosome occurs in many stages. The 40S subunit (already bound to eIF3, eIF4B, eIF1 and eIF1A) interacts with eIF2-GTP-Met-tRNA to form the 43S preinitiation complex. This is then bound by the eIF4F initiation complex, which aids in the scanning of the structured 5' UTR of the mRNA until the start codon is recognised by eIF1, forming the 48S initiation complex. Once the start codon is recognised, eIF2 bound GTP is hydrolysed and partially lost. This then paves the way for 60S subunit and eIF5B-GTP binding, which displaces the other initiation factors, allowing 80S subunit formation and subsequent protein synthesis.

binding [148–150] and contains the main docking site for GTP/GDP. The β subunit is important for the interaction with eIF2B, and the α subunit contains the phosphorylation site (Ser51) which controls the activity of the protein [151,152]. The binding of Met-tRNA requires eIF2 to be in its active, GTP-bound state. As the non-enzymatic guanine-nucleotide-exchange reaction is very slow, it requires catalysis by eIF2B. Although eIF2B shows little similarity to other GTP-exchange proteins, it is classed as a GEF [153]. eIF2B comprises five subunits: α, β, γ, δ, ε which are divided into a catalytic subcomplex (δ,ε) and a regulatory subcomplex (α,β,γ) [154]. The ε subunit of eIF2B interacts with the β subunit of eIF2, facilitating the recruitment of eIF2 to the GEF and allowing guanine nucleotide exchange to occur [152]. eIF2Bε can also be phosphorylated, and its phosphorylation state can affect the GEF activity of eIF2B [153,155]. Phosphorylation of eIF2α at Ser51 does not directly inhibit its function, but increases the affinity of eIF2/GDP for binding to the regulatory subcomplex of eIF2B, inhibiting its GEF activity. However, when eIF2 is GTP bound, it associates with a molecule of Met-tRNA producing a ternary complex (TC). As well as the roles detailed later in the chapter, eIF5 has also been described as a GDP dissociation inhibitor for eIF2 [156], suggesting another step in eIF2 regulation.

Four eIF2α kinases have been identified in mammals that phosphorylate eIF2α at its Ser51 residue. These kinases are activated by different types of cellular stress to inhibit translation initiation. Viral infection activates protein kinase R (PKR), haem deprivation and oxidative stress activate haem-regulated inhibitor (HRI), endoplasmic reticulum stress (ER) activates PKR-like ER kinase (PERK) and nutrient deficiency/UV stress activates general control non-depressible kinase 2, (GCN2) [157].

PKR is activated by the presence of double-stranded RNA (dsRNA), which is produced as an intermediate of viral infection. As well as inhibiting translation through eIF2α, PKR activates several pro-inflammatory and pro-apoptotic

transcription factors [158–160] and the expression of genes encoding components of the death-inducing signalling complex (DISC) [161,162].

GCN2 has been shown to be activated by accumulation of uncharged tRNAs during amino acid starvation [163], and as such inhibits translation via eIF2α. GCN2 has also been observed to become active following incubation of cells with proteasomal inhibitors such as MG132, suggesting an alternative role in ubiquitination or degradation of proteins [164].

PERK is a transmembrane protein which has both an ER-lumenal sensor domain and a carboxy-terminal cytoplasmic protein kinase domain. In non-stressed cells, the luminal domain of PERK is bound to an abundant ER chaperone, GRP78 (also known as BiP), thus keeping PERK inactive. During ER stress, unfolded proteins accumulate in the ER, resulting in GRP78 dissociating from PERK to bind to the unfolded proteins. The dissociation of GRP78 from PERK leads to activation of the cytoplasmic domain and phosphorylation at its Thr980 site [165,166], resulting in phosphorylation of eIF2α at the Ser51 site, inhibiting protein synthesis. The activation of PERK via the unfolded protein response is the most commonly studied mode of activation, yet is not the only one. PERK activation has also been observed in pancreatic β cells during low glucose concentrations, brought about by sarcoplasmic/ER Ca^{2+}-ATPase (SERCA) pump inhibition, which results in reduced levels in Ca^{2+} in the ER lumen [167].

1.22 Recruitment of the 43S pre-initiation complex to the mRNA

When the ternary complex containing eIF2/GTP and Met-tRNA has been formed, it then associates with the 40S ribosomal subunit, eIF3, eIF1A, eIF1 and possibly eIF5 to form a 43S pre-initiation complex (Fig.1.7) [143,168,169].

eIF3 is a large complex with at least 13 different subunits which stabilises the binding of Met-tRNA-eIF2-GTP to the 40S ribosomal subunit, prevents premature binding of the 60S ribosomal subunit [168] and also promotes the dissociation of the 40S and 60S ribosomal subunits[170]. During recruitment to the mRNA, eIF3 also physically interacts with eIF4G, localising the 40S

ribosome to the mRNA [171]. The large amount of non identical subunits that comprise eIF3 and their possible individual functions make it an interesting topic for research, for a detailed review of the multiprotein complex, see review [172].

The 43S complex is competent to bind mRNA non-specifically by itself. However, assembly at the 5' end of the mRNA requires the cap-binding complex, eIF4F. Eukaryotic initiation factor 4F (eIF4F) is a multi-protein complex comprising eIF4E, eIF4A and eIF4G, which is often deregulated in tumour cells (Fig.1.8) [75,140,142].

Mammalian eIF4A is a 46-kDa protein that exhibits bi-directional RNA helicase activity [173–176], which is negatively regulated by PDCD4 [177]. The phosphorylation of PDCD4 by p70 S6K [178,179] results in its ubiquitination and degradation, allowing eIF4A to participate in the eIF4F complex where its activity is enhanced by eIF4B, eIF4H and eIF4G [144,180]. It has been shown that the phosphorylation of eIF4B at its Ser406 and Ser422 sites is essential for its positive influence of eIF4A activity, and therefore in protein translation [181]. It has also been recently shown that p70 S6K can phosphorylate eIF4B [179], suggesting yet another link between mTORC1 signalling and cap-dependent translation. Using ATP, eIF4A unwinds mRNA in the 5' UTR of mRNA to allow 40S ribosomal subunit binding [173]. There are currently three known mammalian isoforms, eIF4AI, eIF4AII and eIF4AIII [182,183], yet only eIF4AI and eIF4AII have been observed *in vivo* to partake in protein synthesis [176]. Although no evidence has yet be found to support the role of eIF4AIII in protein synthesis, it has been identified as a component of the exon junction complex (EJC) [184]. The EJC is extremely important as it acts as a regulatory checkpoint during translation of mRNA. The EJC binds to the exon join sites (after splicing has occurred) in mRNA and if the mRNA has not been formed correctly, and a nonsense mutation is identified before reaching the EJC, nonsense mediated decay of the mRNA occurs.

eIF4G is a large protein that serves as a scaffold during translation initiation, binding to eIF4A, eIF4E, eIF3, poly(A)-binding protein (PABP) and mRNA. Three forms of the protein have been identified to date, eIF4G1, eIF4G2 and

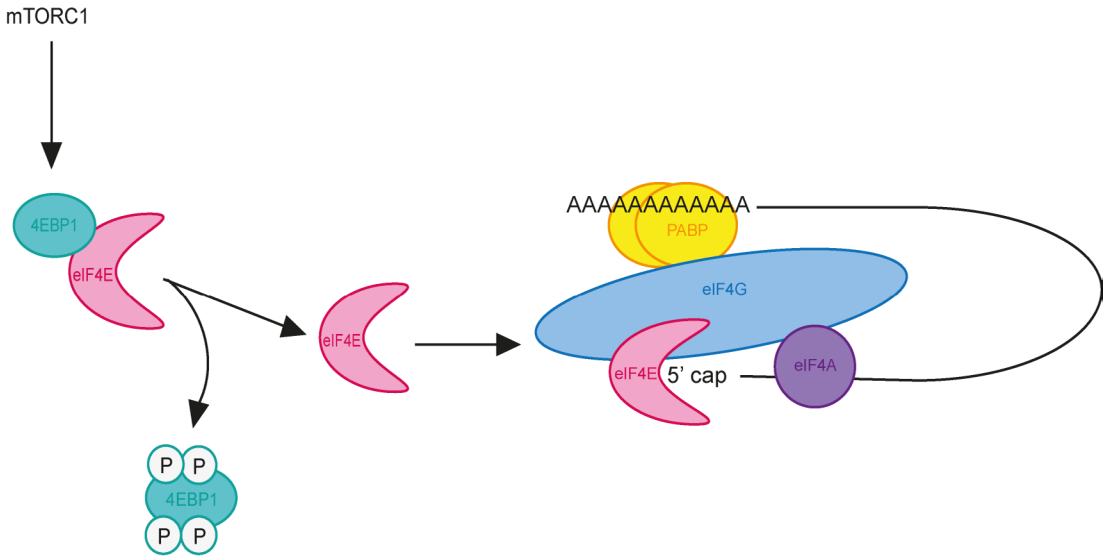

Figure 1.8 Schematic representation of eIF4F formation and mRNA circularisation

Activation of mTORC1 phosphorylates 4E-BP1 which prevents it binding to eIF4E enabling eIF4E to bind eIF4G and participate in the formation of the eIF4F initiation complex (eIF4E, eIF4A, eIF4G) along with the poly (A)-binding protein (PABP) and eIF4B. The eIF4F initiation complex binds to the m^7 GTP cap at the 5' end of mRNA and mediates small ribosomal subunit binding.

eIF4G3. Whilst eIF4G1 and eIF4G2 are structurally similar, and both play a part in cap-dependent translation, eIF4G3 has been implicated in alternative ribosomal entry during cellular stress [185,186]. The N-terminal fragment of eIF4G interacts directly with eIF4E [187–189] and PABP [188,190–192], whereas the central region of eIF4G contains binding sites for eIF4A [193] and eIF3 [194] and possesses RNA-binding activity [195]. The C-terminal domain of eIF4G contains a second, independent binding site for eIF4A and a conserved region at the extreme C-terminus of eIF4G, which has been shown to interact with Mnk1/2 and suggested to interact with eIF5 and eIF2Bε [152,196]. The C-terminus of eIF4G also contains phosphorylation sites at Ser1108, Ser1148, and Ser1192 [197], which PKC has recently been implicated in phosphorylating, this inhibits the interaction between eIF4G and Mnk1/2 [198]. Alongside serving as a scaffold for the assembly of the translational machinery, eIF4G has also been shown to increase the binding affinity of eIF4E for the mRNA cap [199] and to increase the helicase activity of eIF4A [200]. eIF4G contains a HEAT domain [201], and has been observed to be cleaved by picornavirus, therefore inhibiting cap-dependent translation initiation [202].

eIF4E is a 25-kDa protein that is highly conserved from yeast to humans [203,204]. Given its key role in the formation of the eIF4F initiation complex, it is not surprising that it has been the subject of much discussion. There is currently only one known phosphorylation site on eIF4E, Ser209, which has been observed to become phosphorylated in response to cellular stress, and growth factor stimulation of cells [205–209]. The phosphorylation of eIF4E is mediated by Mnk1/2 [210–213]. The Mnk proteins bind to the C-terminus of eIF4G and only phosphorylate eIF4E in *cis*, which means that phosphorylation only takes place if the eIF4E is bound to the same eIF4G [143]. Although the phosphorylation of eIF4E has previously been thought to be essential for translation to occur, double-knockout mice with a mutated eIF4E phosphorylation site do not exhibit a negative phenotype, suggesting that this is not the case [214]. However, it has been observed that excessive eIF4E

phosphorylation can promote malignancies possibly through enhanced export of selected mRNA into the cytoplasm [215].

The formation of the eIF4F complex relies on the availability of eIF4E to participate. Using a conserved motif, 4E-BPs (eIF4E-binding proteins) compete with eIF4G for a common surface on eIF4E. This binding of eIF4E to 4E-BPs therefore inhibits eIF4E from participating in eIF4F assembly, resulting in the inhibition of cap-dependent ribosome recruitment to the mRNA [216] (Fig.1.7). In mammals, three 4E-BP isoforms have been identified so far; 4E-BP1, 4E-BP2, and 4E-BP3 [217–219], the most studied of which is 4E-BP1.

Hypophosphorylated 4E-BP1 binds efficiently to eIF4E, reducing the availability of eIF4E for the translation initiation process. In contrast, multisite phosphorylation of 4E-BP at Thr37/46, Ser65 and Thr70 inhibits this interaction, allowing initiation complex assembly [144,197]. The phosphorylation of Thr37/46 by mTORC1 is thought to prime 4E-BP1 for subsequent phosphorylation at Ser65 and Thr70 [144] (Fig.1.8). 4E-BP1 contains two important motifs that are specifically bound by either raptor or mTOR. The TOS motif present on the C terminus of the protein is bound by raptor, and the RAIP motif on the N terminus is bound by mTOR, both motifs require binding to promote phosphorylation at the multiple residues on 4E-BP1 and therefore it's full activation [220].

Activation of mTORC1 phosphorylates 4E-BP1 and p70 S6K1 (S6K1)(Fig.1.5), both of which encourage protein synthesis [221]. As discussed earlier, phosphorylation of 4E-BP1 prevents it binding to eIF4E which enables eIF4E to bind eIF4G and participate in the formation of the eIF4F initiation complex along with PABP (Fig.1.8).

When the eIF4F initiation complex is formed it then binds to the m^7GTP cap at the 5' end of mRNA. This causes circularisation of the mRNA, mediated by PABP binding to both the poly (A) tail of the mRNA, and eIF4G (Figs.1.7&and 1.8). The eIF4A helicase component of the eIF4F complex then unravels the mRNA; this activity is enhanced by eIF4B and eIF4H. The 40S small ribosomal subunit is then recruited to the mRNA by the binding of eIF3 to both eIF4G and the 43S initiation complex [171].

1.23 Scanning of the mRNA and localisation of the AUG start codon

After attachment, the 43S complex scans the mRNA downstream of the 5' cap until it reaches the AUG initiation codon. Although the scanning model of translation initiation is widely accepted as accurate [222], direct evidence that this is what happens has still not been demonstrated.

The 'scanning' of the mRNA has shown to be directly mediated by the small eukaryotic initiation factors 1 and 1A, associated with eIF3. These factors have both been shown to be essential for start codon recognition [223]. Although both have also been shown to accelerate the formation of the eIF2-GTP-Met-tRNA ternary complex in vitro, only eIF4A has been shown to stabilise this complex [224].

Interestingly, the ternary complex associated with eIF1 has also been observed to be able to carry out ribosomal scanning of unstructured 5' UTRs without the need for the eIF4F complex. However, this is only the case for unstructured mRNAs, as this does not occur when secondary structures are present [223].

When the start codon is reached, the ribosome halts, binds stably at the initiation codon (Fig.1.7) and the 40S ribosome undergoes a GTP-mediated conformational change to stabilise this interaction. The start codon is usually (but not always) the AUG closest to the mRNA 5' end and the binding occurs primarily through the RNA-RNA interaction between the AUG codon and the CAU anticodon of the bound initiator Met-tRNA.

1.24 60S ribosomal subunit joining

Following the binding of the ribosome to the start codon, the GTPase activating protein (GAP), eIF5, binds to the β subunit of eIF2 and induces the hydrolysis of the GTP bound eIF2-Met-tRNA by the γ subunit of eIF2. Previous to this, eIF1 prevents premature hydrolysis of GTP and subsequent release of eIF2 by stabilisation of the complex. However, during codon-anticodon pairing, eIF1 is displaced, allowing GTP hydrolysis and eIF2-GDP release [225,226]; eIF2-GDP is then able to be recycled for the next round of initiation.

Joining of the 60S ribosomal subunit and dissociation of eIF1, eIF1A, eIF3 and residual eIF2-GDP is mediated by eIF5B [227]. eIF5B is a GTPase that hydrolyses bound GTP, resulting in the release of all previously bound initiation factors, promoting the binding of the 60S subunit, resulting in the formation of the 80S ribosome. The GTPase activity of eIF5B is triggered by ribosomal binding, resulting in the hydrolysis of eIF5B bound GTP, and release of eIF5B-GDP and eIF1A [228].

1.25 Research aims

The research undertaken during this project aims to select potential chemical compounds that could downregulate the levels of the MGMT protein so as to be used in conjunction with TMZ and radiotherapy to increase the efficacy of anticancer therapies, yet while remaining non-cytotoxic to the cells when used alone. In addition to this, I also aim to elucidate how the selected compounds influence cell signalling in both glioblastoma lines that over express the MGMT protein, and those that are MGMT null.

Chapter II

Materials and methods

2 Materials and Methods

2.1 Buffers

Lysis Buffer; 20mM MOPS-KOH pH 7.2, 20mM sodium fluoride, 1µM microcystin LR, 75mM KCl, 2 mM $MgCl_2$, 2mM benzamidine, 2mM Na_3VO_4, complete protease inhibitor mix (-EDTA (Roche, UK)), 0.1% (v/v) SDS

Sample buffer; 1.4M β-Mercaptoethanol, 530mM Tris-HCl pH6.8, 0.85% (v/v) SDS, 42.5% (v/v) glycerol, 0.05% (w/v) bromophenol blue and 0.05% (w/v) phenol red

Running buffer; 25mM Tris-HCl pH 8.5, 0.16% (w/v) SDS, 192mM glycine

Anode 1 buffer; 0.3M Tris base pH10, 20% (v/v) methanol

Anode 2 buffer; 25mM Tris base, 20% (v/v) methanol

Cathode buffer; 25mM Tris base, 6-NH_2 hexanoic acid, 20% (v/v) methanol

Buffer A; 20mM MOPS-KOH pH 7.2, 75mM KCl, 2mM benzamidine, 7mM mercaptoethanol, 2mM $MgCl_2$, 0.1mM GTP, complete protease inhibitor mix (-EDTA), 25mM NaF.

Hypertonic lysis buffer; 150 mM Tris-HCl pH7.5, 10mM KCl, 15mM $MgCl_2$, 1% (v/v) Igepal, 0.5%(v/v) DOC, 40mM β-glycerophosphate, complete protease inhibitor mix (-EDTA), 2mM DTT, 100µg/ml cycloheximide, 10 U/ml RNase inhibitor, 0.1% TritonX-100.

PBS; 137mM NaCl; 2.7mM KCl, 6.5mM Na_2HPO_4; 1.5mM KH_2PO_4 , pH 7.3.

TBS-Tween; 50mM Tris-HCl pH7.4, 150mM NaCl, 0.5% (v/v) Tween-20.

ECL developing solution; 0.5mg/ml 5-amino-2,3-dihydro-1,4-phthalazinedione (luminol) and 11µg/ml parahydroxy-coumaric acid in 0.1M Tris-HCl pH 8.6 containing 0.01% (v/v) hydrogen peroxide.

2.2 Cell Culture

T98G glioblastoma cells (obtained from the ECACC) were cultured to confluency in minimum essential medium (MEM) supplemented with 5% non essential amino acids (Invitrogen, UK), 10% foetal calf serum (Biosera, UK) and 5% GlutaMax (Invitrogen, UK). U87-MG glioblastoma cells (obtained from the ECACC) cells were cultured in the same manner but with Hyclone foetal calf serum. All cell lines were grown at 37°C in humidified atmosphere with 5% CO_2.

When treating with chemicals, cells were allowed to grow to 75% confluency if being treated for 24 hours, or 50% confluency if being treated for 48-72 hours.

2.3 Preparation of cell extracts for Western blotting

To prepare cell extracts, tissue culture dishes of cells were transferred onto ice and the medium was removed. The cells were scraped into 0.5ml of PBS and isolated by centrifugation in a microfuge at 15,000 rpm for 1min at 4°C. Cell pellets were then lysed in 200µl of Lysis buffer containing 0.5% (v/v) Igepal and 0.5% (v/v) deoxycholate. After thorough vortexing, the cell debris was isolated by centrifugation at 15,000 rpm for 5 minutes at 4°C and the supernatant was flash-frozen in liquid nitrogen and stored at -80°C for further analysis.

2.4 Estimation of protein concentration

Coomassie dye (Bradford reagent) stock solution was diluted 1:4 with distilled H_2O. 1µl of cell lysate was added to 200µl of diluted Bradford reagent. The colour reaction was quantified by measuring absorbance (A_{620}) minus background absorbance (A_{405}) using a standard curve of known bovine serum albumin protein concentrations to calculate the amounts of protein in the extracts.

2.5 SDS-PAGE and Immunoblotting

SDS-PAGE was used to separate denatured proteins according to their molecular weight by electrophoresis. SDS-PAGE was performed following the standard protocol for the mini-gel systems, Protean II or Protean III (Bio-Rad).

Polyacrylamide resolving gels were composed of 375mM Tris-HCl pH 8.8, 0.2% (v/v) SDS, 0.1% (w/v) ammonium persulphate (APS), 0.1% (v/v) N,N,N',N'-tetramethylethylene diamine (TEMED), and a mixture of acrylamide and bis-acrylamide in a ratio of 37.5:1. The percentage (w/v) of acrylamide contained in the resolving gel was varied to suit the molecular weight of the proteins of interest, ranging from 7.5 to 15%. Stacking gel contained 125mM Tris-HCl pH 6.8, 0.2% (v/v) SDS, 5% (w/v) acrylamide, 0.13% (w/v) bis-acrylamide, 0.1% (w/v) APS and 0.1% (v/v) TEMED. Samples containing equal amounts of protein (10µg) were mixed with SDS-PAGE Sample buffer and resolved next to a track of marker proteins at 100 volts.

Following SDS-PAGE, proteins were transferred to a PVDF membrane (GE Healthcare, UK) using a semidry transfer apparatus (Semi-Phor, Hoefer, USA). A 'sandwich' composed of 4 sheets of filter paper soaked in Anode1 buffer, followed by 2 sheets of filter paper soaked in Anode2 buffer, PVDF membrane wetted in methanol, the polyacrylamide gel, and 4 sheets of filter paper soaked in Cathode buffer was assembled. The 'sandwich' was then placed in the apparatus and the proteins transferred to the membrane by applying 0.8 mA/cm^2 for 2 hours.

After the protein had been transferred to PVDF membrane, non-specific binding sites of the membrane were blocked by immersion in TBS-Tween with 3% (w/v) bovine serum albumin for at least 30minutes. Afterwards, the membrane was rinsed three times in TBS-Tween at room temperature, prior to being incubated in primary antibody (diluted in TBS-Tween with 3% (w/v) bovine serum albumin) overnight at 4°C on a shaker. Next, the membrane was rinsed and washed three times for 10minutes in TBS-Tween, followed by one-hour incubation in 2000-fold diluted horseradish peroxidase-conjugated secondary antibody, and then another three brief rinses and three 10 minute washes in TBS-Tween. Finally, the membrane was incubated for 1 minute in ECL Developing Solution, excess solution removed, the membrane wrapped in cling film and exposed on film for varying length of time according to the intensity of the signal. The antiserum used were raised against: eIF4A, p-eIF4E, eIF4G,

eIF4E [229,230]; MGMT, p-eIF2α, (Abcam, UK); total 4E-BP1, p-4E-BP Ser65, p-4E-BP1 Thr70, p-p70 S6K Thr389, total S6K, α-tubulin, cleaved PARP, p-AMPKα T172, p- ERK1/2, p-p38 MAPK, p-rpS6 Ser240/44, p-Akt Thr308, p-Akt Ser473, $p21^{cip1}$ (Cell signalling, UK). Western blotting experiments presented are representative of 3 separate experiments unless specified in the figure legend.

2.6 Cell Treatments

Temozolomide (TMZ), Rapamycin, LY294002, Thalidomide, Spiperone, Resveratrol, Beta Escin, 4,5-Dianilinophthalimide and AICAR were obtained from Sigma Aldrich, UK. KU0063794, A769662, Thioridazine and PI-103 were obtained from Tocris Biosciences, UK. RAD001 was a gift from Novartis, Basel. Stock solutions were made up in DMSO and mixed thoroughly with tissue culture media to achieve the required final concentrations.

2.7 [^{35}S]-methionine labelling of cellular protein

One hour prior to harvesting, cells were pulse-labelled with [^{35}S]-methionine (MP Biomedicals, UK; 10μCi/ml) and cell extracts prepared as above and 5μl of extract were then spotted in triplicate onto Whatman filter papers. Filters were transferred to 10% (v/v) trichloroacetic acid (TCA) containing 5mM unlabelled methionine for 15 minutes then boiled in 5% (v/v) TCA. Once cooled, the filters were washed in ethanol, then acetone, dried and subjected to liquid scintillation counting. Protein synthesis, expressed as cpm/μg protein, is shown as a % of the rate obtained in cells incubated in the absence of drugs.

2.8 MTS Assay

Metabolism in viable cells produces reducing equivalents such as NADH or NADPH which pass their electrons to an intermediate electron transfer reagent that can reduce the tetrazolium product, MTS, into an aqueous, soluble formazan product. At death, cells rapidly lose the ability to reduce tetrazolium products. Therefore, the production of a coloured formazan product is

proportional to the number of viable cells in culture. To measure cell viability, cells were cultured in a 96 well plate in 100µl of complete medium. Following incubation in the absence or presence of drugs (see individual figure legends for details), 20µl of MTS/PMS solution (Promega, UK) was added to each well, and cells left for 2 hours at 37^{o}C. The colour reaction was quantified by measuring absorbance at A^{490} using the control wells for comparison. All assays were carried out in triplicate.

2.9 RNA extraction and Illumina Microarray analysis

RNA was extracted using Tri reagent and 1-bromo-3-chloropropane (Sigma, UK). The media was aspirated from each well, and the monolayer of cells washed once with 1ml of PBS. The PBS was aspirated and 500µl of TRI reagent (Sigma, UK) added to each well. The TRI reagent was thoroughly pipetted to ensure all cells were removed from the plate, and then transferred into microfuge tubes for storage at -80°C or immediate RNA isolation. If the cells were frozen, the samples were allowed to defrost for 5 minutes at room temperature. 100µl of 1-bromo-3-chloropropane (Sigma, UK) was added to each sample which was then mixed vigorously for 15 seconds. The samples were incubated at room temperature for 2 minutes and then centrifuged at 12,000 rpm for 14 minutes at 4°C. The upper aqueous phase was transferred to a new microfuge tube and mixed thoroughly at a 1:1 ratio with isopropanol (Fisher Scientific, UK). The samples were incubated at room temperature for 10 minutes and centrifuged at 12,000 rpm for 10 minutes at 4°C.

The supernatant was discarded, and the pellet washed twice with 75% ice-cold ethanol (75% absolute ethanol, Fisher Scientific, UK, 25% molecular biology grade water, VWR, UK), then centrifuged at 12,000 rpm for 5 minutes at 4°C. The supernatant was discarded, and the last traces of ethanol removed with gel-loading pipette tips. The RNA pellet was dried in a Savant DNA Speed-Vac for 2 minutes and resuspended in 25µl of molecular biology grade water. The RNA concentration was measured by 260/280 nm absorbance ratio on a Nanodrop spectrophotometer.

RNA integrity was then measured by microfluidics analysis using the Agilent 2100 bioanalyzer and RNA Nano 6000 kit (Agilent Technologies, UK) according to the manufacturer's instructions. Briefly, 1µl of sample containing 50-500ng of RNA was pipetted into a chip containing glass micro-channels filled with a gel containing RNA intercalating fluorescent dye. A current was applied to the gel, separating the RNA molecules by size. The RNA was detected by fluorescence and used to construct gel-like images. RNA quality was assessed by the relative widths of the 18S and 28S ribosomal bands, and expressed as an RNA Integrity Number (RIN) [231]. A RIN of between 8 and 10 indicates RNA integrity sufficient for microarray analysis.

Genome-wide gene expression analysis was carried out using the Illumina Microarray platform. Illumina microarrays are single-channel microarrays with 50mer oligonucleotide probes attached to beads mounted to a mirrored glass slide.

RNA obtained from MCF7 cells treated with 10µM KU0063794 for 6 hours, cells treated with 20µM A769662 for 6 hours and untreated control cells was converted to biotinylated cRNA using an Illumina TotalPrep RNA amplification kit (Ambion, UK). The cRNA was prepared according to the manufacturer's instructions. 500ng of RNA was reverse transcribed to cDNA using a master mix containing oligo (dT) primer, buffer, dNTP mix, RNase inhibitor and ArrayScript (reverse transcriptase) and incubated for 2 hours at 42°C.

Second strand cDNA synthesis was performed by adding a master mix made up of nuclease-free water, buffer, dNTP mix, DNA polymerase and RNase H. The sample was then incubated for 2 hours at 16°C. The cDNA was purified using cDNA filter cartridges and several centrifugation and wash steps, before being eluted in nuclease-free water. The purified cDNA was transcribed to biotinylated cRNA by adding a master mix of buffer, T7 enzyme mix (RNA polymerase), and a biotin-NTP mix and incubated at 37°C for 14 hours. The biotinylated cRNA was purified using cRNA filter cartridges and several centrifugation and wash steps, before being eluted in nuclease-free water. The

integrity of the resulting cRNA was measured by microfluidics analysis using the Agilent 2100 bioanalyzer and RNA Nano 6000 kit as outlined above.

Microarray hybridization was carried according to Illumina manufacturer's instructions. Briefly, 750ng of cRNA was prepared in a volume of 5µl of nuclease free water. The cRNA was mixed with 10µl of hybridization buffer, and denatured at 65°C for 5 minutes. The cRNA samples for MCF7 cells exposed to estradiol were then injected onto Illumina HT-12 v3 Expression BeadChips (Illumina, USA). The cRNA was hybridized to the BeadChips in a humidified hybridization chamber over an 18 hour incubation period at 58°C.

The Illumina BeadChips were washed and scanned according to the manufacturer's instructions. The BeadChip was blocked using a block buffer, and stained with cy3-labelled streptavidin. This was followed by several more wash steps, before the BeadChip was dried by centrifugation at 275 g for 4 minutes. The BeadChip was immediately loaded into an Illumina BeadArray Reader and scanned at a wavelength 532 nm using a laser at default power and PMT parameters.

2.10 Microarray data analysis and connectivity mapping

Raw probe expression values are stored in .IDAT files. The .IDAT files were imported into GenomeStudio Data Analysis Software. During the import process, fluorescence values for repeated probes were combined to produce one mean fluorescence value per probe. The data was then exported in .txt file format. Microarray data was normalized, stored and handled using ArrayTrack software [232] and a storage account kindly set up by ArrayTrack on their server. Illumina microarray data, in .txt file format, was imported into ArrayTrack and normalised using a quantile normalisation algorithm. Control and treated normalised microarray datasets were compared using a Welch t-test. Differentially expressed genes were filtered by p value (<0.05).

In order to query the original connectivity map, microarray data must be in the same naming format as the connectivity map database - Affymetrix (HT) HGU113A probe identifiers. Therefore, in-house generated Illumina microarray

data had to be converted to Affymetrix probe identifiers. Illumina probe identifiers were converted to HUGO gene names using ArrayTrack software loaded with Illumina annotation files. Microarray data in HUGO gene naming format was exported from ArrayTrack in .txt file format. The .txt files were imported into a Microsoft Access database loaded with an Affymetrix annotation file, and a query set up to match the HUGO gene names of the microarray dataset with the annotation file. The microarray dataset was assigned Affymetrix probe identifiers. Where several Affymetrix probes represented a gene, all the Affymetrix probes were included, and the file exported in .txt format.

The most differentially expressed genes were selected as gene signatures to query the connectivity map. These were selected primarily by highest absolute log2 fold change. Where possible, *p* value (<0.05) was used to filter out genes with a higher sample variation. In some cases with Affymetrix data, where background fluorescence can be a problem, filtering out differentially expressed genes with low mean channel intensities was employed. Connectivity mapping was carried out using the sscMap connectivity mapping program with either the standard connectivity map database (in Affymetrix probe identifier format) or the HUGO connectivity map database (in HUGO gene name identifier format).

A product of converting a non-Affymetrix microarray dataset to Affymetrix format is that it necessitates the inclusion of all the Affymetrix probes representing a gene. The impact that this has on connectivity mapping accuracy was modelled using an Affymetrix dataset for MCF7 cells exposed to 10nM estradiol for 6 hours in charcoal-stripped serum conditions. The 30 most changed genes were selected by highest absolute log2 fold change and used as a gene signature to query the connectivity map. This was repeated using the same gene signature with all of the probes representing each gene included.

The 6100 microarray datasets which make up the connectivity map database were converted from Affymetrix probe identifier format to HUGO gene name format. To achieve this, a VBA macro was designed to automate the process. The connectivity map algorithm cannot deal with duplicated gene names. Where

several gene names were present only the gene with the highest absolute log2 fold change was maintained, the others were removed

2.11 Fluorescence activated cell sorting

Following incubation of cells as described in the figure legends, cells were washed with warm PBS then trypsinised and removed from culture dishes. Cells were washed in PBS and fixed in 70% ethanol/30% PBS at 4ºC overnight. Immediately before analysis, the cells were washed in PBS and resuspended in 500µl PBS containing 0.1mg/ml RNase A (Sigma, UK) and 30µg/ml propidium iodide (Invitrogen, UK) and analysed by a FACSCanto^{TM} flow cytometer (BD Biosciences) using BD FACSDiva^{TM} software. Data shown are representative of those obtained in at least three separate experiments.

2.12 Quantitative real–time RT-PCR

RNA was extracted from cell extracts using an RNA easy mini-kit (Qiagen, UK) as per manufacturer's instructions. RNA concentrations were then quantified using a Nanodrop and 1µg of RNA was used for cDNA synthesis using the Promega ImpromII kit. The SYBR real-time PCR system (Kapa Biosystems, UK) was used to quantify transcript abundance for genes of interest and 18S mRNA was used as a control. Template equivalent to 5ng of RNA in cDNA library per reaction was added to each 20µl reaction with a final primer concentration of 200nM per reaction. Crossing thresholds were determined using MxPro software (Agilent), and fold-difference in RNA quantity was calculated using the relative quantification method ($2^{-\Delta\Delta ct}$).

Dissociation curves for both 18S primers and MGMT primers were calculated to ensure amplicons were the correct length, and therefore the primers were binding specifically.

2.13 Immunofluorescence analysis of MGMT in T98G cells

Cells were plated on glass coverslips 8 hours before treatment. Cells were then fixed with 4% (w/v) paraformaldehyde for 20 minutes at room temperature

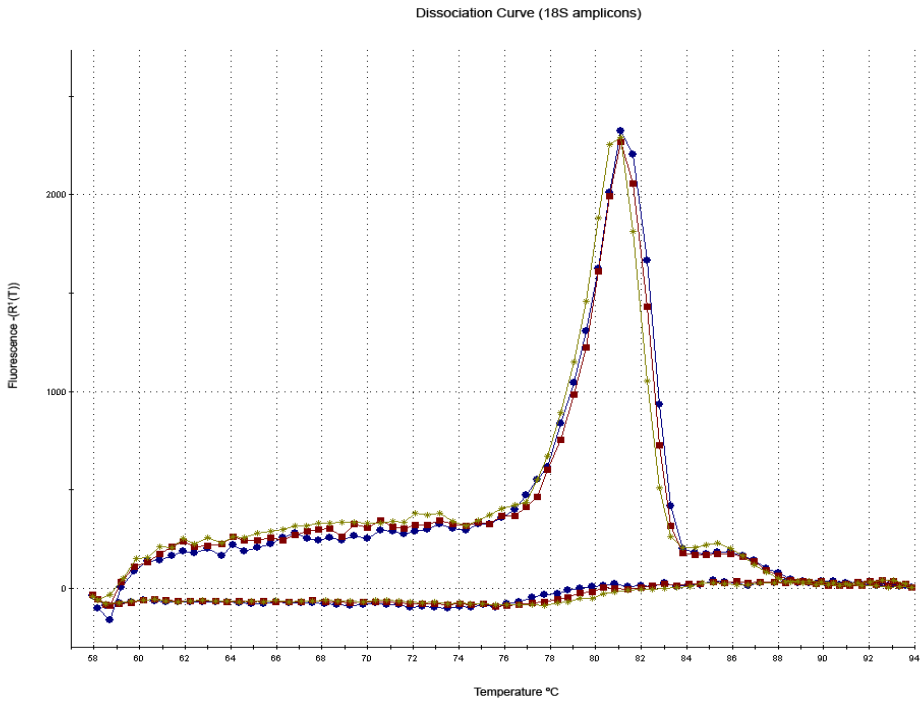

Figure 2.1 Dissociation curve of 18S amplicons

The dissociation curve shows the melting temperature of the RNA strands amplified by the specific primers.

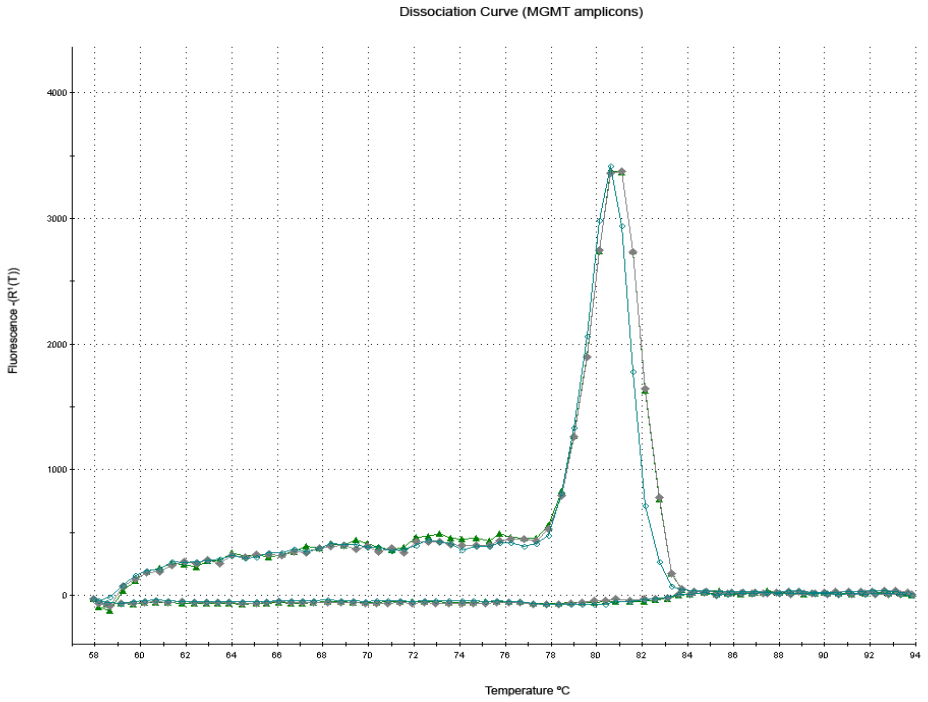

Figure 2.2 Dissociation curve of MGMT amplicons

The dissociation curve shows the melting temperature of the RNA strands amplified by the specific primers.

and permeabilised for 5 minutes in 0.1% (v/v) Triton X-100/PBS. Cells were blocked for 20 minutes with 5% (w/v) gelatin/PBS in a humidified chamber. Cells were incubated with anti-MGMT (Abcam, UK) for 1 hour at room temperature also in a humidified chamber. Alexa Fluor 555-conjugated anti-rabbit secondary antibody was added for 1 hour at room temperature. Alexa Fluor 488 phalloidin was also used in the secondary antibody incubation. Following further extensive washing, nuclei were stained with DAPI (4', 6-diamidino-2-phenylindole) for 5 minutes. After a further two washes, coverslips were mounted on microscope slides with Mowiol mounting solution (0.2 M Tris-HCl pH 8.5, 33% (w/v) glycerol, 13% (w/v) Mowiol and 2.5% (w/v) DABCO (1, 4-diazobicyol [2, 2, 2]-octane)) and sealed with clear nail polish. Images were collected on a Zeiss Axiovert LSM510 scanning confocal microscope using a ×100 objective. Single stain, bleed-though controls and antibody cross-reaction controls were prepared for each sample.

2.14 Optical Microscopy

Cells were grown in 5cm plates then visualised with a Nikon eclipse t5100 microscope. Images were collected using a Moticam 2000 2 megapixel mounted camera.

2.15 M^7GTP sepharose affinity chromatography

To isolate eIF4E and associated proteins [229,230], cells were lysed as described and aliquots containing 100µg were incubated with 30µl m^7GTP-Sepharose resin (50% v/v in 1mg/ml cytochrome c) for 15 minutes on ice, with mixing. The resin was washed twice in 200µl Buffer A then eluted in SDS-PAGE sample buffer containing 10% w/v β-mercaptoethanol, prior to Western blotting.

2.16 Polysome profiles

Cells were treated with 10µg/ml of cycloheximide (Sigma, UK) for 3 minutes before harvesting. The cells were then washed twice in PBS containing 10µg/ml cycloheximide and lysed in Hypertonic lysis buffer for 10 minutes at room

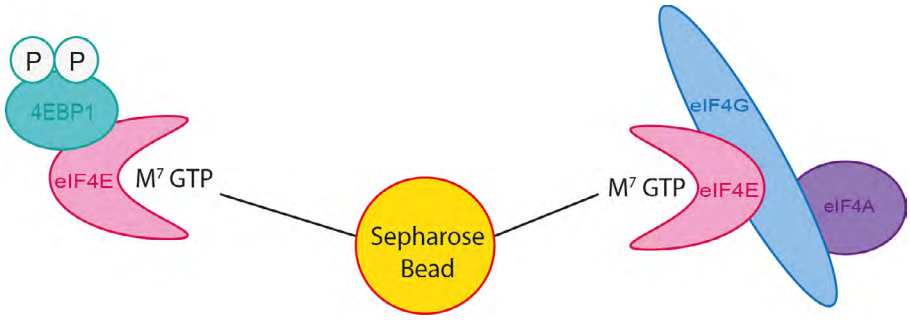

Figure 2.3 A schematic representation of the M^7GTP sepharose beads actively bound to initiation factors

temperature, then a further 20 minutes on ice. The cell lysate was centrifuged at 14,000rpm for 3 minutes and the supernatant was separated on a 7.6ml sucrose gradient (10-60% (w/v) in hypertonic lysis buffer) for 130 minutes at 38,000 rpm using a Beckman SW40 rotor. Optical density profiles and gradient fractions were obtained by upward displacement of the sucrose gradients with pumping sucrose (60% (w/v) sucrose) through an ISCO UA6 gradient fractionation machine coupled to a UA5 spectrophotometer measuring the absorbance at 254nm.

The RNA was precipitated from each fraction by adding 150μl 2M NaCl, 10μg Glycogen and 1ml of filtered Isopropanol. The tubes were then vortexed until thoroughly mixed and left at room temperature for 20 minutes to initiate the precipitation, before being frozen at -20ºC. The samples were then thawed before being centrifuged at 14,000rpm for 45 minutes at 10ºC. The samples were then washed twice in 1ml of cold ethanol and centrifuged at 14,000rpm and 4ºC to remove the salt. The supernatant was removed and the pellets left to dry in the fume hood. The pellets were resuspended in 100μl of Ambion Lysis/Binding buffer, left for 5 minutes and then 100μl of Phenol (Ambion) was added. The samples were then centrifuged at room temperature and 10,000rpm for 10 minutes and then the upper phase was removed and placed in a clean cold microfuge tube. The RNA was then purified according to the NucleoSpin RNA II isolation kit (Macherey-Nagel) and qRT-PCR was carried out as described above.

2.17 eIF4A helicase reporter assays

To assay eIF4A activity in cells, assays were carried out by Dr. Thomas Webb (University of Nottingham), using the technique outlined in [233]. Briefly, SH-SY5Y cells were co-transfected in triplicate with pGL3-(6x) HRE–firefly luciferase and TK–Renilla luciferase reporters. The cells were then incubated overnight with chemicals and concentrations specified in the corresponding figure legends. 24 hours post-transfection, cells were freeze–thawed and lysed in 1× passive lysis buffer (Promega). The cell samples were assayed for

luciferase activity using LarII and Stop and Glo reagents (Promega) and a GloMax luminometer (Perkin Elmer).

Chapter III

Identifying potential therapeutic candidates using patient material: Connectivity mapping

3 *Identifying potential therapeutic candidates using patient material: Connectivity mapping*

3.1 Aims

- To identify compounds that will decrease MGMT protein levels
- To use connectivity mapping with patient data to identify these compounds
- To ensure the compounds are not cytotoxic to cells

3.2 Introduction

3.2.1 Connectivity mapping: an overview

Connectivity mapping is a technique that combines a reference collection of gene expression profiles derived from cultured human MCF7 breast cancer cells treated with bioactive small molecules, with an algorithm that searches for similarities or differences between these profiles. The technique is based upon the principle that a transcription pattern can be used as a fingerprint to describe a chemical-induced biological condition. By identifying similarities between the transcription patterns produced by different chemicals, functional similarities or "connections" can be identified between those compounds. Connectivity mapping was originally designed and implemented by Lamb *et al.* in 2006 [234]. The technique was then refined by Zhang *et al.* in 2009. I have implemented this refined technique as it normalises the data, making the analysis less error prone than the original format.

There are three main stages to connectivity mapping (Fig.3.1). Firstly, there is a reference database that contains gene profiles of MCF7 breast cancer cell lines. The gene profiles are generated by treating the cells with a known concentration of a compound for 6 hours. A genome-wide mRNA microarray is then performed on both the treated cells, and an untreated control. The changes in mRNA expression between the two samples are then quantified, and a list compiled of the top 30 or top 100 most changed genes (whichever describes the changes best). The list is arranged in descending order, with the most changed

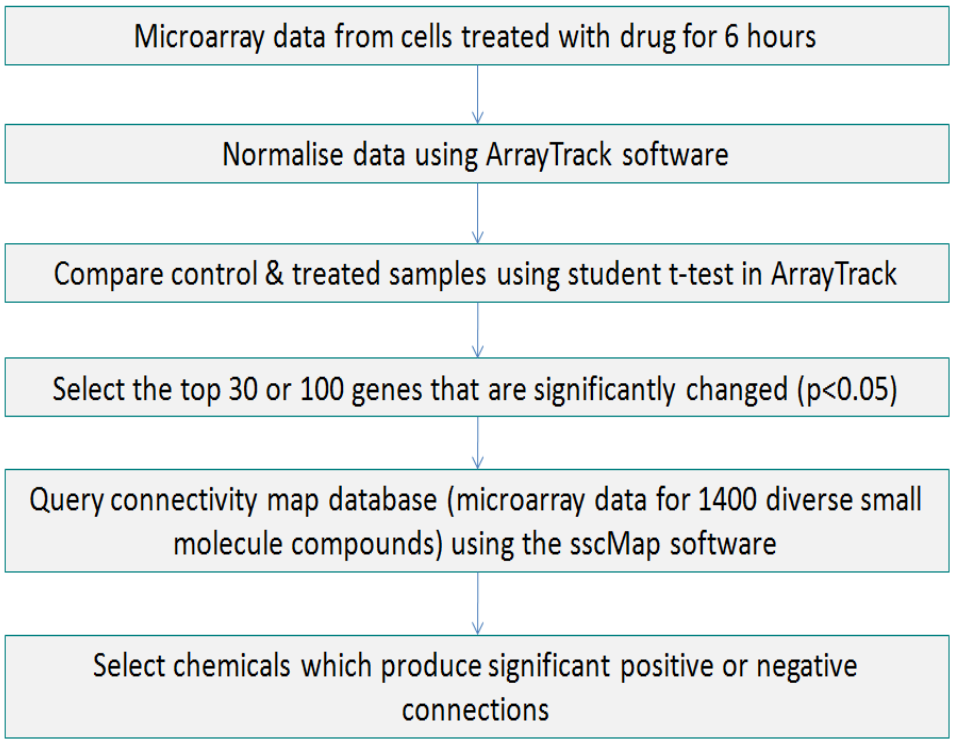

Figure 3.1 Flow diagram representing the stages of connectivity mapping

This flow diagram outlines the main stages of connectivity mapping. First MCF7 cells are treated for 6 hours with a compound. A microarray is then performed on these cells and an untreated control. The treated and untreated samples are then compared and the top 30 or 100 (depending on which is most descriptive of the gene change) are selected. The most changed genes list then represents this compound. The connectivity map database is made up of thousands of compounds that have been processed in this fashion. The connectivity map can then be queried to find chemicals that produce a similar (or dissimilar) expression pattern.

genes at the top (“most changed” gene expression includes both up-regulated and down-regulated genes).

The second stage of connectivity mapping involves either creating a query gene signature by doing an “in house” microarray on cells treated with a compound of interest, or obtaining microarray data from the original database created by Lamb *et al.* [234]. For the approach to be successful, the query gene signature has to accurately define the biological state change compared to the control, whilst being shorter than the genome-wide list of genes. The query gene signature, therefore, is simply a list of genes whose expression changed as a result of a disease state or induced by treatment with a compound (compared to a control). This list is then ranked in descending order, with the genes which had the highest fold change in gene expression at the top.

The third and final stage of the connectivity mapping procedure is the use of an algorithm that determines similarities between the query gene signature, and the reference gene signatures in the database. The connection strength of a query signature to a reference signature is determined by multiplying the values assigned to genes (the fold change in gene expression) in the query signature with the values assigned to genes in the reference database (Fig.3.2).

$$C(\mathbf{R}, \mathbf{s}) = \sum_{i=1}^{n} R(g_i)s(g_i),$$

Figure 3.2 The sscMap scoring scheme

The sscMap algorithm scoring scheme involves the multiplication of values associated with genes contained in the gene signature, with the values associated with the corresponding genes in each reference profile. Where **C** is the connection strength; **R** is a reference profile; **s** is a gene signature; **n** is the number of genes in a gene signature, **gi** is a gene in the gene signature and **R(gi)** and **s(gi)** are the gene ranks in the reference profile and gene signature respectively [235].

The connection strength can then be used to generate a connection score, which is calculated by dividing the connection strength by the maximum possible connection strength (Fig.3.2).

$$c = C(R, s)/Cmax(N, n)$$

Figure 3.3 Connection score calculation

The connection score is calculated by dividing the connection strength by the maximum possible connection strength. Where **c** is the connectivity score; **C** is the connection strength; **R** is a reference profile; **s** is a gene signature; **N** is the total number of genes in the reference profile and **n** is the number of genes in a gene signature [235].

The connection score calculated by these formulae can be a positive or a negative value. A positive score indicates similarities between the gene changes in the reference profile data and the query profile data. Alternatively, a negative connection score indicates an inverse transcriptional change between the gene signature and reference profile. In order to establish a measurement of statistical significance, the connection strength for a particular gene signature is compared with the connection strength of 10000 random gene signatures of the same length.

3.2.2 Connectivity mapping: applications

Connectivity mapping has a wide range of applications, yet being a relatively new technique, not all of these applications have been explored thoroughly. Connectivity mapping has been most commonly implemented to find novel chemical functions by identifying similarities between compounds effects on

gene expression. Examples of this include the identification of a transcription pattern induced by a specific HSP90 inhibitor and the subsequent identification of novel HSP90 inhibitors (celastrol and gedunin) [236] and the detection of novel inhibitors of HIF2α activity using transcription patterns for the HIF2α-inhibitor PGJ2 [237]. The use of connectivity mapping to detect novel chemical function based on a transcription pattern for a pathological process has also been tested. A transcriptional profile for glucocorticoid resistance identified the mTORC1 inhibitor rapamycin as a novel glucocorticoid sensitising agent [238].

These examples suggest many new and exciting applications for connectivity mapping, especially in aiding the discovery of novel chemical functions of chemicals that may otherwise have been discarded as ineffective for their intended use. Here I will use both disease states and chemical compounds to identify new and exciting chemical functions that could have therapeutic effect on MGMT protein levels in GBM cells.

3.3 Results

3.3.1 Connectivity mapping using patient material

Initially, microarray data was obtained from Lambiv *et al.* [239] from patients with temozolomide and radiotherapy-resistant GBM. The data was derived by comparing the gene changes shown in microarray profiles between samples of GBM that were unresponsive to treatment, compared to those that were responsive to therapy. The gene changes used to define the TMZ resistant GBM samples are listed in Table 3.1.

These sample data underwent connectivity mapping analysis, and the negatively scored results (therefore chemicals that created a gene signature inverse to that of the disease state and the resistance) are listed in Table 3.2. Interestingly the majority of compounds were antipsychotics, but positive connections were also produced by PI3K inhibitors, RTK inhibitors and angiogenesis inhibitors.

Table 3.1 Top 30 most changed genes in TMZ resistant GBM patient samples

The top 96 genes in TMZ resistant GBM samples that had the highest fold change compared to a non-resistant GBM control were used to define the query gene signature, of these, the top 30 are displayed.

Gene name	Fold change
RTP4	1.134483822
CHST8	-1.110915901
CD55	-1.104076998
CA10	-1.089574327
ISG15	0.968717474
IFI44L	0.957023083
PCP4	0.939377047
CLIC2	-0.932085986
ANXA3	-0.914031546
IL20RA	0.90126274
MX1	0.900567372
RSAD2	0.888226952
NF2	0.877979773
CCRL1	0.87530826
IFIH1	0.791689067
LRRC48	0.790021308
PTGER3	0.767570056
WDR78	0.756510956
HIGD2A	-0.711228033
HAP1	-0.710755715
MECP2	0.673013615
IFIT3	0.659924558
SELENBP1	0.649385529
STAT1	0.630125852
CYP39A1	0.627886946
EIF1	0.620492574
CHEK1	0.6098495
PDE3B	0.58168868
IGF1R	-0.57949065

Table 3.2 Candidate drugs suggested to reverse the gene changes brought about by Temozolomide resistance in human samples

The cMap build 2 database was searched for negative connections to a gene signature derived from patient samples of TMZ resistant GBM. The top 96 genes that had the highest fold change compared to a non-resistant GBM control were used to define the query gene signature. The database contained 3738 sets of reference profiles and the expected number of false connections to tolerate was 1. The threshold p value was therefore set at 2.675227394328518e-4 (1/3738) and any connection with a p value lower than this declared significant. All chemicals shown in the table are deemed significant. The top 40 candidate drugs are shown.

Reference set name	Reference set score
triamterene	-4.89966926
dequalinium chloride	-4.875095613
spiperone	-4.667354237
digoxin	-4.412556603
methylbenzethonium chloride	-4.369968855
butoconazole	-4.338523302
altretamine	-4.261400367
mitoxantrone	4.110896614
tonzonium bromide	-4.100504909
proscillaridin	-4.091748982
antimycin A	-4.072536566
lanatoside C	-4.055869411
pyrvinium	-4.051160489
NU-1025	-4.030434451
ouabain	-4.010658905
pipenzolate bromide	-3.976884464
alexidine	-3.974620998
flumetasone	-3.974353309
sulfadiazine	-3.966747222
thioridazine	-3.926260218
octopamine	-3.902298628
tiabendazole	-3.878739069
beta-escin	-3.870456348
colchicine	-3.851894778
Prestwick-682	3.84700215
oxedrine	3.820716804
terfenadine	-3.80995331
metrifonate	-3.807393122
cycloheximide	-3.806058845
ciclacillin	-3.786550231
LY-294002	-3.785180231
thalidomide	-3.741528782
lycorine	-3.738504899
buspirone	-3.71854776
trifluprom azine	-3.686221853
felodipine	-3.627822445
R-atenolol	-3.59555864

3.3.2 Initial treatment of T98G cells with rapamycin, LY294002, PI103 and Torin 1

Mutations in the mTOR signalling pathway is commonly seen in GBM cells can result in hyperactive PI3K/ERK/mTOR signalling, promoting cell survival and protein synthesis [75,142,240]. The hyperactivity of these signalling pathways allows cancerous cells to grow quickly and to effectively resynthesise proteins. One particular protein whose constant synthesis has the potential to cause problems during chemotherapeutic treatment with TMZ is the DNA repair protein, MGMT. MGMT is a “suicide” repair protein that binds irreversibly to a DNA adduct (such as those caused by TMZ) and is destroyed by the proteasome once repair has taken place (Fig.1.3). Therefore, the ability of the cell to resynthesise MGMT and repair DNA damage could be the basis for TMZ resistance in GBM cells.

With this in mind, the initial inhibitors that were screened for potentially reducing MGMT protein levels in GBM cells included the PI3K inhibitor LY294002 which was identified by connectivity mapping of the TMZ-resistant GBM patient samples. Other compounds were chosen because they were also PI3K inhibitors, or affected proteins directly upstream or downstream of PI3K.This included the mTORC1 inhibitor rapamycin, the PI3K inhibitor PI103 and the dual mTOR inhibitor Torin 1.

During the compound treatments T98G cells were treated with four different final concentrations of each inhibitor for 24 hours. Before compound treatments commenced, I ensured that complete cell lysis was being achieved from the T98G cells by using Lysis buffer containing differing concentrations of SDS detergent. I wanted to ensure that all of the MGMT was being extracted from the cells, as it is possible that if a protein is associated with an intracellular component, such as the ER, and cell lysis is incomplete, the proteins can be separated from the lysate during the centrifugation step of protein extraction and discarded. However, the lysis of the cell in the presence of SDS confirmed this was not occurring.

Western blotting was then used with anti-serum against eIF4A and MGMT to visualise protein levels (Fig.3.4). The eIF4A loading control showed that 0.1-0.2% SDS was optimal for protein recovery in this experiment. MGMT protein is present in both the cytoplasm and the nucleus and the data shown in Figure 3.4 suggests that at least 0.1% SDS is optimal for MGMT protein recovered from the cells. Increasing detergent concentrations does not have a huge impact on MGMT protein recovery in these cells. I therefore continued to use 0.1% SDS in the Lysis buffer throughout my experiments to ensure whole cell lysis.

In addition to western blotting analysis, possible cytotoxicity of these compounds was also measured using an MTS assay and the morphology of the cells was assessed under the microscope. A drawback of the MTS assay is that lower readings from the cells as a result of increased mitochondrial toxicity could be disguised by an increase in cell number in the well; this is why I also observed the cells growth and morphology under a light microscope.

3.3.3 Rapamycin treatment leads to increased steady state levels of MGMT in T98G cells

Rapamycin is a macrolide antibiotic, produced by *Streptomyces hygroscopicus* which inhibits mTORC1 activity by forming a complex with FKBP-12 and binding to mTOR [72]. The data presented in Figure 3.5 shows that in T98G cells, complete inhibition of mTORC1 with rapamycin is only complete at the high concentrations. This is suggested by the fact that rapamycin does not lead to the complete dephosphorylation of 4E-BP1 (Fig.3.5 A, lanes 1-5). However, this could also be a result of the speed at which 4E-BP1 becomes dephosphorylated after mTORC1 inhibition. Surprisingly, even though the recovery of eIF4A was constant between treatments, MGMT protein levels were seen to increase as the concentration of rapamycin increases. In addition the level of phosphorylated-eIF2α was also shown to increase with increasing concentrations of rapamycin (lanes 3-5), suggesting that the cells are undergoing an alternative form of stress [241]. Rapamycin is not cytotoxic at any of the concentrations used (Fig.3.5B) but Figure 3.5C shows that, relative to

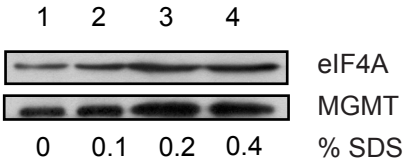

Figure 3.4 Effects of SDS on the recovery of MGMT

T98G cells were grown for 24 hours in complete medium. Cells were harvested and samples were lysed in the absence (lane 1) or presence of differing percentage concentrations of SDS (lanes 2,3 and 4). Aliquots containing 10μg of protein were resolved by SDS-PAGE and proteins visualised by Western blotting using the antiserum indicated (n=1).

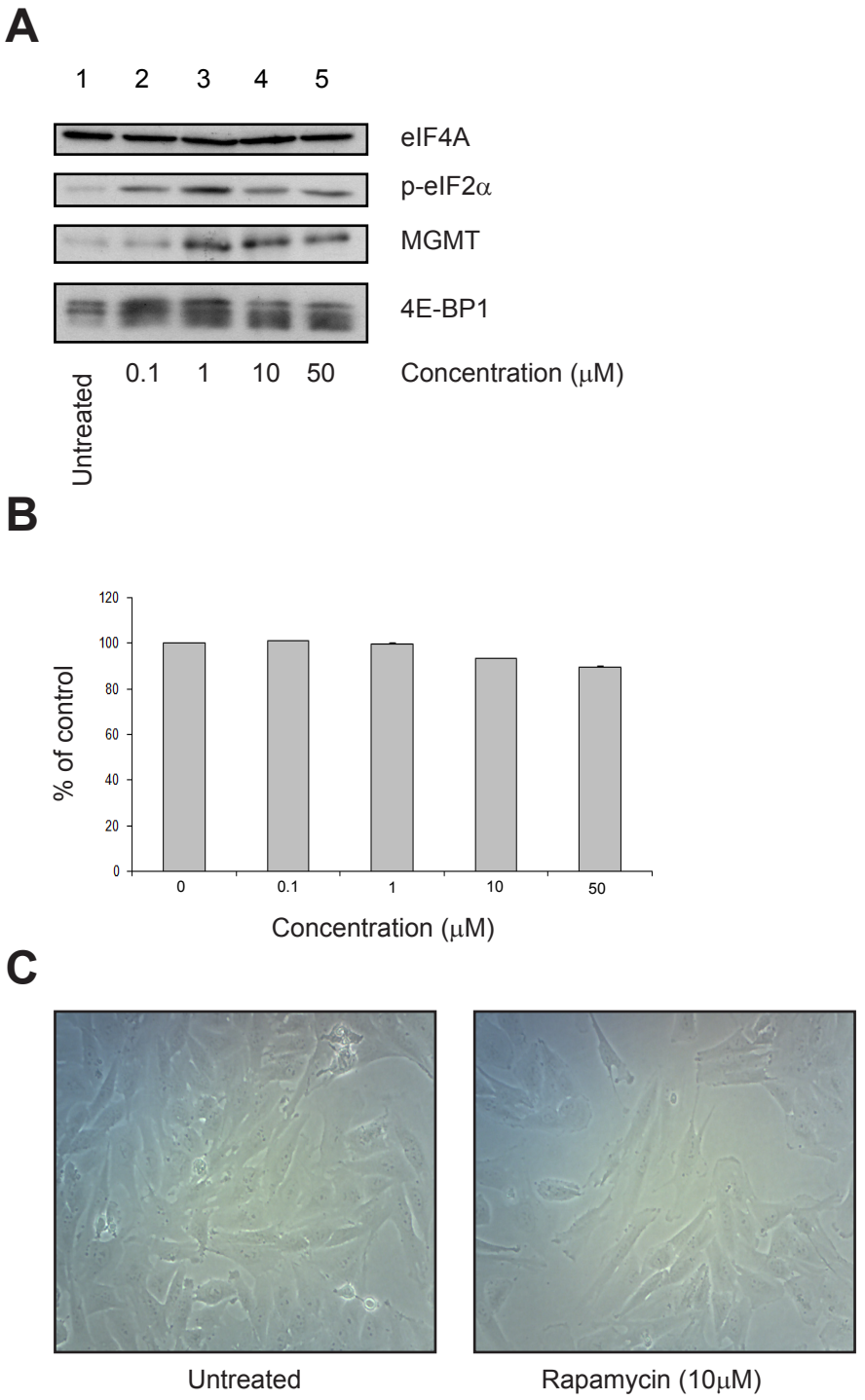

Figure 3.5 High concentrations of rapamycin prevent 4EBP1 phosphorylation without promoting cell death

Panel A. T98G cells were incubated for 24 hours in the absence (lane 1) or presence of differing concentrations of rapamycin (lanes 2-5). Extracts were prepared and aliquots containing 10μg of protein were resolved by SDS-PAGE and proteins visualised by Western blotting using the antiserum indicated (n=2) **Panel B.** T98G cells were treated as in **(A)** and cell viability was assessed using an MTS assay as described in Materials and Methods. Results are expressed relative to those obtained in untreated cells (set at 100%). Error bars are the S.D (n=3). **Panel C.** T98G cells were incubated for 24 hours in the absence or presence of 10 μM rapamycin. Cells were subjected to light microscopy using a Nikon eclipse T5100 and images captured with a Moticam 2000 camera.

untreated cells; incubation of cells with 10μM rapamycin inhibits cell growth over 24 hours.

3.3.4 LY294002 did not reduce MGMT levels in T98G cells

LY294002 is a highly selective PI3K inhibitor which also has the ability to directly inhibit mTOR when used at high concentrations [242]. To investigate the effect of LY294002 on steady state levels of MGMT, T98G cells were incubated with different concentrations of LY294002 for 24 hours. Figure 3.6A (lane 4 vs. lanes 1-3) shows that at concentrations above 10μM, there was a dephosphorylation of 4E-BP1, characteristic of an inhibition of mTOR signalling. Alongside this, MGMT protein levels were maintained up to levels of 10μM LY294002 (lane 2-4 vs. lane 1), then decrease with 50μM of LY294002 (lane 5 vs. lanes 2-4). As with cells incubated with rapamycin (Fig.3.5), the phosphorylation of eIF2α was also seen to increase in cells incubated with LY294002 (lanes 2-4 vs. lane 1). An MTS assay showed no increase in mitochondrial toxicity following incubation of cells with LY294002 (Fig.3.6B) but light microscopy (Fig.3.6C) shows that LY294002 inhibits cell proliferation.

3.3.5 PI103 does not increase steady state levels of MGMT and promotes apoptosis

PI103 is a kinase inhibitor that has been suggested to inhibit PI3K, mTOR and DNAPK [243,244]. In T98G cells treated with PI103 for 24 hours, only a high concentration of drug showed an inhibition of mTOR signalling, as characterised by dephosphorylation of 4E-BP1 (Fig.3.7, lane 5 vs. lanes 1). In contrast to rapamycin, there was no general increase in levels of MGMT with increasing drug concentrations. An MTS mitochondrial toxicity assay (Fig.3.7B) showed no significant inhibition of mitochondrial function with increasing concentrations of PI103 over 24 hours. However, analysis of cells by light microscopy suggests that high concentrations of PI103 inhibit cell growth; furthermore, blebbing can be seen in these cells suggesting that they are beginning to enter apoptosis (Fig.3.7C).

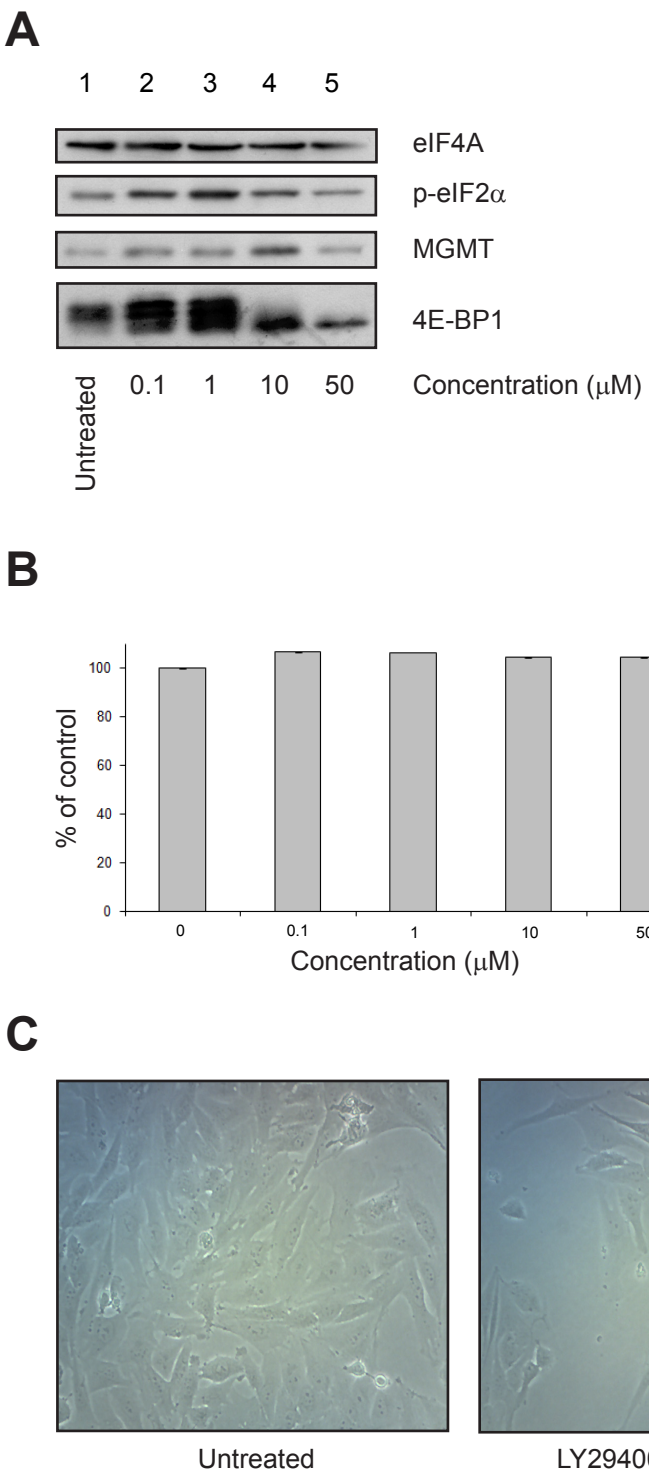

Figure 3.6 LY294002 inhibits mTOR signalling when used at high concentrations

Panel A. T98G cells were incubated for 24 hours in the absence (lane 1) or presence of differing concentrations of LY294002 (lanes 2-5). Extracts were prepared and aliquots containing 10 μg of protein were resolved by SDS-PAGE and proteins visualised by Western blotting using the antiserum indicated. (n=2) **Panel B.** T98G cells were treated as in **(A)** and cell viability was assessed using an MTS assay as described in Materials and Methods. Results are expressed relative to those obtained in untreated cells (set at 100%). Error bars are the S.D (n=3). **Panel C.** T98G cells were incubated for 24 hours in the absence or presence of 10 μM LY294002. Cells were subjected to light microscopy using a Nikon eclipse T5100 and images captured with a Moticam 2000 camera.

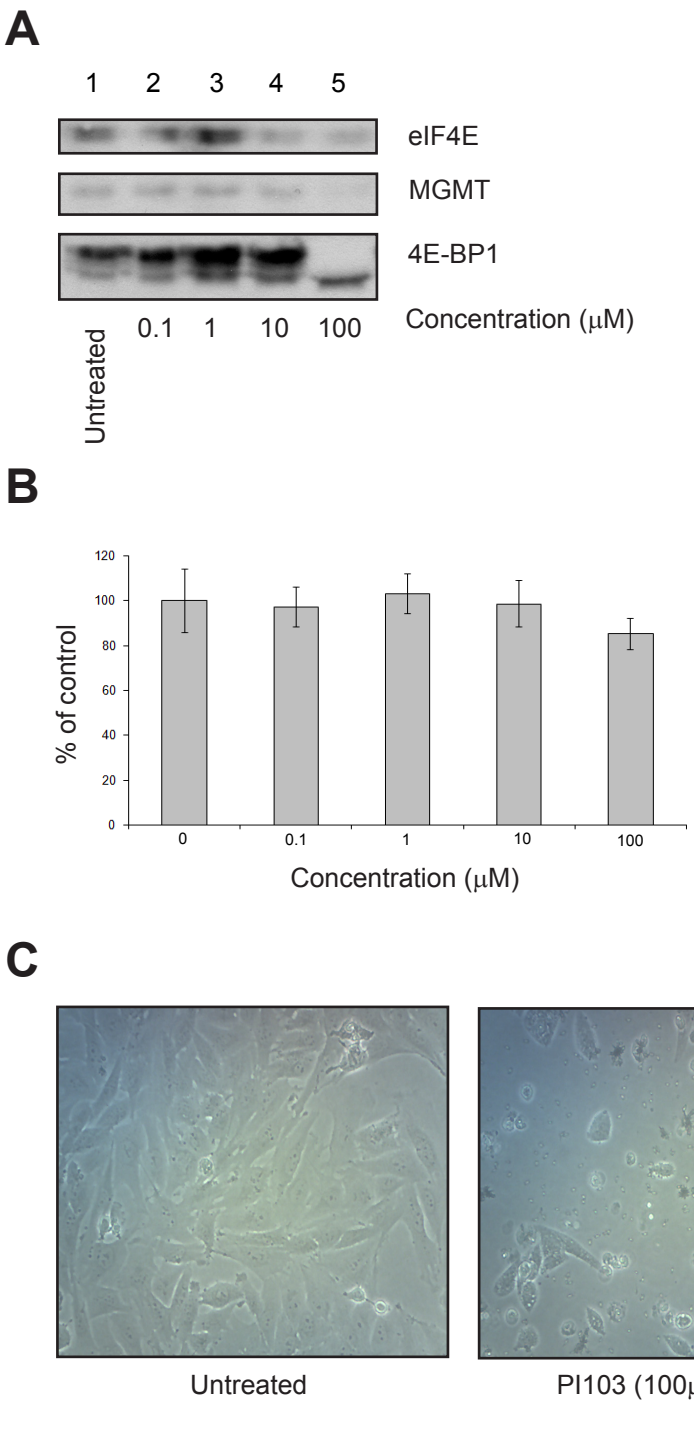

Figure 3.7 PI103 inhibits mTOR signalling at high concentrations but is cytotoxic

Panel A. T98G cells were incubated for 24 hours in the absence (lane 1) or presence of differing concentrations of PI103 (lanes 2-5). Extracts were prepared and aliquots containing 10 μg of protein were resolved by SDS-PAGE and proteins visualised by Western blotting using the antiserum indicated (n=1) **Panel B.** T98G cells were treated as in **(A)** and cell viability was assessed using an MTS assay as described in Materials and Methods. Results are expressed relative to those obtained in untreated cells (set at 100%). Error bars are the S.D (n=3). **Panel C.** T98G cells were incubated for 24 hours in the absence or presence of 100 μM PI103. Cells were subjected to light microscopy using a Nikon eclipse T5100 and images captured with a Moticam 2000 camera.

3.3.6 Torin 1 is an effective mTORC1/2 inhibitor in T98G cells

Torin 1 is a selective dual mTORC1/2 inhibitor which targets the active site of the mTOR kinase [245]. Over a 24 hour incubation period in T98G cells, at low concentrations, Torin 1 results in the dephosphorylation of 4E-BP1 (Fig.3.8, lanes 2-5 vs. Lane 1), indicating that incubation with the compound results in an inhibition of mTOR signalling. However, in contrast to rapamycin (Fig.3.5A) and LY294002 (Fig.3.6A), incubation of cells with Torin 1 did not result in an increase in steady state levels of MGMT, and actually showed a reduction in MGMT when treated with 0.5μM for 24 hours (Fig.3.8A). A cell viability assay using MTS alongside light microscopy showed a slight increase in mitochondrial toxicity in cells treated with Torin 1 compared to an untreated control and a moderate inhibition of cell proliferation (Figs. 3.8B and 3.8C, respectively).

3.3.7 The effect of rapamycin, LY294002, PI103 and Torin 1 on protein synthesis rates in T98G cells

The initial drugs tested here were either identified directly, or were closely related to those that were identified by connectivity mapping of TMZ resistant GBM samples. However, they had different effects on the steady state level of MGMT protein and mTOR signalling over a 24 hour incubation period with varying concentrations of the compounds. Therefore, in an attempt to correlate MGMT protein levels, mTOR signalling and translation, in parallel I measured the effect of these compounds on cell viability (Fig.3.9A) and the rate of protein synthesis (Fig.3.9B). I also investigated the effect of TMZ on protein synthesis rates under these assay conditions. At the concentrations of compounds used here, there was no significant decrease in cell viability under any condition (Fig.3.9A). In contrast, effects of the rate of protein synthesis varied dramatically. As shown in Figure 3.9B, treatment of cells with PI103 or TMZ had a moderate effect on protein synthesis rates. High concentrations of rapamycin resulted in a reduction in [^{35}S] methionine incorporation into protein but resulted in an increase in the steady state levels of MGMT. This is discussed in more

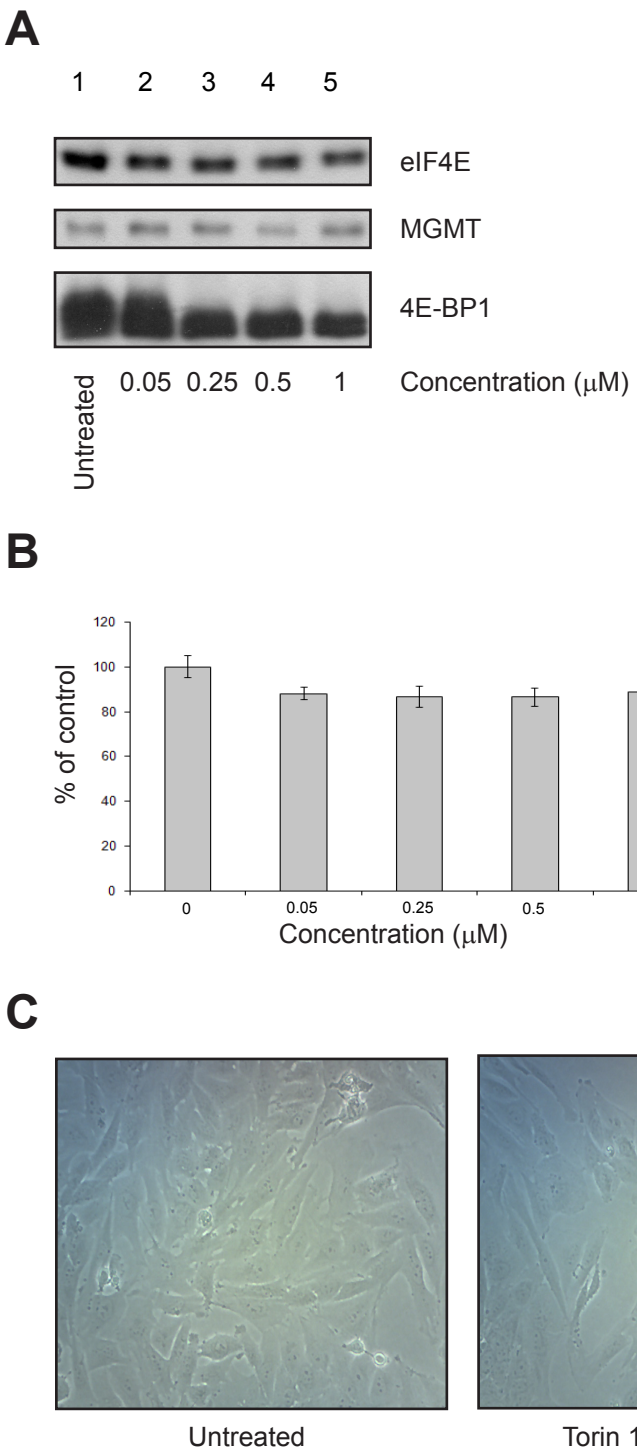

Figure 3.8 Torin 1 inhibits mTOR signalling and reduces MGMT levels

Panel A. T98G cells were incubated for 24 hours in the absence (lane 1) or presence of differing concentrations of Torin1 (lanes 2-5). Extracts were prepared and aliquots containing 10μg of protein were resolved by SDS-PAGE and proteins visualised by Western blotting using the antiserum indicated (n=2) **Panel B.** T98G cells were treated as in **(A)** and cell viability was assessed using an MTS assay as described in Materials and Methods. Results are expressed relative to those obtained in untreated cells (set at 100%). Error bars are the S.D (n=3). **Panel C.** T98G cells were incubated for 24 hours in the absence or presence of 0.5 μM Torin1. Cells were subjected to light microscopy using a Nikon eclipse T5100 and images captured with a Moticam 2000 camera.

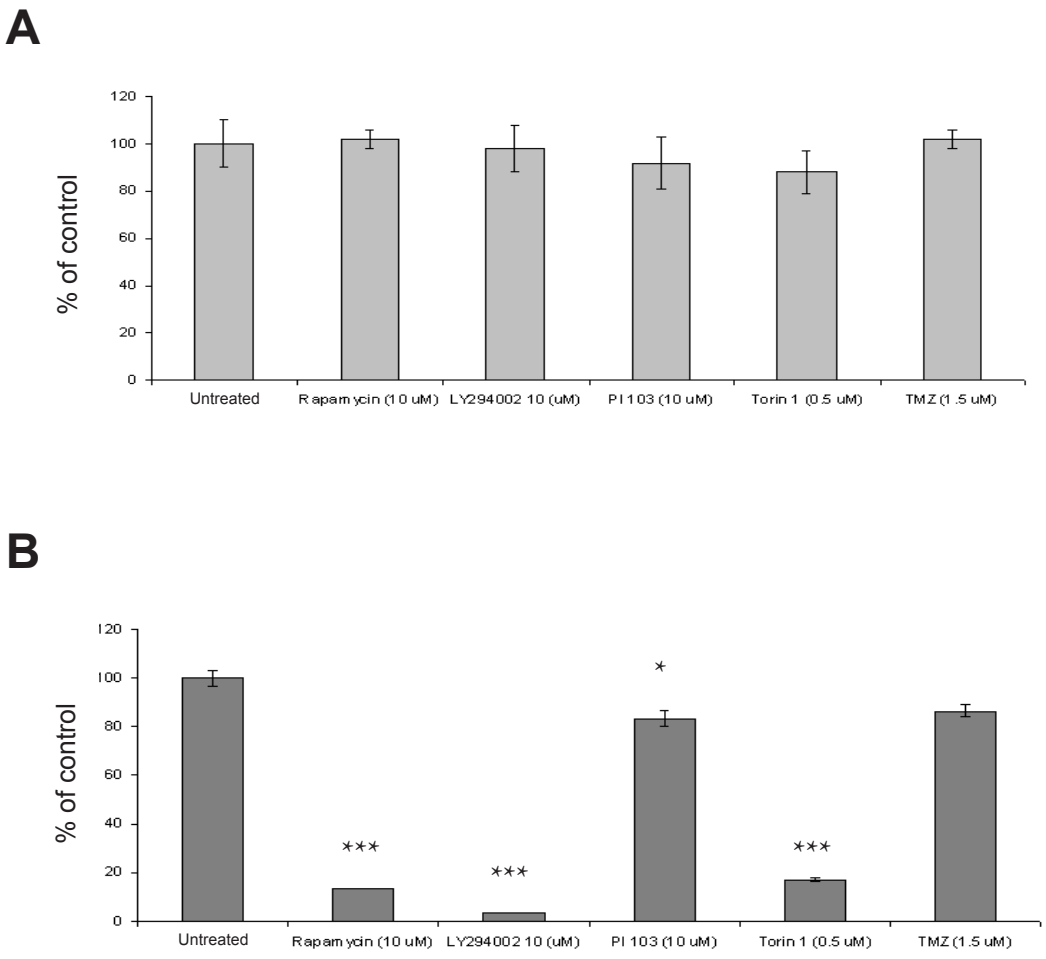

Figure 3.9 Effects of compounds on mitochondrial function and protein synthesis

Panel A. T98G cells were treated with the final concentrations of the drugs and incubated for 24 hours. Cell viability was assessed using an MTS assay as described in Materials and Methods. Results are expressed relative to those obtained in untreated cells (set at 100%). Error bars are the S.D (n=3). **Panel B.** T98G cells were treated as in **(A)** and one hour prior to harvesting, cells were incubated with 10μCi/ml [^{35S}] methionine, as described in Materials and Methods. Cells were harvested, extracts were prepared and incorporation of radioactive methionine into protein determined as cpm/μg protein; results are presented as a % of the rate obtained in cells incubated in the absence of drugs. Error bars are the S.D (n=3). A standard T Test was performed and p values were assigned limits where * <0.05, **<0.005, ***<0.001.

detail later in the thesis. However, as previous studies showed little effect on 4E-BP1 phosphorylation status (Fig.3.5A) and could reflect the phosphorylation of eIF2α.

Incubation of cells with LY294002 promoted a dephosphorylation of 4E-BP1 and a severe inhibition of protein synthesis rates; however, it did not reduce MGMT protein levels at most concentrations and was therefore not carried forward in this study. The mTOR inhibitor, Torin 1, did show some promising results, with low toxicity and mTOR inhibition. However, due to availability issues, it was replaced with commercially available, KU0063794, which is a very similar dual mTORC1/2 inhibitor.

3.4 Summary

- Torin 1 was the only compound screened that reduced MGMT protein levels over a 24 hour treatment.
- LY294002 was the only compound screened that was directly identified using connectivity mapping and it did not reduce MGMT protein levels over 24 hours.
- None of the compounds screened were cytotoxic at low levels.

3.5 Conclusions

The initial experiments carried out to screen compounds abilities to reduce MGMT levels in T98G cells produced some interesting findings. Firstly, rapamycin treatment of cells was shown to increase MGMT protein levels in a dose dependent manner, yet while reducing protein synthesismost probably through inhibition of cap dependent translation. Secondly, although LY294002 did not reduce MGMT protein levels when used alone, it did reduce protein synthesis rates, and did not increase levels of MGMT protein, making it a possible therapeutic candidate for using in addition to another compound. Thirdly, a dual mTOR inhibitor, Torin 1, did reduce levels of MGMT protein at certain concentrations, making it an attractive compound for further research.

Chapter IV

Using custom gene signatures and chemical compounds to identify mTOR signalling inhibitors

4 *Using custom gene signatures and chemical compounds to identify mTOR signalling inhibitors*

4.1 Aims

- To identify compounds that will reduce MGMT protein levels
- To use connectivity mapping with known compounds and custom gene signatures to identify these compounds
- To ensure the compounds are not cytotoxic to cells

4.2 Introduction

During the previous chapter I showed that rapamycin and LY294002 both reduced protein synthesis rates in T98G glioblastoma cells. I also showed that a dual mTOR inhibitor reduced levels of MGMT protein in T98G cells. Because of this, I used connectivity mapping to mine for compounds that are known to inhibit PI3K and mTOR, whilst avoiding the possible cytotoxicity faced if multiple compounds were administered concomitantly.

In addition to the connectivity mapping experiments that were used to identify compounds that gave similar outputs to LY294002, rapamycin and the custom gene list, I also wanted to search for other possible direct dual mTORC1/2 inhibitors, and explore if any of the compounds found in the previous searches were produced in response to an mTORC1/2 inhibitor query. Furthermore, as many of the compounds produced in the connectivity mapping were AMPK activators (which generally cause little cytotoxicity); I also wanted to query the database for compounds that showed positive connections to other AMPK activators.

It was important at this stage to discontinue using drugs that were cytotoxic to the cells when used alone, as the purpose of the chosen compounds was to sensitise the cells to current treatments (i.e. TMZ chemotherapy and radiotherapy) by down-regulating levels of MGMT protein, which in the short term, should not be cytotoxic to cells.

4.3 Results

4.3.1 Using custom gene signatures, rapamycin and LY294002 to identify novel functions of compounds

Table 4.1 lists the custom gene changes I used to mine for compounds and Tables 4.2 and 4.3 show which gene changes were induced by treatment of cells with rapamycin and LY294002 respectively. I chose the 17 genes in the custom gene list as they either directly affect MGMT expression or PI3K/mTOR signalling. I also wanted to see if a gene expression profile that had changes in these specific genes would identify similar compounds to the rapamycin and LY294002 queries, as well as the TMZ resistant GBM patient samples. These gene changes define the compounds and were the “signatures” I used to search the database. Although the search generated 50 compounds as a result of the query search, I only focused on those that had a known effect on the mTOR signalling pathway, as these were of primary interest for my project because this pathway is commonly upregulated in GBM cells. The full list of compounds produced can be found in the Appendix. As shown in the Venn diagram (Fig.4.1), the only compounds that produced positive connections to all query profiles (rapamycin, LY294002 and the custom gene list containing 17 genes) were DAPH, beta escin (both of which are tyrosine kinase receptor inhibitors [246,247]) and resveratrol, which has been suggested as an AMPK activator [248]. I also screened thalidomide and thioridazine for potential benefits as they were both identified by the connectivity mapping, and I found thalidomide in particular to be of interest as it is a known angiogenesis inhibitor and is also being currently used for chemotherapy.

4.3.2 Connectivity mapping using KU0063794 and A769662

To do this I created my own microarray gene signatures (as described in the Materials and Methods), by treating MCF7 cells with 10μM KU0063794 or 20μM A769662 for 6 hours. I then used these gene expression profiles for connectivity mapping (Fig.4.2). Interestingly, the resulting connections did contain compounds that had been identified both in the connectivity mapping

Table 4.1 Custom gene list

The connectivity mapping database was queried using a custom gene expression profile. The genes were chosen either because they are known to be mutated in GBM and/or because they influence cap dependant translation.

Gene name	Fold change
MGMT	-1
PIK3CA	-1
EIF4G1	-1
EIF4G2	-1
EIF4G3	-1
EIF4E	-1
EIF4A1	-1
EIF4A2	-1
EIF4A3	-1
EIF4B	-1
EIF4EBP1	1
FRAP1	-1
AKT1	1
MAPK1	-1
PTEN	-1
TSC1	1
TSC2	1

Table 4.2 Top 30 most changed genes in MCF7 cells treated with rapamycin

The top 30 genes that had the highest fold change in MCF7 cells treated with 0.1μM rapamycin for 6 hours compared to untreated MCF7 cells.

Gene name	Fold change
TXNIP	11887.6
IFRD1	-11689.96
JMJD6	-11454.92
EIF5	-11388.88
HBP1	11138.44
CCDC86	-10891.68
KLHL24	10715.28
RGS16	-10681.84
CCDC28A	10633.48
CCNG2	10628.68
RRS1	-10525.48
NOL1	-10521.4
GPRC5A	10429.8
ARPC5L	-10370.72
HSPC111	-10293.8
UTP18	-10280.68
HSPH1	-10092.72
DNAJA1	-9909.68
MAK16	-9786.32
CABC1	9772.68
PIGV	9757.84
DDX21	-9756.44
BNIP3L	9749
YPEL5	9582.16
MRPS12	-9474.08
TARS	-9453.56
PUS1	-9410.16
BYSL	-9398.24
LOC100133166	9391.44

Table 4.3 Top 30 most changed genes in MCF7 cells treated with LY294002

The top 30 genes that had the highest fold change in MCF7 cells treated with 10μM LY294002 for 6 hours compared to untreated MCF7 cells.

Gene name	Fold change
TXNIP	12820.46154
CCNG2	12794.19231
HIST1H3H	12667.19231
DNAJA1	-12646.34615
HBP1	12631.42308
HIST1H2BC	12545.07692
CCDC86	-12503.84615
SFN	-12454.69231
BTG1	12416.34615
HSPH1	-12379.57692
RRS1	-12374.61538
PHLDA2	-12362.65385
PPIF	-12356.84615
RRP15	-12356.15385
UTP18	-12300.26923
TCF3	-12269
CTPS	-12241.84615
CCDC28A	12233.07692
HIST2H2BE	12232.76923
IFRD1	-12231.5
JMJD6	-12224.19231
HIST1H2BD	12190.61538
HIST1H2AC	12167.69231
IER3	-12136
FARSA	-12082.84615
DNAJB1	-12053.73077
EIF5	-12037.03846
MARS	-11881.69231
HSPA1A	-11879.80769

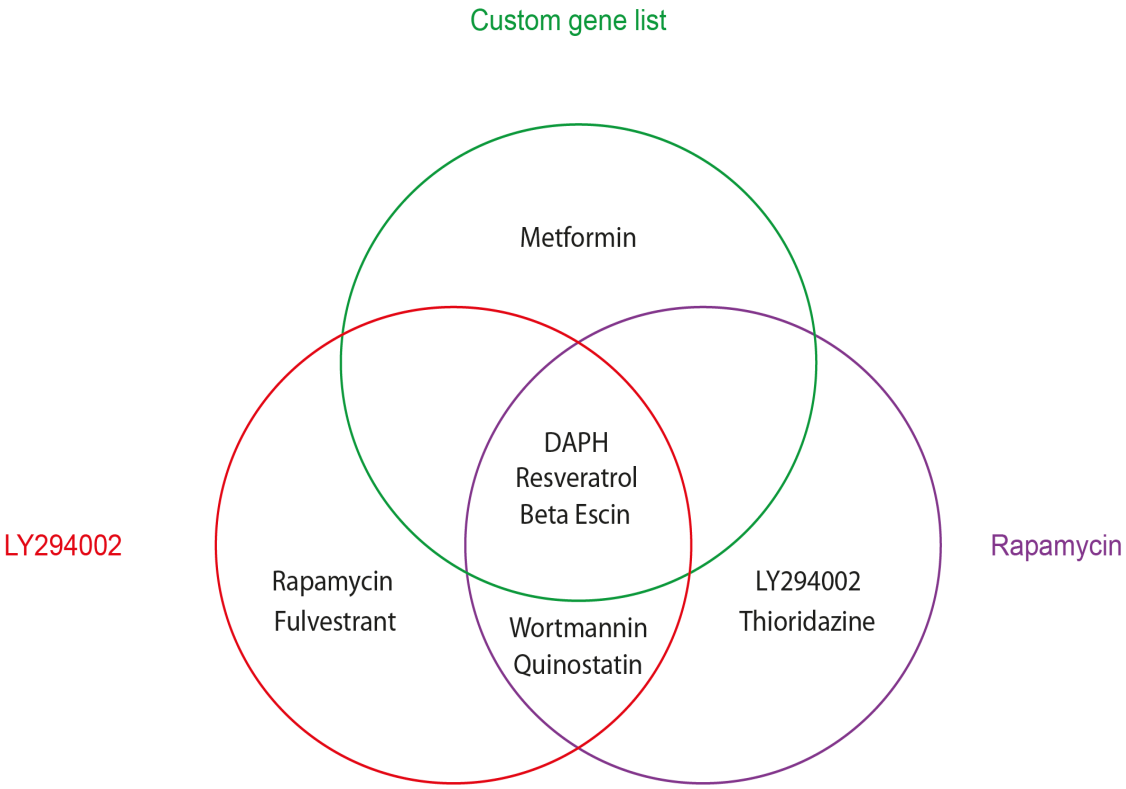

Figure 4.1 Candidate drugs derived from connectivity mapping

The cMap build 2 reference database was searched for chemicals that had a positive correlation with gene signatures obtained from microarray data of MCF7 cells treated for 6 hours with 10μM LY294002 or 0.1μM rapamycin. The top 30 genes in each treatment that had the highest fold change compared to an untreated control were used to define the query gene signatures. The database was also used to search for gene changes that showed a positive correlation with a custom generated gene list (Table 4.1). The Venn diagram shows which chemicals were derived from which searches in the database and indicates where similar results were found.

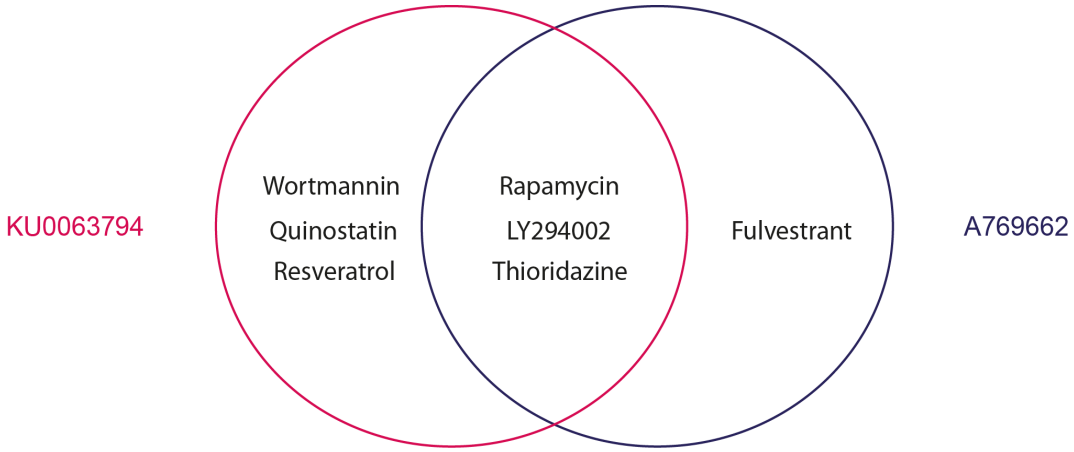

Figure 4.2 Connectivity mapping results derived from 'in house' KU0063794 and A769662 treatment of cells

MCF7 cells were incubated with 10μM KU0063794 or 20μM A769662 for 6 hours. A genome-wide mRNA microarray analysis was performed on treated and untreated cells using the Illumina platform, as described. The top 30 genes in each treatment that had the highest fold change compared to those observed from untreated cells were identified and used to define the query gene signatures for each chemical (see appendix). The cMap build 2 database was searched for other chemicals that showed a positive correlation to gene signatures obtained with KU0063794 and A769662 (see appendix for full list). The Venn diagram shows matched chemicals that have been suggested to also affect the PI3K/mTOR pathway.

experiment using rapamycin, LY294002 and the custom gene signature, and the connectivity mapping performed on the human TMZ-resistant GBM patient samples. It was also drawn to my attention that many of the compounds with high connections to the query gene signatures in these connectivity mapping experiments displayed inhibitory effects on neurotransmitter transduction and many were also antihistamines in the piperazine family of chemicals. However, these compounds were not carried forward as they have no known connection to mTOR signalling. Table 4.4 summarises the compounds that were identified through connectivity mapping; these data also show which query gene signature produced that result, and what the known properties of the compounds are (see Appendix for more details).

4.3.3 Resveratrol does not significantly affect mTOR signalling, but does affect cell cycle progression

Resveratrol is a phytoestrogen [249] that is found in low levels in foods, such as red grape skins and Japanese knotweed roots. Resveratrol was initially trialled at multiple concentrations to ascertain whether it was cytotoxic to T98G cells. Cells were incubated for 24 hours and cell viability monitored by MTS assay. As shown in Figure 4.3A, even at high concentrations mitochondrial function assays showed no toxicity to resveratrol. As resveratrol has been suggested to activate AMPK, I monitored mTOR signalling as a read-out for the activation of AMPK [248]. Cells were incubated with 25μM resveratrol over a period of 72 hours, cell extracts were prepared, and Western blotting was carried out (Fig.4.3B). These data show that resveratrol did not affect the phosphorylation status of 4E-BP1 (lanes 2-5 vs. lane 1); suggesting that under these conditions, in T98G cells, resveratrol did not activate AMPK. Resveratrol did not affect the steady state level of MGMT protein, did not promote the phosphorylation of eIF2α or increase the phosphorylation of AMPK at Thr172 (data not shown). Figure 4.3C shows that similar results were obtained when cells were incubated with resveratrol in the absence or presence of TMZ.

A

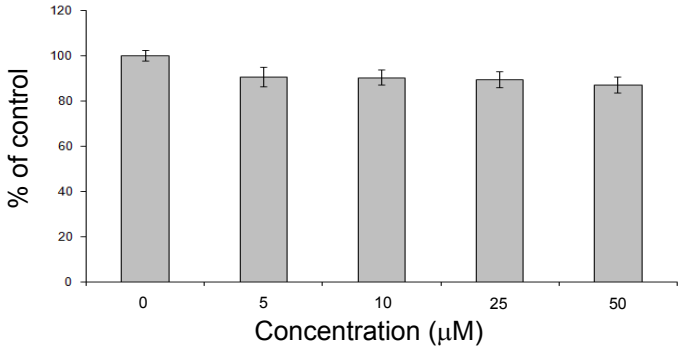

B

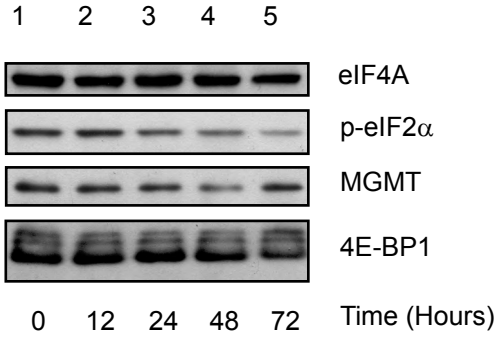

C

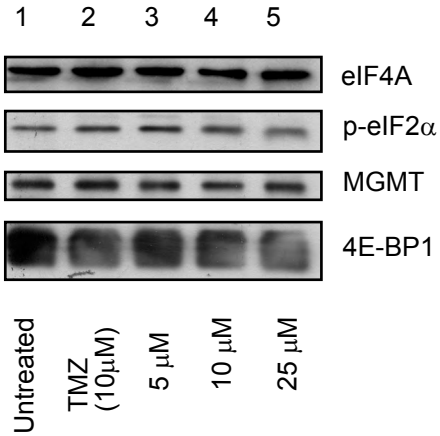

Figure continues on the next page

D

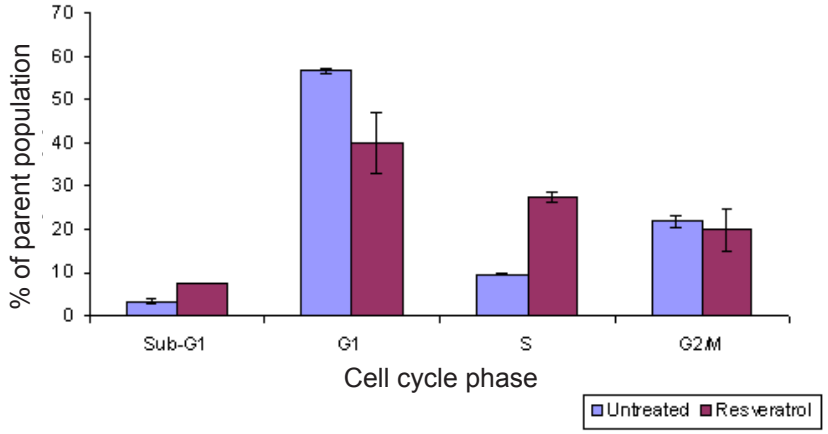

Figure 4.3 Resveratrol does not inhibit mTOR, but does affect cell cycle progression

Panel A. T98G cells were incubated with different concentrations of resveratrol for 24 hours and A cell viability was assessed using an MTS assay as described in Materials and Methods. Values are expressed relative to that obtained in untreated cells (set at 100%). **Panel B.** Cells were incubated in the presence of 25μM of resveratrol for 0-72 hours (lanes 1-5). Extracts were prepared and aliquots containing 10μg of protein were resolved by SDS-PAGE and proteins visualised by Western blotting using the antiserum indicated (n=2). **Panel C.** Cells were incubated in the absence (lane 1) or presence (lanes 2-5) of 10μM TMZ for 24 hours with different concentrations of resveratrol (lanes 3-5). Extracts were prepared and aliquots containing 10μg of protein were resolved by SDS-PAGE and proteins visualised by Western blotting using the antiserum indicated (n=2). **Panel D.** Cells were treated with 25μM of resveratrol for 24 hours and then harvested for FACS analysis, as described in Materials and Methods. Error bars are the S.D (n=3).

To determine if resveratrol had any effect on cell cycle progression in T98G cells, cultures were incubated with resveratrol for 24 hours and the cells were processed for FACS analysis (Fig.4.3D). Following incubation with resveratrol for 24 hours, there was a 20% increase in cells in S phase, and a small decrease in cells in G1 phase and little increase in cells with sub-G1 DNA content. S phase cell cycle arrest with high concentrations (300μM) of resveratrol has also been seen in other cancer cell lines [250]. However, under such conditions, there was an increase the cytotoxicity of the drug, reflected in an increased number of cells with sub-G1 DNA content. As resveratrol showed no effect on mTOR signalling or on MGMT protein levels, the compound was not considered further here.

4.3.4 Beta escin is cytotoxic to T98G cells, even at low concentrations

Beta escin is composed of a mixture of triterpenoid saponins and is found in the seeds of the horse chestnut plant (*Aesculus hippocastanum*). Beta escin has been implicated as a receptor tyrosine kinase (RTK) inhibitor [247], and was therefore investigated for its effect on mTOR signalling. As described above, cells were incubated for 24 hours with different concentrations of compound and cell viability monitored by MTS assay. As shown in Figure 4.4A, even at concentrations below 5μM, beta escin was cytotoxic; increased concentrations of beta escin resulted in 70% cell death at 20μM levels. Cells were incubated with 1μM beta escin over a period of 72 hours, cell extracts were prepared, and Western blotting was carried out. As shown in Figure 4.4B, beta escin had little effect on the phosphorylation of 4E-BP1, eIF2α or the steady state levels of MGMT. Mitochondrial toxicity assays carried out in parallel (Fig.4.4C) indicated that the cells were no longer viable after 72 hours of treatment with 1μM of beta escin. Consequently, as the cytotoxicity of beta escin was deemed to be too great, this compound was not used in further work described here.

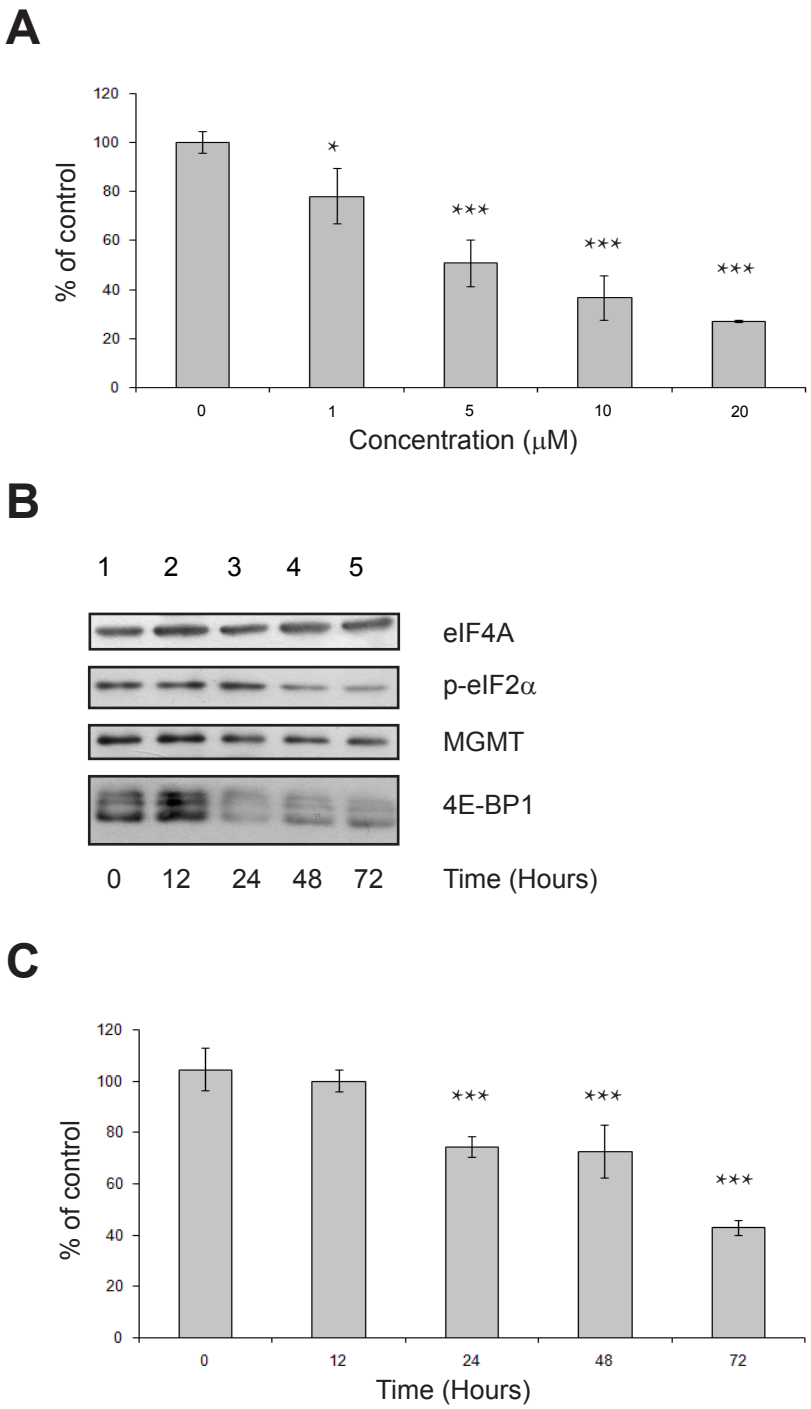

Figure 4.4 Beta escin is cytotoxic to T98G cells

Panel A. T98G cells were treated with different concentrations of Beta escin for 24 hours and cell viability was assessed using an MTS assay as described in Materials and Methods. Values are expressed relative to those obtained in untreated cells (set at 100%). A standard TTest was performed and p values were assigned limits where *<0.05, **<0.005 and ***<0.001. **Panel B.** Cells were incubated in the presence of 1μM of Beta Escin for 0-72 hours (lanes 1-5). Extracts were prepared and aliquots containing 10 μg of protein were resolved by SDS-PAGE and proteins visualised by Western blotting using the antiserum indicated (n=3). **Panel C.** Cells were treated as in Panel B and cell viability was assessed using an MTS assay as described in Materials and Methods. Cell viability is expressed relative to those obtained in untreated cells (set at 100%). A standard TTest was performed and p values were assigned limits where *<0.05, *<0.005 and ***<0.001.

4.3.5 A769662 treatment of cells promotes protein synthesis and the hyperphosphorylation of 4E-BP1

A769662, (6,7-Dihydro-4-hydroxy-3-(2'-hydroxy[1,1'-biphenyl]-4-yl)-6-oxo-thieno[2,3-*b*]pyridine-5-carbonitrile), is known to be a potent activator of AMPK, reflecting its ability to allosterically bind AMPK and prevent dephosphorylation of the kinase [251]. The compound was not derived directly from the connectivity mapping study; however, as many of the chemicals that produced strong connections to PI3K/mTOR inhibitors also displayed activity towards AMPK, a direct AMPK activator was chosen to investigate this relationship in glioblastoma cells. Cells were incubated for 24 hours and cell viability monitored by MTS assay. As shown in Figure 4.5A, at concentrations up to 20μM, A769662 was not toxic. However, a 10% decrease (Student's t-test, $p<0.05$) in mitochondrial toxicity was seen in cells treated with 50μM A769662 compared to an untreated control, this might reflect the high level of DMSO present in the cultures when A769662 was used at a high concentration. To look at the effect of A769662 on PI3K/mTOR signalling, cells were incubated for different times in the presence of 20μM A769662, extracts prepared and the phosphorylation of 4E-BP1 monitored by Western blotting. Figure 4.5B shows that A769662 had little effect on the phosphorylation status of 4E-BP1, even over 72 hours, indicating that it is not affect mTORC1 signalling in T98G cells under these conditions. Levels of phosphorylated eIF2α did not increase over 48 hours and may have decreased at 72 hours incubation with A769662. However, a reduction in the steady state levels of MGMT protein was observed as the incubation time increased (Panel B, lanes 2-4 vs. lane 1), suggesting that A769662 warranted further investigation.

As with described above, these assays were repeated with different final concentration of A769662, in the absence or presence of 10μM TMZ. Cells were incubated for 24 hours and 4E-BP1 phosphorylation, eIF2α phosphorylation and steady state levels of MGMT protein levels monitored by Western blotting. As shown in Figure 4.5C, in contrast to A769662 or TMZ alone (lanes 1 and 2,

A

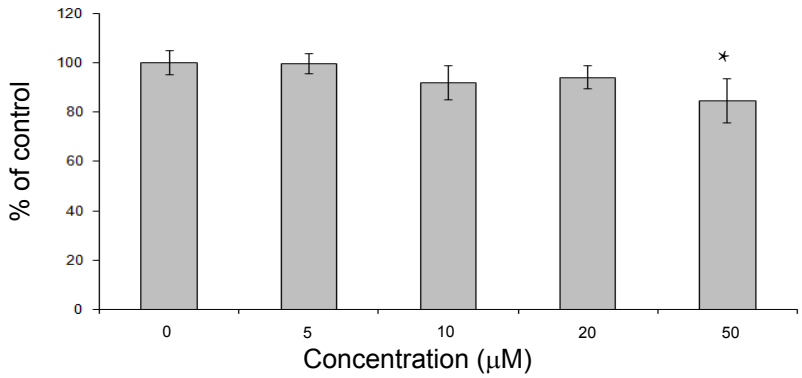

B

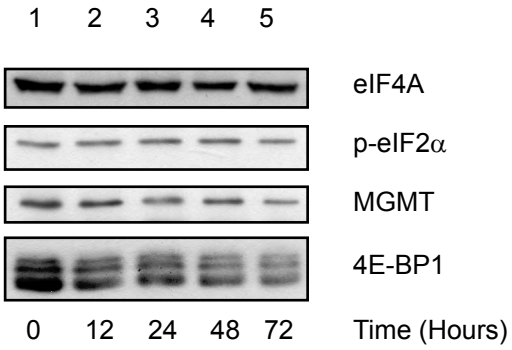

C

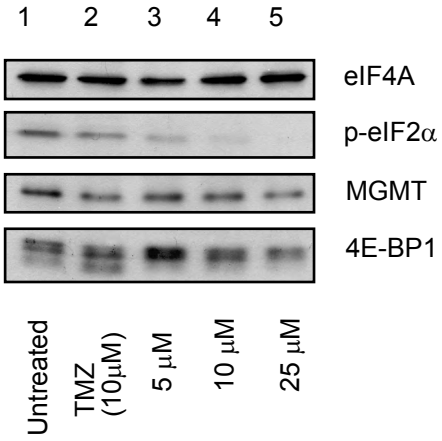

Figure continues on the next page

D

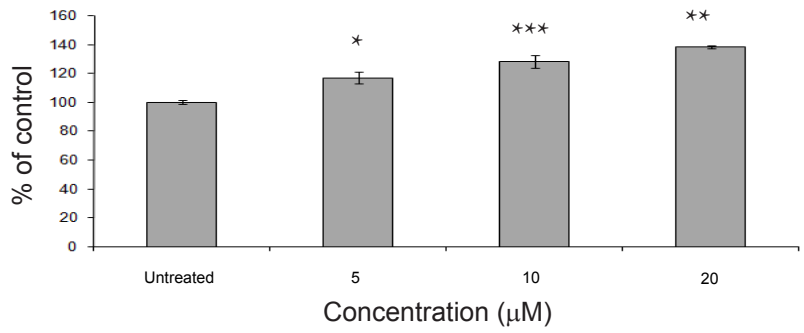

Figure 4.5 Incubation of cells with A769662 leads to hyperphosphorylation of 4EBP1 when combined with TMZ

Panel A. T98G cells were treated with different concentrations of A769662 for 24 hours and cell viability was assessed using an MTS assay as described in Materials and Methods. Values are expressed relative to those obtained in untreated cells (set at 100%). A standard TTest was performed and p values were assigned limits where *<0.05, **<0.005 and ***<0.001. **Panel B.** Cells were incubated in the presence of 20μM A769662 for 0-72 hours (lanes 1-5). Extracts were prepared and aliquots containing 10μg of protein were resolved by SDS-PAGE and proteins visualised by Western blotting using the antiserum indicated (n=3). **Panel C.** Cells were incubated in the absence (lane 1) or presence of 10μM TMZ (lanes 2-5), in combination with different concentrations of A769662 (lanes 3-5) for 24 hours. Extracts were prepared and aliquots containing 10μg of protein were resolved by SDS-PAGE and proteins visualised by Western blotting using the antiserum indicated (n=3). **Panel D.** Cells were incubated with 10μM TMZ, combined with different concentrations of A769662 and one hour prior to harvesting, cells were incubated with 10μCi/ml [^{35S}] methionine, as described in Materials and Methods. Extracts were prepared and incorporation of radioactive methionine into protein determined as cpm/μg protein; results are presented as a % of the rate obtained in cells incubated in the absence of A769662 and TMZ. Error bars are the S.D (n=3). A standard TTest was performed and p values were assigned limits where *<0.05, **<0.005 and ***<0.001.

respectively), 25μM A769662 combined with 10μM TMZ (lane 5) did not result in a change in MGMT protein levels but did cause the hyperphosphorylation of 4E-BP1, and decreased levels of eIF2α phosphorylation. To complement this, I also measured the rate of protein synthesis in the cells. Figure 4.5D shows that incubation of T98G cells with increasing concentrations of A769662 actually stimulated translation. The reasons for this are unclear but might reflect the finding that levels of eIF2α phosphorylation decreased and the hyperphosphorylation of 4E-BP1 was maintained under these conditions (Fig.4.5B).

4.3.6 Incubation of cells with DAPH leads to dephosphorylation of 4E-BP1 and reduced rates of protein synthesis

DAPH (4,5-dianilinophthalimide) is a selective EGFR inhibitor, that also inhibits α and β fibril formation associated with Alzheimer's disease [246]. RTK inhibitors can often be cytotoxic due to the broad range of RTKs that they can affect. To assess the cytotoxicity of DAPH in T98G cells, a cell viability assay was carried out using increasing final concentrations of DAPH over 24 hours. The data shown in Figure 4.6A indicates that at the concentrations employed here, DAPH did not cause a loss of cell viability. To ascertain the effect of DAPH on PI3K/mTOR signalling, cells were incubated with 5μM of DAPH for 24 hours, extracts prepared and the phosphorylation of 4E-BP1 monitored by Western blotting (Fig.4.6B). These data show that there was a clear dephosphorylation of 4E-BP1 between 48-72 hours (lanes 4 and 5), as visualised by the increased mobility of 4E-BP1 on SDS-PAGE, indicating that mTORC1 was inhibited. Up to 24 hours, there appeared to be an increase in both MGMT protein levels and eIF2α phosphorylation (lanes 2-3 vs. lane 1), but levels of both decreased at 48 and 72 hours (lanes 4-5 vs. lane 3). When cells were incubated with both DAPH and TMZ (Fig.4.6C), the steady state level of MGMT protein was not reduced, and levels of eIF2α phosphorylation also was not affected (lanes 4-5 vs. lanes 1 and 2). Surprisingly, in contrast to DAPH alone (B), under these conditions the

A

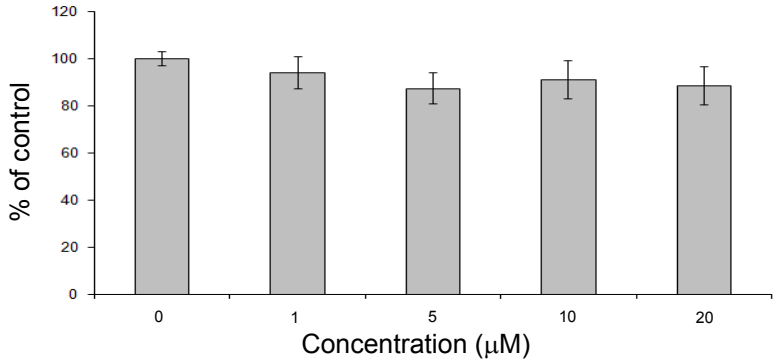

B

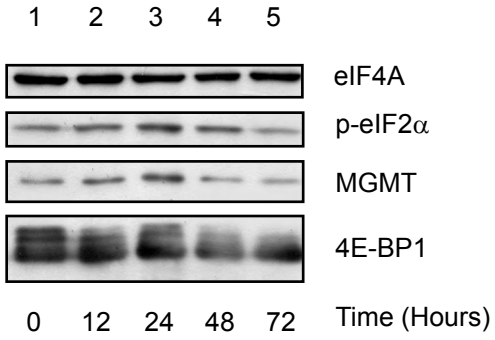

C

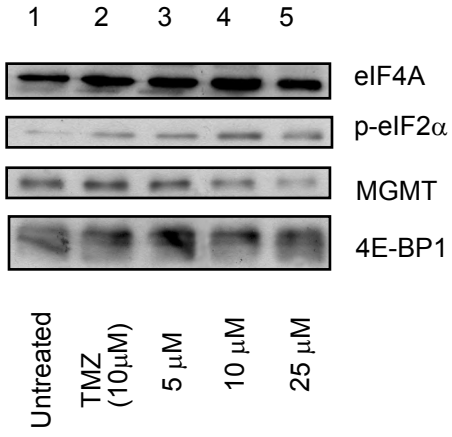

Figure continues on the next page

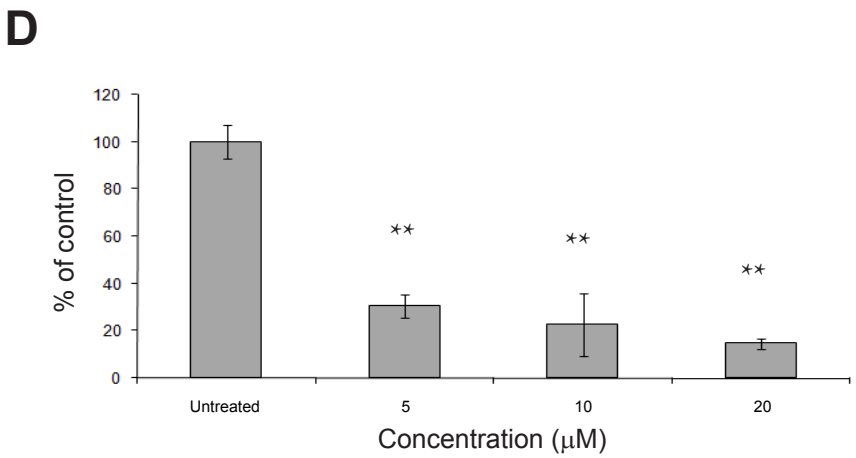

Figure 4.6 Incubation of T98G cells with DAPH leads to dephosphorylation of 4EBP1 when used alone, but not when used in combination with TMZ

Panel A. T98G cells were treated with different concentrations of DAPH for 24 hours and cell viability was assessed using an MTS assay as described in Materials and Methods. Values are expressed relative to those obtained in untreated cells (set at 100%). A standard TTest was performed and p values were assigned limits where *<0.05, **<0.005 and ***<0.001. **Panel B.** Cells were incubated in the presence of 5μM of DAPH for 0-72 hours (lanes 1-5). Extracts were prepared and aliquots containing 10μg of protein were resolved by SDS-PAGE and proteins visualised by Western blotting using the antiserum indicated (n=3). **Panel C.** Cells were incubated in the absence (lane 1) or presence of 10μM TMZ (lanes 2-5), in combination with different concentrations of DAPH (lanes 3-5) for 24 hours. Extracts were prepared and aliquots containing 10μg of protein were resolved by SDS-PAGE and proteins visualised by Western blotting using the antiserum indicated (n=3). **Panel D.**Cells were incubated in 10μM TMZ combined with different concentrations of DAPH and one hour prior to harvesting, cells were incubated with 10μCi/ml [^{35S}] methionine, as described in Materials and Methods. Extracts were prepared and incorporation of radioactive methionine into protein determined as cpm/μg protein; results are presented as a % of the rate obtained in cells incubated in the absence of DAPH and TMZ. Error bars are the S.D (n=3). A standard TTest was performed and p values were assigned limits where *<0.05, **<0.005 and ***<0.001

level of 4E-BP1 phosphorylation did not decrease, suggesting that mTORC1 signalling was unaffected here. Incubation of T98G cells with DAPH resulted in an inhibition of protein synthesis (Fig.4.6C), even at the lowest concentrations tested. As this could not be directly ascribed to either changes in 4E-BP1 phosphorylation or eIF2α phosphorylation, the reason for this inhibition is unclear.

4.3.7 KU0063794 selectively inhibits mTOR and is not cytotoxic to cells

KU0063794 is a small molecule kinase inhibitor, which inhibits both mTOR complexes (mTORC1/mTORC2) whilst displaying a reduced activity towards other kinases [252]. Its specificity is very similar to Torin 1, the mTOR inhibitor used in earlier experiments. Cell viability assays (Fig.4.7A) indicated that, over a period of 24 hours, KU0063794 was only cytotoxic to cells when used at concentrations greater than 20μM. This was demonstrated by a 20% decrease (Student's t-test, $p<0.05$) in dye produced compared to the untreated control. Western blotting analysis confirmed that over 72 hours, incubation of cells with 10μM KU0063794 promoted the dephosphorylation of 4E-BP1, reduced levels of eIF2α phosphorylation and yet maintained MGMT protein levels (Fig.4.7B). These data are consistent with KU0063794 being an effective inhibitor of mTOR signalling.

4.3.8 Thalidomide does not have a significant effect on T98G cell signalling or cell viability

The next compound used in the initial screening programme shown here, and suggested by the connectivity mapping study, was thalidomide. Thalidomide is famously known as a teratogen. It is now known to also display anti-inflammatory and anti-proliferative effects, as well as inhibiting TNF-α synthesis [253], but currently has no known activity towards the PI3K/mTOR pathway. Its current use as a treatment of multiple myeloma [254] prompted me to include it in my initial screening of compounds which might alter the steady state level of MGMT protein in T98G cells. Unfortunately, as well as showing no cytotoxic

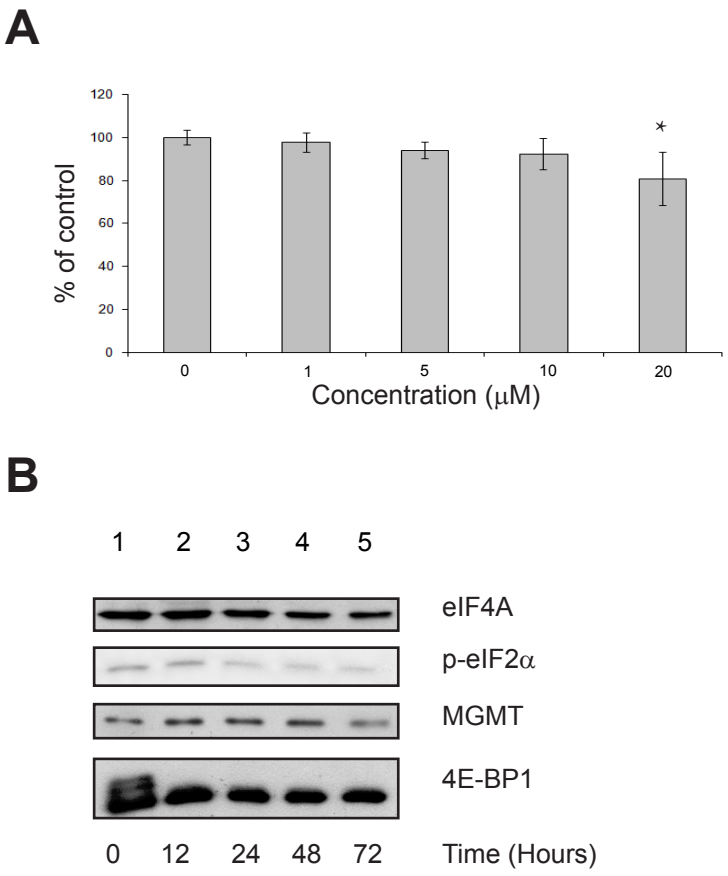

Figure 4.7 KU0063794 inhibits mTOR signalling and is not cytotoxic to the cells

Panel A. T98G cells were treated with different concentrations of KU0063794 for 24 hours and cell viability was assessed using an MTS assay as described in Materials and Methods. Cell viability is expressed relative to that obtained in untreated cells (set at 100%). A standard TTest was performed and p values were assigned limits where *<0.05, **<0.005 and ***<0.001. **Panel B.** Cells were incubated in the presence of 10μM of KU0063794 for 0-72 hours (lanes 1-5). Extracts were prepared and aliquots containing 10μg of protein were resolved by SDS-PAGE and proteins visualised by Western blotting using the antiserum indicated (n=3).

effects on these cells (Fig.4.8A), it did not show any significant effect on MGMT protein levels, 4E-BP1 phosphorylation or eIF2α phosphorylation (Fig.4.8B). A similar lack of effect was seen even when the compound was used in the presence of TMZ (C). Consequently, I decided not to use this compound in any further studies reported here.

4.3.9 Thioridazine inhibits protein synthesis when used in conjunction with TMZ

The final compound that I used as part of this preliminary screening process was thioridazine, a dopamine receptor antagonist that belongs to the family of drugs known as the phenothiazines. It has been widely used to treat psychotic disorders such as schizophrenia and psychosis [255];however, it has more recently been considered as a possible cancer therapeutic as it has been shown to induce apoptosis by inhibiting the PI3K/Akt/mTOR pathways in HeLa cells [256]. To look at the effect of thioridazine on cell viability, cells were incubated with increasing final concentrations of the compound over 24 hours. The data shown in Figure 4.9A indicates that at the concentrations employed here, thioridazine did not cause a loss of cell viability. To look at potential effects on mTOR signalling and MGMT protein levels, cells were incubated with different final concentrations of thioridazine. Western blotting did not show any significant effect on MGMT protein levels, 4E-BP1 phosphorylation or on eIF2α phosphorylation (data not shown). Additional assays were carried out with thioridazine in the presence if TMZ. When cells were treated with a combination of thioridazine and TMZ for 24 hours, the level of phosphorylation of 4E-BP1 was not changed. In contrast, the combination of thioridazine and TMZ decreased the steady state levels of MGMT protein and increased the phosphorylation of eIF2α (Fig.4.9B lanes 4-5 vs. lane1). As the data presented in Panel B suggested that thioridazine might have an effect on protein synthesis rates by the level of eIF2α phosphorylation, cells were incubated with [^{35}S] methionine at the end of incubating cells with thioridazine for 24 hours. As shown in Figure 4.9C, thioridazine promoted a decrease in protein synthesis

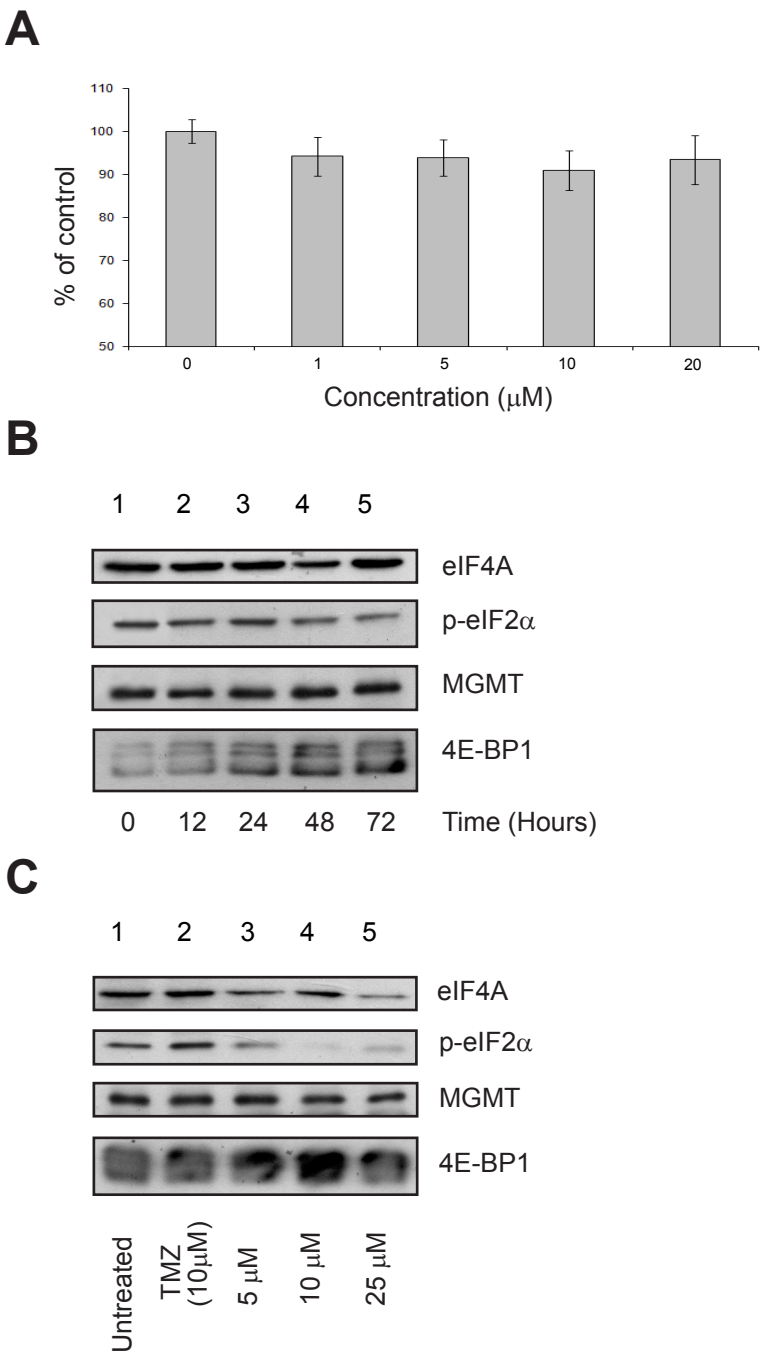

Figure 4.8 Thalidomide does not have a significant effect on mTOR signalling in T98G cells

Panel A. T98G cells were treated with different concentrations of Thalidomide for 24 hours and cell viability was assessed using an MTS assay as described in Materials and Methods. Values are expressed relative to those obtained in untreated cells (set at 100%). A standard TTest was performed and p values were assigned limits where *<0.05, **<0.005 and ***<0.001. **Panel B.** Cells were incubated in the presence of 10μM of Thalidomide for 0-72 hours (lanes 1-5). Extracts were prepared and aliquots containing 10μg of protein were resolved by SDS-PAGE and proteins visualised by Western blotting using the antiserum indicated (n=2). **Panel C.** Cells were incubated in the absence (lane 1) or presence (lanes 3-5) of 10μM TMZ for 24 hours with different concentrations of Thalidomide (lanes 2-5). Extracts were prepared and aliquots containing 10μg of protein were resolved by SDS-PAGE and proteins visualised by Western blotting using the antiserum indicated (n=2).

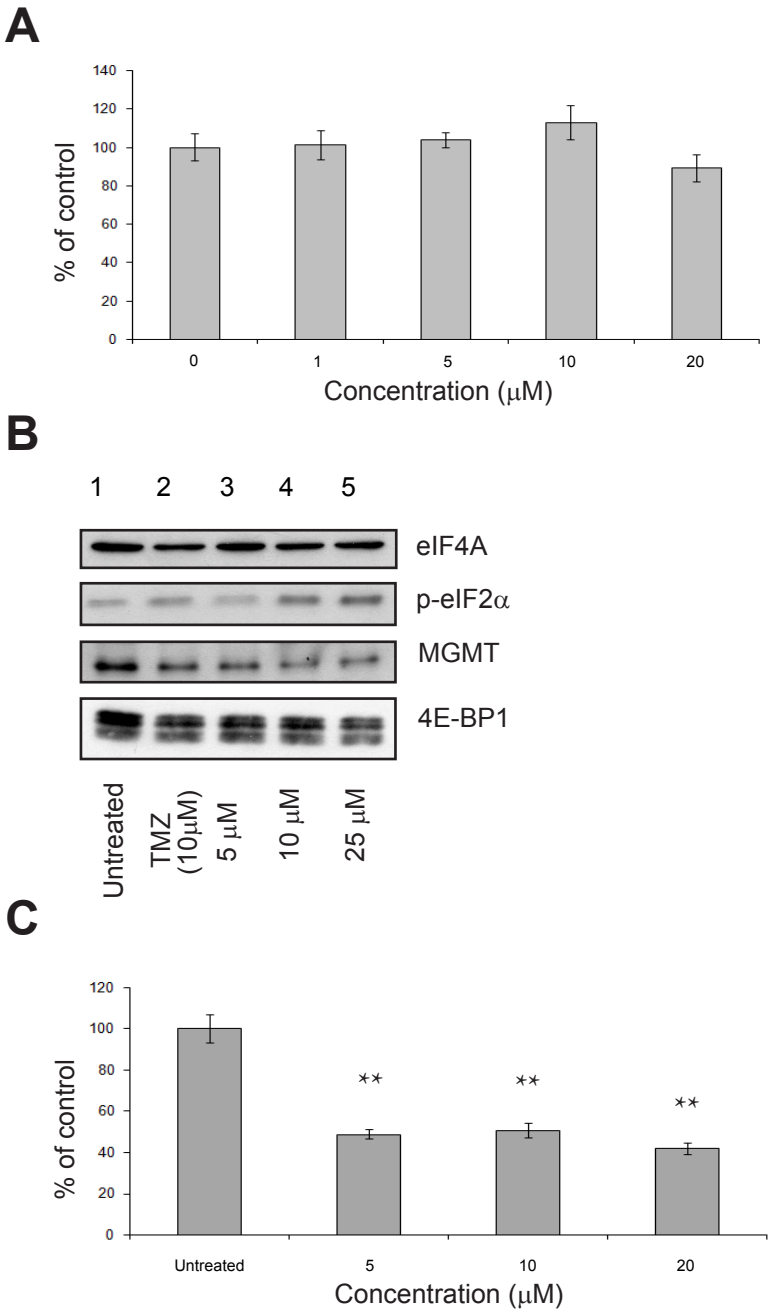

Figure 4.9 Thioridazine inhibits protein synthesis when used in combination with TMZ

Panel A. T98G cells were treated with different concentrations of thioridazine for 24 hours and cell viability was assessed using an MTS assay as described in Materials and Methods. Values are expressed relative to those obtained in untreated cells (set at 100%). A standard TTest was performed and p values were assigned limits where *<0.05, **<0.005 and ***<0.001. **Panel B.** Cells were incubated in the absence (lane 1) or presence of 10μM TMZ (lanes 2-5), in combination with different concentrations of thioridazine (lanes 3-5) for 24 hours. Extracts were prepared and aliquots containing 10μg of protein were resolved by SDS-PAGE and proteins visualised by Western blotting using the antiserum indicated (n=3). **Panel C.** Cells were incubated with 10μM TMZ, combined with different concentrations of thioridazine and one hour prior to harvesting, cells were incubated with 10μCi/ml [^{35S}] methionine, as described in Materials and Methods. Extracts were prepared and incorporation of radioactive methionine into protein determined as cpm/μg protein; results are presented as a % of the rate obtained in cells incubated in the absence of thioridazine and TMZ. Error bars are the S.D (n=3). A standard TTest was performed and p values were assigned limits where *<0.05, **<0.005 and ***<0.001.

rates compared to untreated cells when treated with a combination of Thioridazine and TMZ over a 24 hour time period. Yet this compound did not show any other positive effects on T98G cell MGMT levels during further experiments (data not shown), and so was not considered effective for this project.

4.4 Summary

- The compounds that reduced MGMT protein levels over 72 hours were beta escin, A769662 and DAPH
- The compounds that were effective were identified using known PI3K, mTOR inhibitors, custom gene signatures and the TMZ-resistant GBM patient data
- Beta escin is toxic and therefore was not suitable for future studies.

4.5 Conclusions

Preliminary experiments with the compounds identified with connectivity mapping were used to establish the suitability of each compound for further work. The results of these initial screens suggested that only three compounds were effective at reducing MGMT protein levels whilst remaining non-cytotoxic to cells; DAPH, A769662 and KU0063794. The main aim of using the connectivity mapping database was to find compounds that could reduce rates of MGMT protein synthesis while remaining non-cytotoxic when used by themselves. The summary of drug treatments outlined in Figure 4.10A shows the results of cell viability assays performed on cells treated with differing compounds for 24 hours, both when used alone and when combined with 10μM TMZ. Here it is immediately obvious that beta escin is unsuitable for further work as it is the only compound that is cytotoxic over this short incubation time. The data in Figure 4.10B shows a comparison of the effects of the compounds alone and in combination with TMZ on protein synthesis. Here it is noticeable that thalidomide has no significant effect on protein synthesis rates, both when used alone or when used in combination with TMZ. Although resveratrol did have a

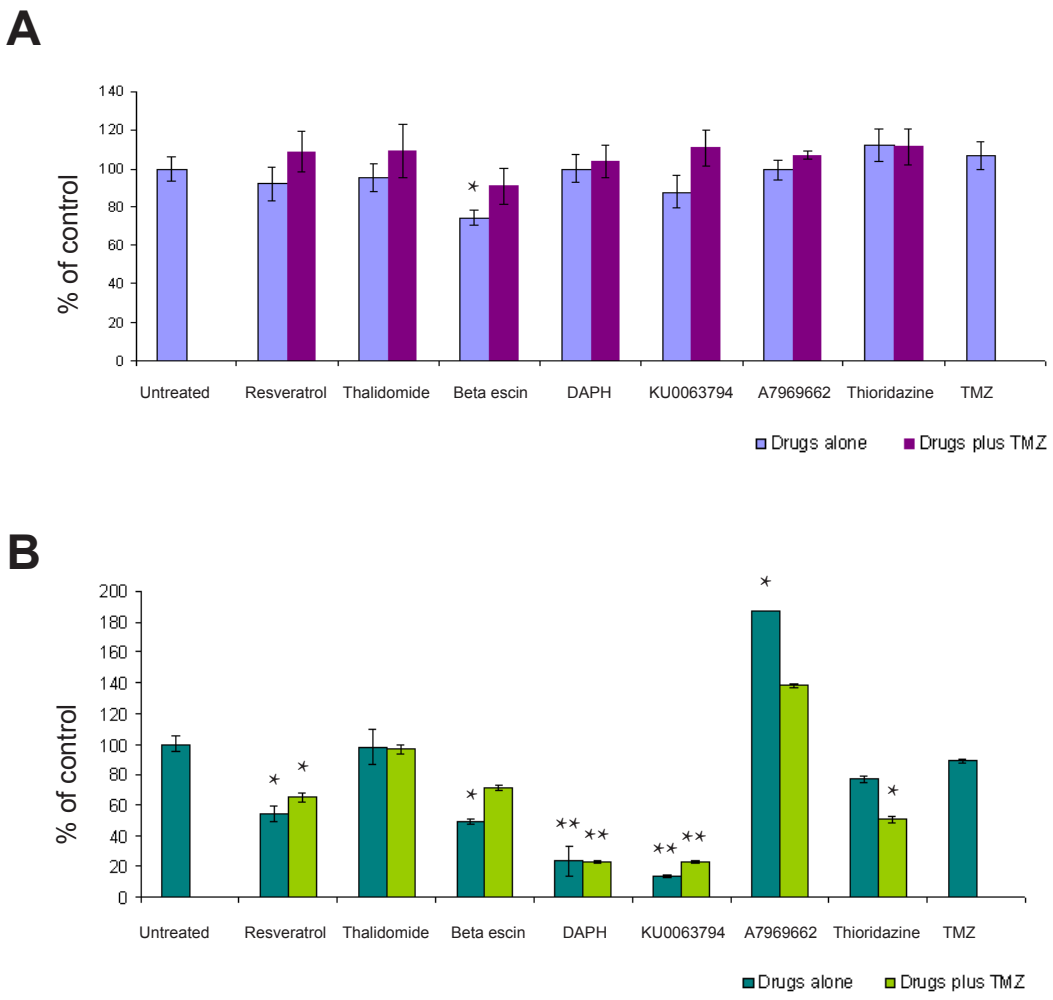

Figure 4.10 Effect of different drugs on cell viability and rates of protein synthesis

Panel A. T98G cells were incubated with set concentrations of drugs; Resveratrol 25μM, Thalidomide 10μM, Beta Escin 1μM, DAPH 5μM, KU0063794 10μM, A769662 20μM, Thioridazine 5μM and TMZ 10μM and incubated for 24 hours either alone, or in combination with 10μM TMZ. Cell viability was assessed using an MTS assay as described in Materials and Methods and is expressed relative to that obtained in untreated cells (set at 100%). Error bars are the S.D (n=3). A standard TTest was performed and p values were assigned limits where *<0.05, **<0.005 and ***<0.001. **Panel B.** T98G cells were incubated as in **(A)** and one hour prior to harvesting, cells were incubated with 10μCi/ml [^{35S}] methionine, as described in Materials and Methods. Extracts were prepared and incorporation of radioactive methionine into protein determined as cpm/μg protein; results are presented as a % of the rate obtained in cells incubated in the absence of drug treatments. Error bars are the S.D (n=3). A standard TTest was performed and p values were assigned limits where *<0.05, **<0.005 and ***<0.001.

Table 4.4 Summary of initial compounds trialled, and which candidates are appropriate for continued research

A summary of initial compounds trialled as a result of connectivity mapping and the decision as to whether to carry on researching them or not. This table summarises the effect the compound has on the cells when used alone, not in conjunction with TMZ

Chemical	Continuation decision	Effect on MGMT protein levels	Additional notes
Resveratrol	Discontinue	No effect	No significant effect on mTOR signalling
Thalidomide	Discontinue	No effect	No significant effect on mTOR signalling
Beta Escin	Discontinue	No effect	Cytotoxic to cells, even in low doses
DAPH	Continue	Small reduction	mTOR inhibition
KU0063794	Continue	No effect	Good positive control for mTOR inhibition
A769662	Continue	Reduction	Lack of mTOR inhibition is interesting - how is it affecting the MGMT levels?
Thioridazine	Discontinue	No effect	Protein synthesis inhibition

slight effect on protein synthesis rates, and was not cytotoxic, the lack on an effect on mTOR signalling meant the compound was not used any further in my study. A summary of the compounds carried on to the next stage of analysis can be found in Table 4.4.

Chapter V

Characterising the effect of KU0063794, DAPH, A769662 and TMZ on cellular signalling and protein synthesis

5 *Characterising the effect of selected compounds on cellular signalling and protein synthesis*

5.1 Aims

- To characterise how the compounds are affecting cell signalling
- To understand how the compounds are affecting MGMT protein levels
- To determine if the compounds sensitise the cells to TMZ

5.2 Introduction

The next objective after using the connectivity mapping technique to find compounds that would potentially modulate MGMT was to characterise how the compounds were affecting the T98G glioblastoma cells. For this, I set out to determine the effect the compounds had on cell signalling, MGMT protein localisation, cap dependent translation and protein synthesis rates. Establishing which specific proteins the compounds were affecting, as well as trying to determine whether the compounds sensitised the cells to TMZ was also important. Identifying proteins that are being affected by the compounds could indicate which cellular signalling pathways were being interfered with. To this end, T98G cells were incubated with the indicated concentration of KU0063794, DAPH or A769662, both alone and in combination with TMZ for up to 72 hours and extracts were prepared as described in the Materials and Methods. Western blotting was used to determine the effect of compounds on targets in T98G cells.

5.3 Results

5.3.1 Identifying how the compounds affect cellular signalling in T98G cells

T98G cells were incubated with 10μM KU0063794 alone (Fig.5.1 A) or in combination with 10μM TMZ (Panel B) for the time indicated in the figure. Western blotting analysis demonstrates that phosphorylation of Akt on Thr308 increases upon inhibition of mTOR signalling in comparison to untreated cells

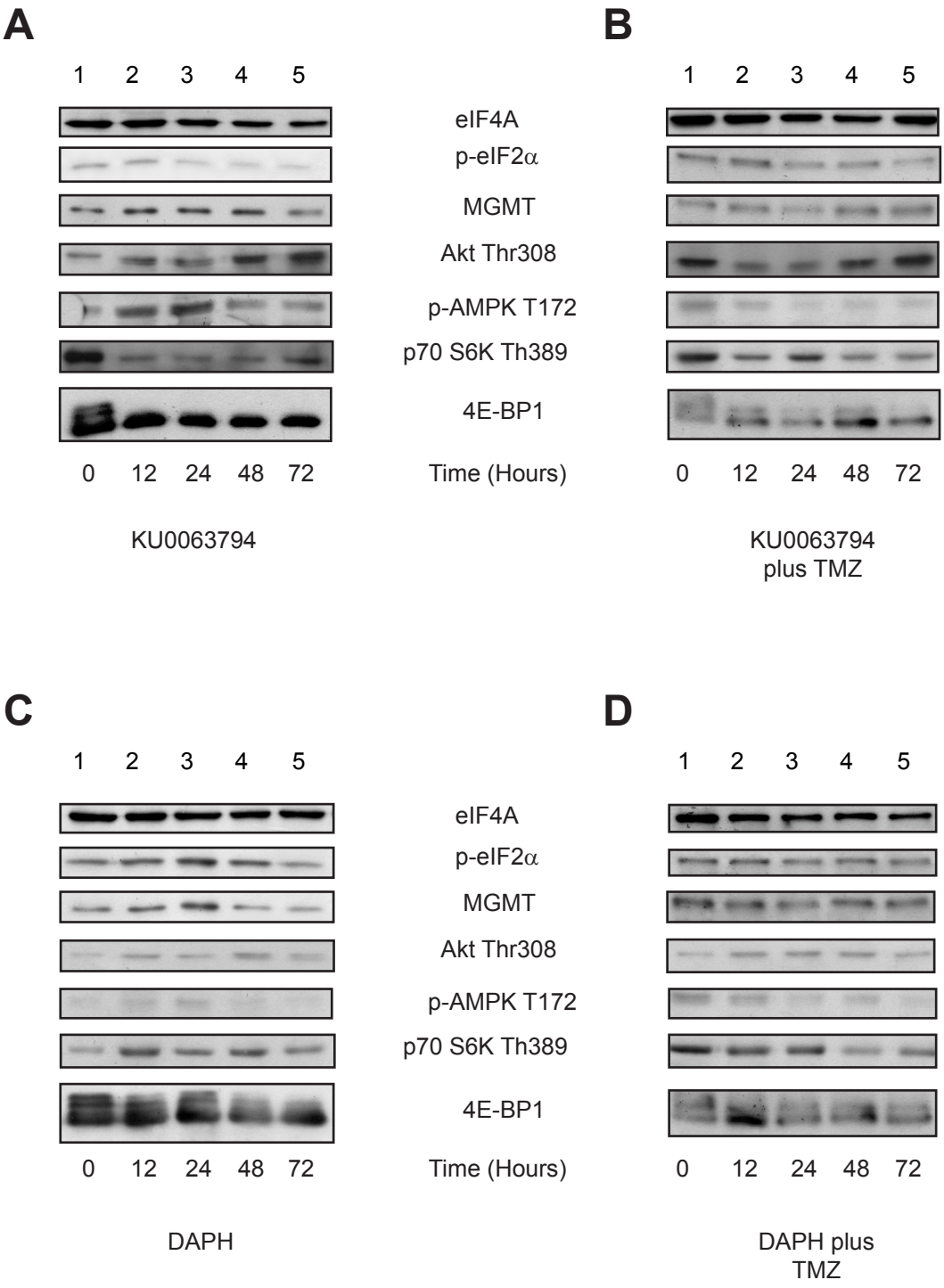

Figure continues on the next page

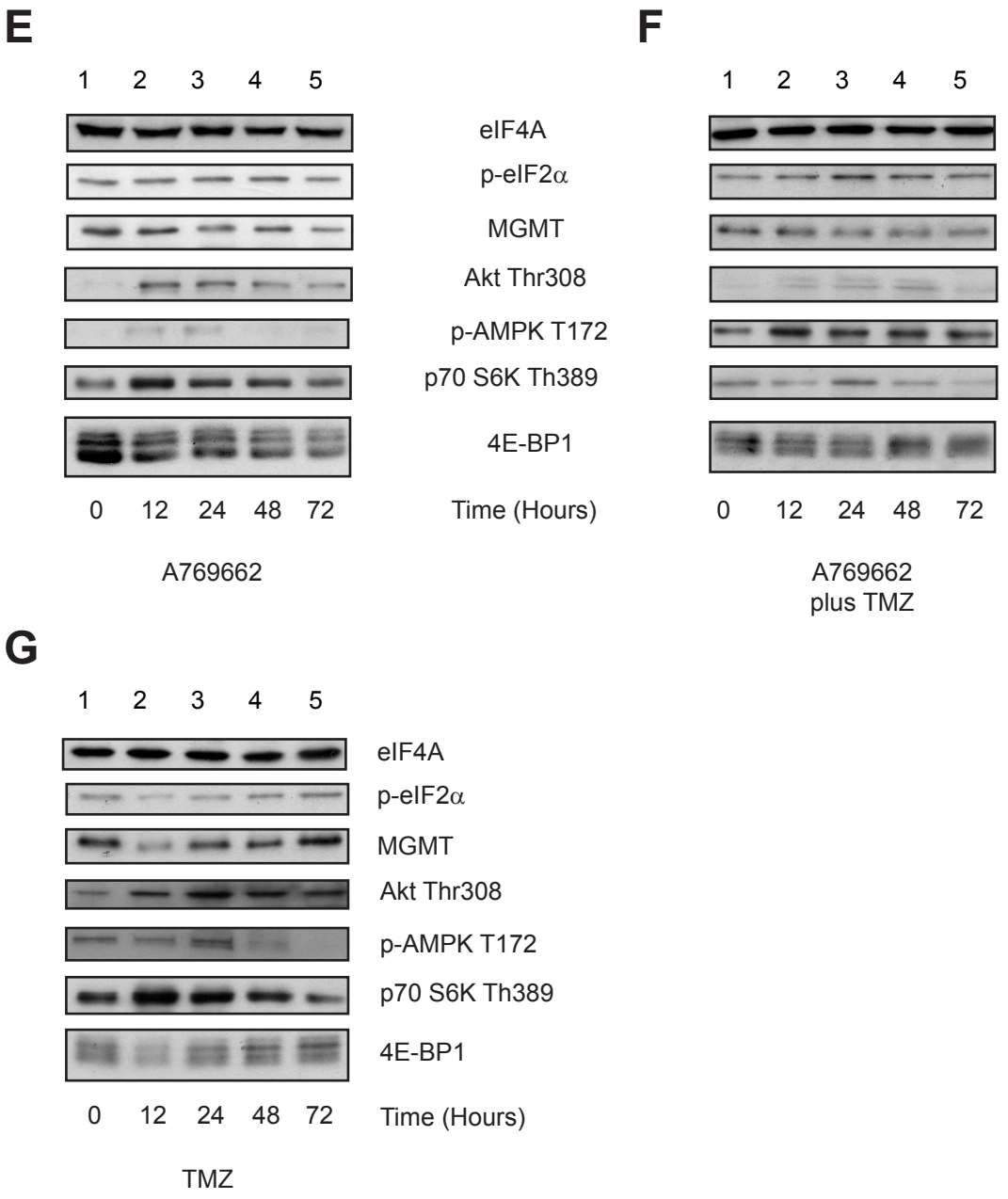

Figure 5.1 All compounds affect proteins associated with the mTOR signalling pathway

Panel A. T98G cells were incubated in the absence (lane 1) or presence of 10μM KU0063794 (n=3). **Panel C.** 5μM DAPH (n=3) **Panel E.** 20μM A769662 (n=3) for 12-72 hours (lanes 2-5). Extracts were prepared and aliquots containing 10μg of protein were resolved by SDS-PAGE and proteins visualised by Western blotting using the antiserum indicated. **Panels B, D, F** Cells were treated as in **(A,C,E)**, but treatments were combined with 10μM TMZ (n=3). **Panel G.** Cells were treated with 10μM TMZ alone for 0-72 hours (lanes 1-5). Extracts were prepared and aliquots containing 10μg of protein were resolved by SDS-PAGE and proteins visualised by Western blotting using the antiserum indicated (n=3).

(lanes 2-5 vs. lane 1).There was little increase in the phosphorylation (and hence activation) of p38MAPK, AMPK or eIF2α phosphorylation. These data suggest that prolonged incubation with KU0063794 may lead to the activation of PI3K signalling, as described for rapamycin [257]. The decrease in phosphorylation of p70 S6K at Thr389 in cells treated with either KU0063794 alone (A) or in conjunction with TMZ (B) compared to the untreated control (lanes 2-5 vs. lane 1) reaffirms the inhibition of the mTOR signalling pathway, as this specific phosphorylation site is directly controlled by mTOR. Surprisingly, incubation of cells with both KU0063794 and TMZ delayed the dephosphorylation of p70S6K Thr389 relative to that seen with KU0063794 alone. In T98G cells incubated with both KU0063794 alone and in combination with TMZ, MGMT levels did not change, (Fig.5.1A).

In cells incubated with 10μM TMZ alone for 24 hours, there were some changes in the activity of intracellular signalling pathways and the steady state level of MGMT protein (Fig.5.1G). The most obvious was a transient increase in p70S6K phosphorylation and a general increase in the activation of Akt, and the absence of stress kinase and/or eIF2α phosphorylation. The level of MGMT protein expression dropped dramatically following treatment of cells with TMZ, reaching a low level at 12 hours; this probably reflects the use of MGMT protein in repairing TMZ-induced DNA damage. However, this level increased as the incubation time with TMZ progressed (lanes 3-5 vs. lane 2), suggesting that MGMT may be synthesised actively during this period.

Cells incubated with DAPH alone and in combination with TMZ over 24 hours (Fig.5.1C and D) only showed a slight increase in Akt 308 phosphorylation. p70 S6K phosphorylation was largely unaffected in cells treated with either DAPH alone or with TMZ (lanes 2-5 vs. lane 1) and only showed a minor decrease during the later time points (lanes 4 and 5 vs. lanes 1-3). There was little change in the phosphorylation (and hence activation) of AMPK under any conditions with DAPH. The level of MGMT protein varied slightly in cells incubated with DAPH alone but not when used in combination with TMZ (Fig.5.1 C, D). This variation was reproducible (data not shown).

As A769662 has shown in previous cell lines that it is an AMPK activator [251], it was surprising that when incubated with T98G cells for 24 hours alone (Fig.5.1E), it did not seem to have an effect on AMPK phosphorylation. There was a transient increase in AMPK Thr172 phosphorylation and p38MAPK phosphorylation at 12-24 hours (lanes 2 and 3), which decreased to basal levels by 48 hours of incubation in the cells incubated with a combination of both A769662 and TMZ however, there was an increase in phosphorylated AMPK (Fig.5.1F) which occurred without activation of p38MAPK or eIF2α phosphorylation. These data suggest that A769662 with TMZ activates AMPK without eliciting a general stress response in T98G cells. However, this activation of AMPK is not sufficient to promote dephosphorylation of 4E-BP1 mediated by inhibition of mTORC1 signalling. Akt phosphorylation at Thr308 and p70S6K Thr389 phosphorylation both increased transiently in cells treated with A769662 alone compared to an untreated control (Panel E, lanes 2-5 vs. lane 1). To a lesser extent, these phosphorylation events were observed in cells incubated concurrently with TMZ. MGMT protein levels were not affected by incubation with A769662 (Fig 5.1E, F).

5.3.2 KU0063794 impairs the cells ability to form the eIF4F complex

Inhibition of the mTOR signalling pathway results in 4EBP1 remaining bound to eIF4E causing it to be unavailable to participate in the eIF4F initiation complex alongside the helicase eIF4A and the scaffold protein eIF4G. To ascertain whether or not the cells are able to form this complex after incubation with KU0063794, DAPH, A769662 or TMZ, cell extracts were prepared and 100μg of total protein was mixed with Sepharose beads coupled to m^7GTP (lanes 1 and 3-9). This cap structure emulates that of the mRNA cap on the 5' end of an mRNA, resulting in eIF4E and associated proteins binding to it. Lysate from cells incubated in the absence of compounds was mixed with Sepharose beads lacking an m^7GTP cap to serve as a negative control for specific interaction of recovered proteins with the cap analogue (lane 2). Figure 5.2 (lane 1 vs. 2) shows that the eIF4F complex (eIF4E, eIF4A, eIF4G) and

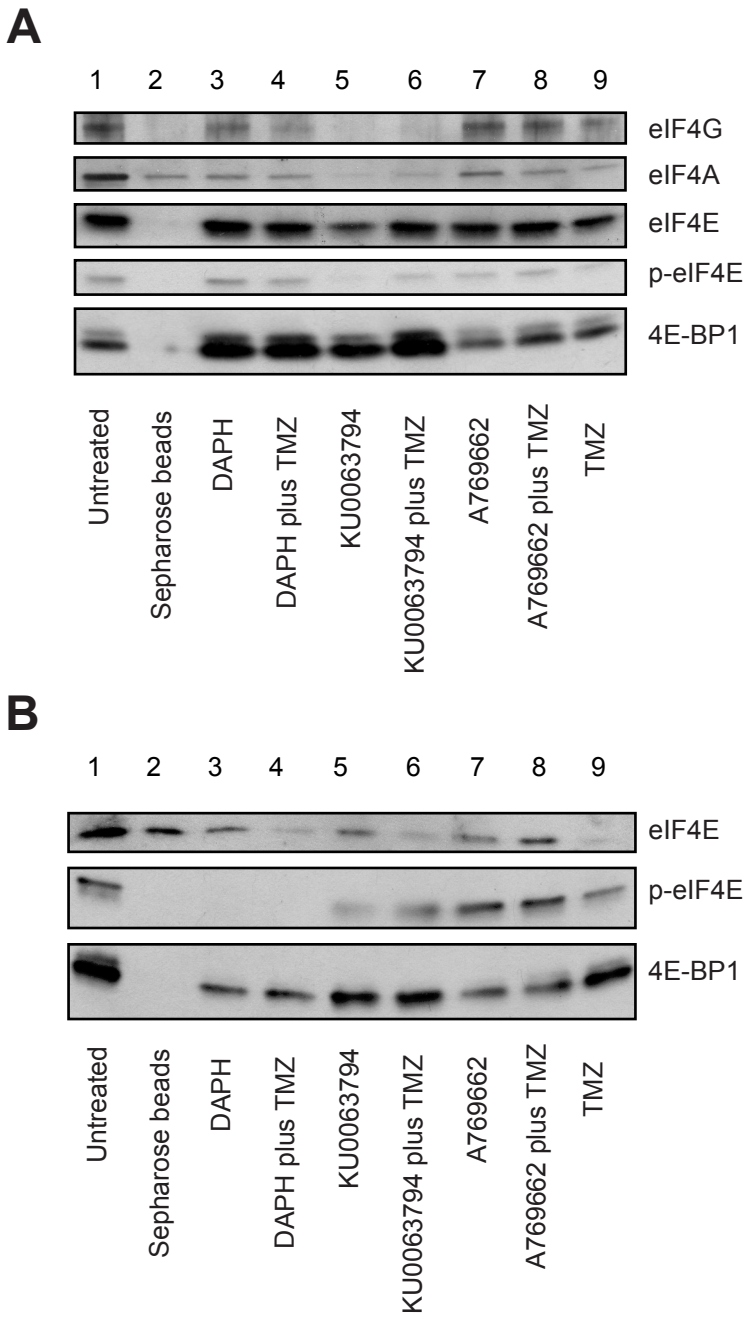

Figure 5.2 KU0063794 inhibits eIF4F complex formation, both when used alone and when combined with TMZ

Panel A. T98G cells were incubated for 24 hours in the absence (lanes 1 and 2) or presence of 5μM DAPH (lane 3), 10μM KU0063794 (lane 5) or 20μM A769662 (lane 7), either alone or in conjunction with 10μM TMZ (lanes 4,6 and 8). Cells were also incubated with 10μM TMZ alone (lane 9). Extracts were prepared and aliquots containing 100μg of protein were subjected to m^7GTP-Sepharose affinity chromatography as described in Materials and Methods (n=3). Sepharose beads lacking an m^7GTP cap were also combined with 100μg of untreated extract as a negative control (lane 2). eIF4E and associated proteins were recovered and resolved by SDS-PAGE and proteins visualised by Western blotting using the antiserum indicated. All lanes were resolved on the same gel. **Panel B.** Cells were treated as in **panel A** but for 72 hours (n=2).

eIF4E/4E-BP1 complexes were specifically recovered with the resin. When cells were incubated with KU0063794 for 24 hours (Fig.5.2A), there was a decrease in the association of eIF4A and eIF4G recovered with eIF4E (lane 5 vs. lane 1), suggesting that this initiation complex is not forming. Furthermore, this decrease in eIF4F complex levels was associated with increased levels of eIF4E associated with 4E-BP1, and decreased levels of phosphorylated eIF4E. A similar response was seen when cells were incubated with both KU00663794 and TMZ (lane 6 vs. lane 5). Incubation of cells with DAPH, in the absence or presence of TMZ has a similar, but less pronounced effect on eIF4F complex levels. In contrast, incubation of the cells with A769662 in the absence or presence of TMZ, or indeed TMZ alone, has little effect on eIF4F complex levels or eIF4E phosphorylation (lanes 7-9 vs. lane 1).

To investigate eIF4E/BP-1 levels further, cells were incubated with compounds, without and with TMZ for 72 hours and eIF4E and associated proteins recovered as above. Figure 5.2B shows that at this time point, in general, results were similar to those seen at 24 hours. However, effects of KU0063794 on eIF4E/4E-BP1 levels were less pronounced relative to untreated cells (lanes 5 and 6 vs. lane 1). These data suggest that cells have adapted to the presence of the compound over this period of time. Alternatively, as recovery of eIF4E here was somewhat variable, this could also reflect a problem with protein complex recovery from the resin.

5.3.3 MGMT protein does not re-localise in cells treated with compounds

MGMT protein is over-expressed in T98G cells relative to other glioblastoma cell lines [258,259] and we show that it is predominantly nuclear in this cell line. With increased levels of MGMT protein in these cells, if the protein were to differentially localise between cellular compartments during incubation with chemotherapeutic agents or other compounds, it could give us an insight in to how the steady state level of the protein is being regulated. Taking this in to account, cells were incubated with compounds for 24 hours, at the concentrations stated in Figure 5.3. Confocal imaging analysis was then

A

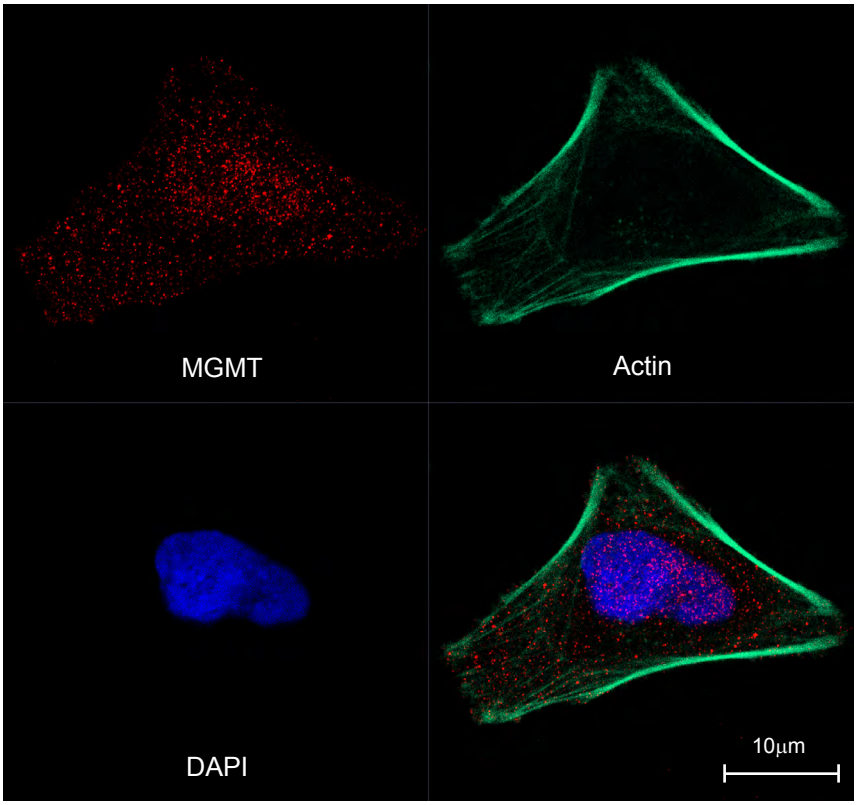

B

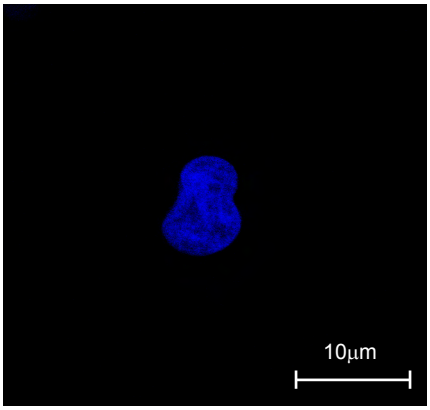

Secondary IgG only

Figure continues on the next page

C

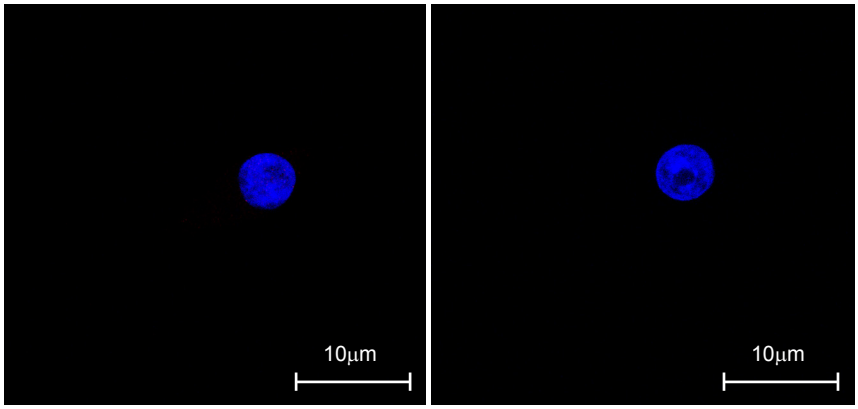

Primary and secondary IgG Secondary IgG only

D

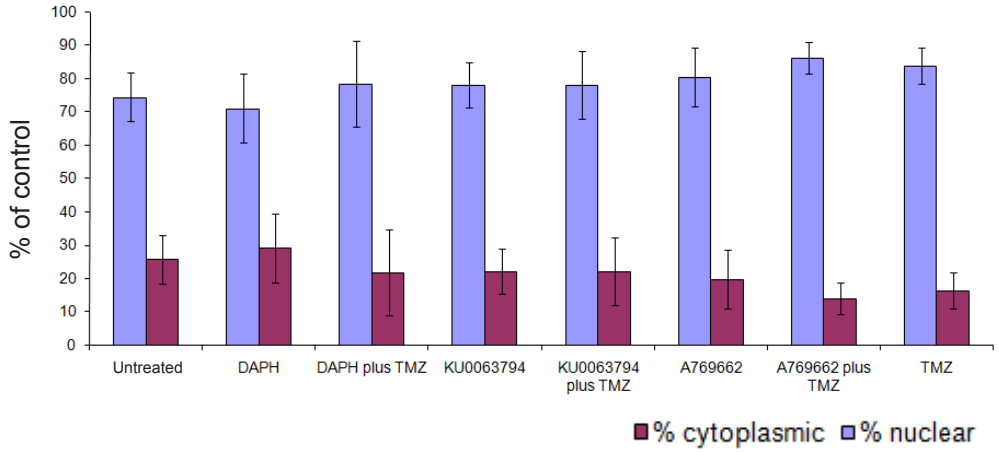

Figure 5.3 MGMT does not relocalise in cells treated with DAPH, KU0063794 or A769662

Panel A. Untreated T98G cells were fixed and permeabilised as described in Materials and Methods. Proteins were visualised using fluor conjugated anti serum against MGMT, actin and DNA, as indicated. Images were collected on a Zeiss Axiovert LSM510 scanning confocal microscope using a ×100 objective. **Panel B.** Untreated T98G cells were fixed and permeabilised as described in Materials and Methods. Proteins were incubated with the secondary antibody only. **Panel C.** Untreated U87- MG cells were fixed and permeabilised as described in Materials and Methods. Proteins were visualised using fluor conjugated anti serum against MGMT, or secondary antibody only and DNA, as indicated. **Panel D.** T98G cells were incubated in the absence or presence of 5μM DAPH, 10μM KU0063794 or 20μM A769662, either alone or in conjunction with 10μM TMZ for 24 hours. Cells were also treated with 10μM TMZ for 24 hours. Cells were then fixed, permeabilised and processed for IF analysis of MGMT, as described in Materials and Methods. Images were collected on a Zeiss Axiovert LSM510 scanning confocal microscope using a ×100 objective. The localisation of MGMT was quantified in the nuclear and cytoplasmic fractions from three separate preparations using ImageJ. Error bars are the S.D (n=3). A standard T Test was performed and p values were assigned limits where *<0.05, **<0.005 and ***<0.001.

performed to determine if the percentage of MGMT protein in the nucleus versus the cytoplasm changed between untreated cells and cells incubated with compounds. The data shown in panel A confirm that although staining for MGMT can be clearly seen in the cytoplasm, the protein is enriched in the nuclear compartment. This did not change appreciably when cells were incubated with any of the compounds, with or without TMZ (data not shown). To ensure the primary and secondary antibodies were not binding to cellular proteins non-specifically, T98G cells were incubated with secondary antibody and DAPI only (Fig.5.3B). These data clearly show the presence of the DNA but no other signal, showing the specificity of the antibody used here. In addition, I have used U87-MG cells which do not express MGMT [260]. As predicted, when these cells were probed with either primary and secondary antibody or secondary antibody only alongside DAPI staining (C), only nuclei were visible, confirming that I was looking at MGMT protein in the T98G cells. Such data were quantified from cells incubated in the absence or presence of the compounds shown, confirming that no significant re-localisation of MGMT protein was observed under these assay conditions (Fig.5.3D).

5.3.4 MGMT mRNA levels do not change significantly in cells treated with compounds

The compounds derived from connectivity mapping experiments were chosen based on their ability to change specific mRNA levels whose protein products had been linked into mTOR inhibition. However, it was important for me to know whether the compounds used in my work were mainly regulating protein synthesis through an inhibition of translation or a down-regulation *via* a transcriptional mechanism. To confirm the changes seen in MGMT protein levels in cells treated with A769662 and DAPH alone were not a reflection of changes in mRNA levels, qRT-PCR was performed to measure the amount of MGMT mRNA present in untreated cells compared to mRNA levels in cells incubated with the compounds for either 24 (Fig.5.4A) or 72 hours (Fig.5.4B). MGMT mRNA levels were also measured in cells treated with the compounds

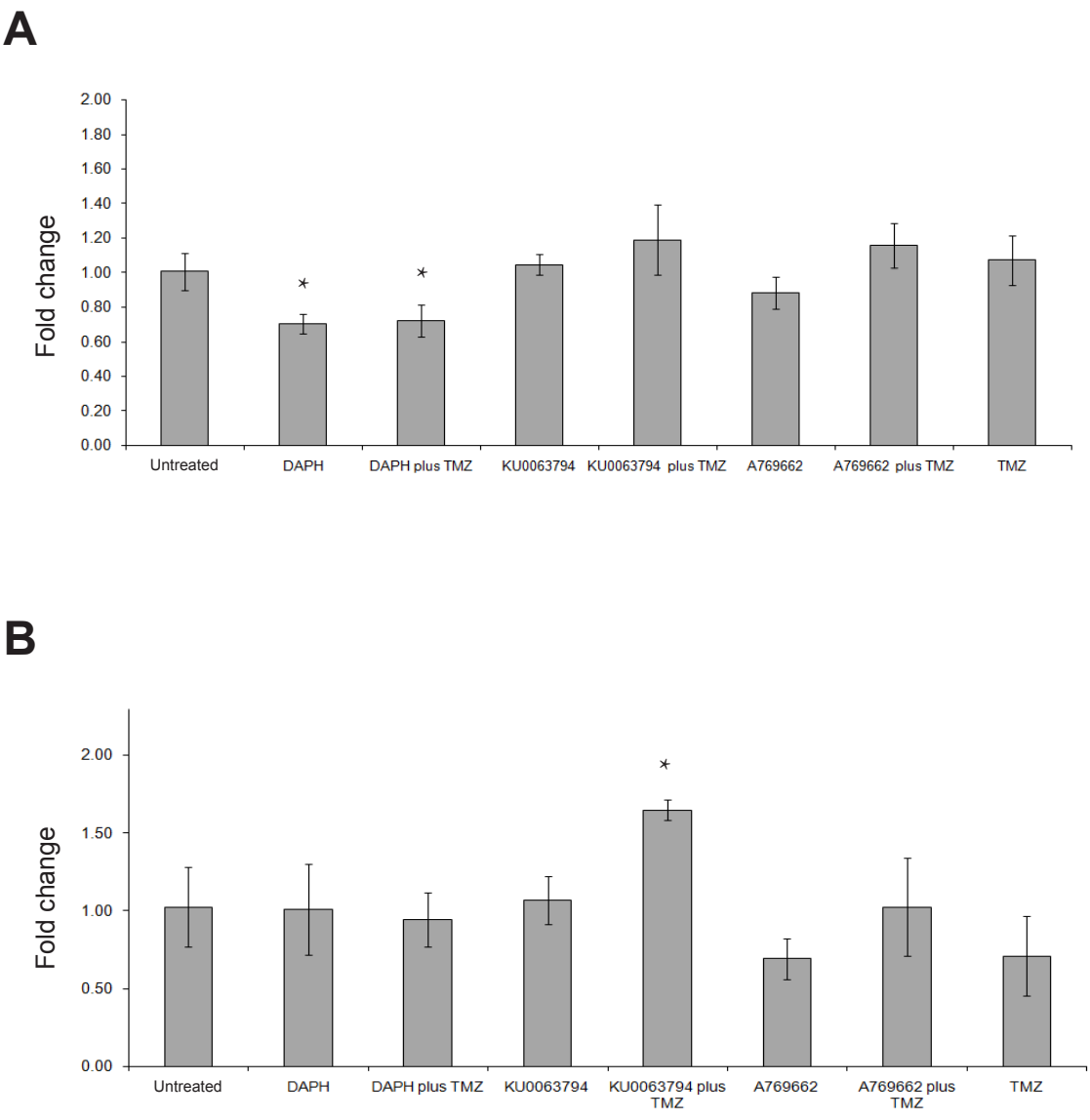

Figure 5.4 MGMT mRNA levels do not change significantly in treated cells

Panel A. Cells were incubated for 24 hours in the absence or presence of 5μM DAPH, 10μM KU0063794 or 20μM A769662, either alone or in conjunction with 10μM TMZ for 24 hours as indicated. mRNA was extracted from cell extracts as described in Materials and Methods. For each treatment, quantitative RT-PCR was used to determine levels of MGMT mRNA relative to 18S rRNA, as described. Data are presented as a fold change in mRNA amount relative to levels observed in untreated cells. Error bars are the S.D (n=3). A standard T Test was performed and p values were assigned limits where *<0.05, **<0.005 and ***<0.001. **Panel B.** Cells were treated as in **(A)** but for 72 hours.

treated with KU0063794 and in combination with KU0063794. These experiments were used to correlate mRNA levels and protein levels across treatments, to allow the results to be observed in a wider context. Levels of MGMT mRNA expression were then expressed relative to the levels of 18S ribosomal RNA in the same cells. As shown, when T98G cells were incubated with the compounds for 24 hours, there was not a dramatic difference in the levels of MGMT mRNA relative to those found in cells incubated in the absence of compounds (Fig.5.4A). However, cells incubated with DAPH or DAPH plus TMZ did show a 30% reduction (Student's t-test, $p<0.05$) in MGMT mRNA which was significant. Similarly, MGMT mRNA levels relative to those found in cells incubated in the absence of compounds varied little following a 72 hour incubation period with the compounds (Fig.5.4B). One exception was when cells were incubated with both KU0063794 and TMZ, where there was a significant (Student's t-test, $p<0.05$) increase in MGMT mRNA levels, yet this is not considered a large fold change in mRNA levels and may be a result of cellular stress as it was only observed in the 72 hour treatment and not the 24 hour treatment. Overall, these data confirm that the change of MGMT protein levels in cells treated with the DAPH and A769662 is not likely to be a reflection of reduced mRNA levels.

5.3.5 Inhibiting mTOR signalling does not fully inhibit eukaryotic translation

To get a complete picture of events in the cells that are being treated with the compounds, I needed to look more closely at the actively translating polysomes. From the connectivity mapping, I already have information providing insight into the transcriptional effects the compounds have on cells, their ability to change protein levels and affect protein synthesis, and their effect on eukaryotic translation initiation. Yet to obtain more information about the functioning cell, I need to understand how the compounds are affecting the amount of ribosomes that are actively translating protein. Polysome profiling separates free material, ribosomal subunits and polysomes to determine the amount of mRNA engaged

on polysomes and hence actively involved in translation at any point. For this, T98G cells were incubated with the compounds for 24 hours at the concentrations specified in the figure legend (Fig.5.5). Cells were then lysed in a hypotonic lysis buffer and the cell extracts centrifuged through a sucrose gradient to separate the ribosomal subunits from the polysomes. As shown in Figure 5.5A, incubation of cells with DAPH had little effect on the recovery of mRNA in heavy polysomes, suggesting that translation is still occurring quite efficiently. This was somewhat surprising considering that whilst DAPH only had a moderate effect on eIF4F levels (Fig.5.2), [^{35}S] methionine incorporation into protein was reduced to about 20% (Student's t-test, $p<0.005$) of that observed in untreated cells (Fig.4.6).

Cells treated with KU0063794 for 24 hours show an increase in 80S monosomes compared to the untreated cells. There are also fewer polysomes in the KU0063794 treated cells compared to the control consistent with an inhibition of protein synthesis (Fig.4.10B) and decreased eIF4F levels (Fig.5.2). However, it is important to note that some polysomes are still present in these cells. In contrast, incubation of cells with either A769662 or TMZ seemed to have had little effect on the association of mRNA into actively translating polysomes, suggesting that these compounds do not inhibit translation at 24 hours. This information does correlate with the data obtained with m^{7}GTP-Sepharose isolation of eIF4F (Fig.5.2A) indicating no change in this complex or protein synthesis rates (Fig. 4.10B) under these conditions

5.3.6 MGMT mRNA remains in polysomes during mTOR inhibition and reduced translation initiation

To determine whether the maintenance of MGMT protein in cells treated with KU0063794 was due to maintenance of MGMT mRNA translation during reduced eukaryotic initiation and protein synthesis, quantitative RT-PCR was carried out on the fractions obtained during polysome fractionation as described in Figure 5.5. The polysome fractions were pooled, so as to measure mRNA in the free material, the ribosomal subunits and monosomes, the light polysomes

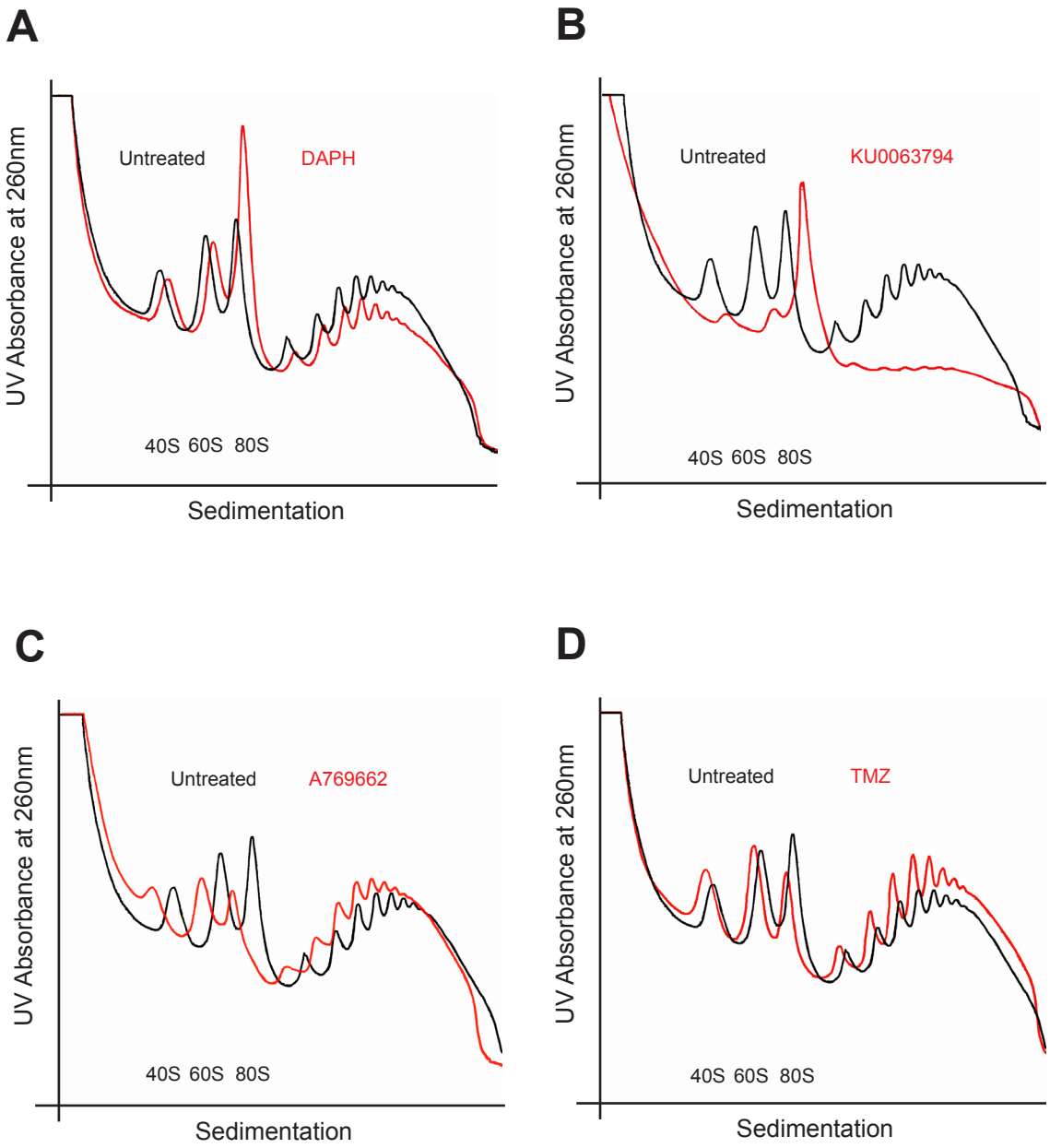

Figure 5.5 DAPH and KU0063794 both inhibit mTOR, but have different effects on polysome levels

T98G cells were incubated for 24 hours in the absence or presence of 5μM DAPH **(Panel A)**, 10μM KU0063794 **(Panel B)**, 20μM A769662 **(Panel C)** or 10μM TMZ **(Panel D)**. Cell extracts were prepared and subjected to polysome profiling as described in materials and methods. The figure represents 3 separate experiments (n=3).

and the heavy polysomes. By measuring the amount of GAPDH and MGMT mRNA in each of these fractions, it is possible to compare the distribution of GAPDH mRNA and MGMT mRNA after incubation of cells with compounds for 24 hours. Untreated cells show a similar distribution of GAPDH and MGMT mRNA across the fractions in the gradient (Fig.5.6A), whereas cells that were incubated with 10μM KU0063794 for 24 hours showed a reduction of GAPDH mRNA in the polysome fractions and an increase in GAPDH mRNA in the subunits and free material. Surprisingly, the MGMT mRNA associated with polysomes was not reduced, even though translation was greatly reduced. Similar amounts of MGMT mRNA were observed in the light and heavy polysomes as seen in the untreated cells (Fig.5.6B). The distribution of MGMT and GAPDH mRNA in cells incubated with A769662 was very similar (Fig.5.6D), although there was more total RNA extracted from this gradient than any of the other gradients (data not shown). When cells were incubated with DAPH, there was a reduction of GAPDH mRNA in the heavy polysome fractions and an increased recovery in the subunit fraction. Although this reduction of GAPDH mRNA was observed in the heavy polysome fraction, MGMT mRNA did not follow the same pattern, and was present in a high percentage in both the light and heavy polysomes (Fig.5.6C).

.

5.3.7 U87-MG and T98G cells respond to the compounds in similar ways

T98G cells show resistance to TMZ, mainly because they express a high amount of MGMT protein in comparison to other GBM cell types [258,259]. To ensure that the effects the selected compounds had on the T98G cells were not cell-specific, I also used U87-MG cells; these brain tumour-derived human cells are MGMT null. Therefore, U87-MG cells were incubated with the compounds for 24 hours (Fig.5.7) and both Western blotting analysis and rates of protein synthesis were performed on the cells, as described previously.

Western blotting analysis of the extracts derived from U87-MG cells (Fig.5.7A) suggested that the compounds had a similar effect to those observed with T98G cells. The dephosphorylation of 4E-BP1 in the cells treated with

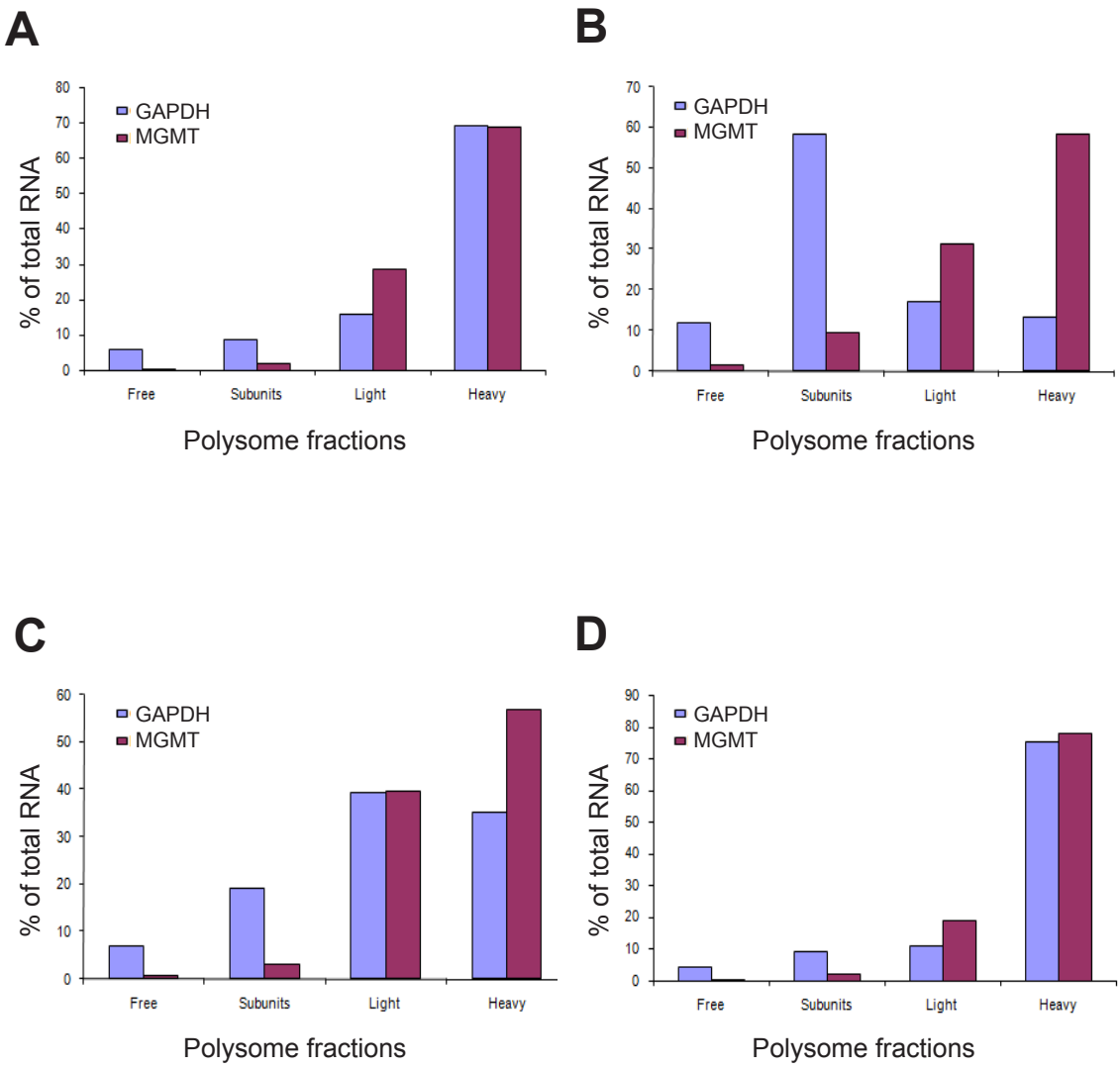

Figure 5.6 MGMT mRNA remains in polysomes during translation initiation inhibition

Cells were incubated for 24 hours in the absence (**Panel A)** or presence of 10μM KU0063794 (**Panel B)**, 5μM DAPH (**Panel C)** or 20μM A769662 (**Panel D)**, lysates were prepared and polysomes resolved and fractionated as described in Figure 6.5. The mRNA from pooled fractions was extracted as described in Materials and Methods. For each gradient, quantitative RT-PCR was used to determine levels of GAPDH and MGMT mRNA distribution across each fraction, with the total mRNA in each gradient set at 100%. Error bars are the S.D (n=3) of 3 technical replicates.

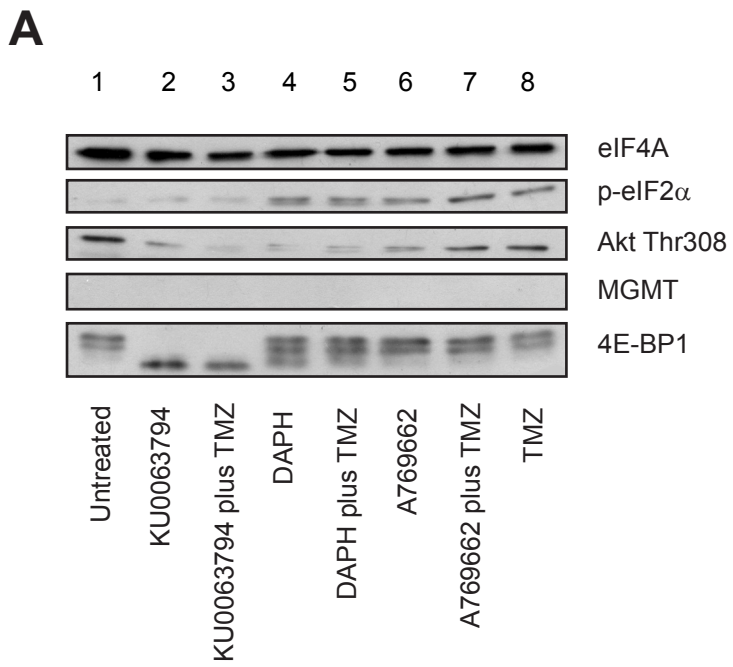

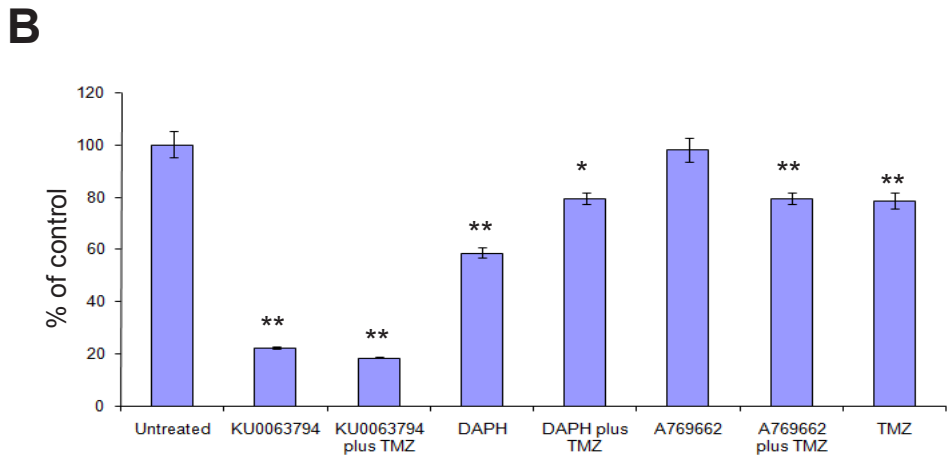

Figure 5.7 U87-MG cells respond to the compounds in a similar way to T98G cells

Panel A. U87-MG cells were incubated in the absence (lane 1) or presence of 10μM KU0063794 (lane 2), 5μM DAPH (lane 4) or 20μM A769662 (lane 6), either alone or in conjunction with 10μM TMZ (lanes 3,5 and 7) for 24 hours. Cells were also incubated with 10μM TMZ alone (lane 8). Extracts were prepared and aliquots containing 10μg of protein were resolved by SDS-PAGE and proteins visualised by Western blotting using the antiserum indicated (n=2). **Panel B.** Cells were treated as in **(A)** and one hour prior to harvesting, cells were incubated with 10μCi/ml [^{35}s] methionine, as described in Materials and Methods. Extracts were prepared and incorporation of radioactive methionine into protein determined as cpm/μg protein; results are presented as a % of the rate obtained in cells incubated in the absence of compounds. Error bars are the S.D (n=3). A standard T Test was performed and p values were assigned limits where *<0.05, **<0.005 and ***<0.001.

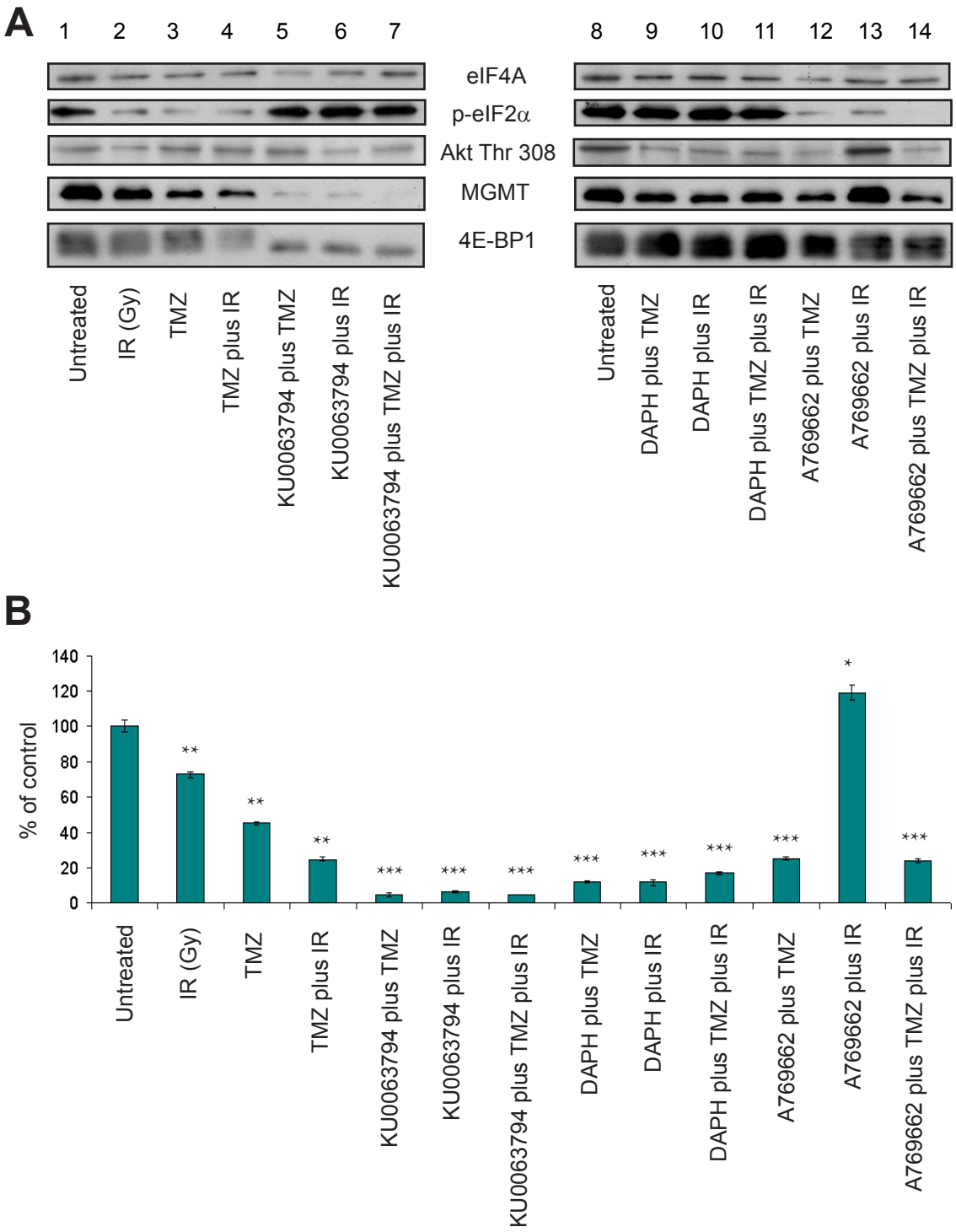

Figure 5.8 Combining KU0063794, TMZ and ionising radiation dramatically reduces MGMT protein levels in T98G cells

Panel A. T98G cells were incubated in the presence of compounds as indicated. KU0063794 was used at 10μM, DAPH at 5μM, A769662 at 20μM, TMZ at 10μM and Ionising radiation at 2Gy. Cells were all incubated with compounds for 72 hours, irradiated, then harvested 24 hours later. Lysates were resolved by SDS-PAGE and proteins visualised by Western blotting using the antiserum indicated (n=2). **Panel B.** T98G cells were incubated as indicated and one hour prior to harvesting, cells were incubated with 10μCi/ml [^{35}S] methionine, as described in Materials and Methods. Extracts were prepared and incorporation of radioactive methionine into protein determined as cpm/μg protein; results are presented as a % of the rate obtained in cells incubated in the absence of drug treatments. Error bars are the S.D (n=3). A standard T Test was performed and p values were assigned limits where *<0.05, **<0.005 and ***<0.001.

KU0063794 or KU0063794 plus TMZ (lanes 3 and 4 vs. lane 1) indicated that mTOR signalling was inhibited. Incubation of these cells with DAPH caused a slight dephosphorylation of 4E-BP1 (lanes 4 and 5 vs. lane 1), but A769662 (lanes 6 and 7 vs. lane 1) or TMZ (lane 8 vs. lane 1) had little effect on the phosphorylation of this protein. Relative to untreated cells, the phosphorylation of Akt on Thr308 decreased with KU0063794 and DAPH (lanes 2-5 vs. lane 1) but actually increased slightly in response to TMZ (lanes 7 and 8 vs. lane 7). The phosphorylation of eIF2α was unaffected by KU0063794 (lanes 1-3) but increased in the presence of DAPH and A769662, without or with TMZ present (lanes 4-8 vs. lanes 1-3). Protein synthesis assays shown in Fig.5.7B suggested that incubation of cells with KU0063794 resulted in an inhibition of protein synthesis rates when compared to cells incubated without the compound. These data are consistent with a central role for mTOR signalling in controlling translation rates in U87-MG cells. Incubation of cells with DAPH also inhibited radioactive methionine incorporation into protein but to a lesser extent. This was also observed with DAPH in T98G cells (Fig.4.6). A769662 and TMZ showed little effect on translation rates even though levels of eIF2α phosphorylation were increased over control cells.

5.3.8 Combining an mTOR inhibitor, TMZ and ionising radiation dramatically reduces MGMT levels in T98G cells

The current strategy for treating GBM combines TMZ chemotherapy with radiotherapy, for maximum efficacy. It was therefore important that I test the compounds of interest with both TMZ and ionising radiation (IR) for effects on signalling and MGMT protein levels. To this end, T98G cells were incubated for 72 hours with the compounds alone or in conjunction with TMZ, as specified in Figure 5.8. Cells were then either transported to the gamma irradiator but not irradiated, or irradiated with 2Gy of ionising radiation and allowed to recover for 24 hours before being harvested. I ensured that the cells which were not irradiated spent the same amount of time outside the incubator as the ones that were irradiated, so that this did not cause a difference in cell behaviour.

Western blotting of cell extracts showed that the dephosphorylation of 4E-BP1 is clear in cells incubated with KU0063794 (Fig.5.8A, lanes 5-7) whilst there was little effect on Akt Thr308 phosphorylation. In contrast, there was a robust increase in eIF2α phosphorylation under these conditions and a decrease in steady state levels of MGMT protein. Treatment of cells with IR (lane 2), TMZ (lane 3) or IR with TMZ (lane 4) had no effect on either 4E-BP1 or Akt Thr308 phosphorylation. However, the phosphorylation of eIF2α decreases quite considerably under these conditions (lanes 2-4 vs. lane 1). DAPH or A769662 treatment of cells did not elicit a dephosphorylation of 4E-BP1 under any assay conditions, and generally lead to a slight decrease in Akt Thr308 phosphorylation (lanes 9-14 vs. lane 8). The reason for the increase in Akt Thr308 phosphorylation in response to A769662 pus IR (lane 13) is unknown and was not reproducible (data not shown). As there was a high basal level of eIF2α phosphorylation in the control extract here, it was impossible to see whether there was any increase in phosphorylation; it certainly did not decrease to the levels observed with A769662 (lanes 12-14 vs. lane 8). MGMT protein levels are reduced in all treatments (lanes 9-12 and 14 vs. lane 8), again except the A769662 plus IR treatment (lane 13). These dramatic changes seen in MGMT protein levels in cells treated with all of the compounds are most likely different from previous results because the cells have been in the treatment plates for an extra 24 hours. Cytotoxicity assays were also difficult to execute in parallel to these experiments, as cells need to be grown in 96 well plates for the MTS assays, which can result in cells that are actively growing lacking space to grow and therefore becoming apoptotic. Because of this, the changes in MGMT levels, and the changes in eIF4A levels could be a result of cell death. The effects on MGMT protein levels are also reflected by the [^{35}S] methionine incorporation data from the same treatments. All of the compound combination treatments (again apart from the A769662 plus IR treatment) showed a large decrease in protein synthesis rates (80-95% inhibition) relative to the untreated cells. IR alone produced only a moderate inhibition of protein synthesis.

5.4 Summary

- KU0063794 inhibits cap dependent translation by inhibiting mTORC1 and mTORC2 signalling
- Whilst DAPH is inhibiting cap dependent translation (but not as effectively as KU0063794) it is also showing an effect on translation elongation and MGMT mRNA levels
- A769662 is not affecting mTOR signalling, or cap dependent translation. Although protein synthesis rates are increased, MGMT protein levels are reduced
- The compounds are not sensitising the cells to TMZ treatment, as there are still large amounts of MGMT protein within the cells. However, MGMT protein levels do stabilise in the presence of KU0063794, DAPH and A769662 when combined with TMZ compared to MGMT protein levels in cells treated with the compounds alone.

5.5 Conclusions

A769662 and DAPH, when used alone are successfully reducing levels of MGMT protein in T98G cells. However, the mechanism by which A769662 and DAPH are doing this is not immediately obvious, and will have to be explored further. MGMT protein levels are not affected to the same extent when any of the three compounds are combined with TMZ. These data indicate that the stability of the MGMT protein should be explored further. The experiment exploring the affect of IR alone and when combined with both the compounds and TMZ highlights another drawback (in addition to those mentioned earlier) with the MTS assay; the small plate size and hence the area available for cells to grow limits the duration of the experiments, especially with fast growing cells such as T98G cells.

Chapter VI

Exploring MGMT protein stability in T98G cells

6 *Exploring MGMT protein stability in T98G cells*

6.1 Aims

- To determine the half-life of the MGMT protein in T98G cells
- To investigate the stability of MGMT protein in the presence of KU0063794 versus KU0063794 and TMZ in T98G cells

6.2 Introduction

Temporarily inhibiting translation of MGMT as a means to improve the efficacy of chemotherapy relies on the MGMT protein having a manageable half life. The half life of MGMT protein had been previously recorded as 15-20 hours in a different cell type [261]. It was important to ascertain the half life of MGMT protein in T98G cells, to ensure that the combination treatments were being administered in the most effective time frame. The experiments described in this chapter were designed to inhibit the synthesis of MGMT in the cells and then monitor the turnover of MGMT protein by Western blotting at different times after incubation with or without KU0063794 and TMZ. These data would then give me important mechanistic information regarding how the compounds used here were affecting steady state MGMT protein levels.

6.3 Results

6.3.1 Cycloheximide inhibits protein synthesis in T98G cells

Temporarily inhibiting translation of MGMT as a means to improve the efficacy of chemotherapy relies on the MGMT protein having a manageable half life. The half life of MGMT protein had been previously recorded as 15-20 hours in a different cell type [261]. It was important to ascertain the half life of MGMT protein in T98G cells, to ensure that the combination treatments were being administered in the most effective time frame. As a first step, I had to determine which concentration of cycloheximide to use to inhibit protein synthesis in T98G cells without causing cell death. As shown in Figure 6.1A, at least 0.5μM was required to inhibit protein synthesis; cells were still viable at this time (data not

shown). To attempt to measure the half-life of MGMT, protein synthesis was inhibited with 10μM cycloheximide and cell extracts were prepared at different times. Western blotting was then used to monitor the steady state level of MGMT protein in these cells. Surprisingly, steady state levels of MGMT protein apparently increased at later times of incubation (Fig.6.1B); this was repeated a number of times (Panels C and D) with similar results. The reasons for this apparent increase in protein level, even though translation rates are inhibited (Panel A) were unclear.

6.3.2 Inhibition of mTOR signalling does not affect the half life of MGMT protein in T98G cells but stabilises MGMT in the presence of TMZ

As cycloheximide generated inconclusive results, I repeated the experiments using emetine, which also blocks translation elongation [262]. Cells were incubated in the presence of emetine alone at a level sufficient to totally block protein synthesis (data not shown; Fig.6.2A), or combined with KU0063794 (Panel B), TMZ (Panel C), or KU0063794 and TMZ together (Panel D). Cell extracts were resolved by SDS-PAGE and MGMT levels visualised by Western blotting. Fig 6.2A shows that MGMT protein is relatively stable in T98G cells, with a half-life of approximately 60 hours (quantified in Panel E). This is unchanged when cells are also incubated in the presence of KU0063794 (Panels B and E). However, incubation of cells with TMZ reduces the half-life of MGMT in T98G cells to less than 12 hours (Panels C and E). This most likely reflects the fact that MGMT is required for the repair of DNA damage induced by TMZ and subsequently being proteolysed; as emetine is entirely blocking protein synthesis, MGMT is unable to be re-synthesised to maintain steady state levels (Panel C). Interestingly, inhibition of mTOR signalling with KU0063794 combined with emetine and TMZ restored steady state levels of MGMT when added to cells (Panel D).

6.4 Summary

- The half-life of the MGMT protein in T98G cells is just under 72 hours

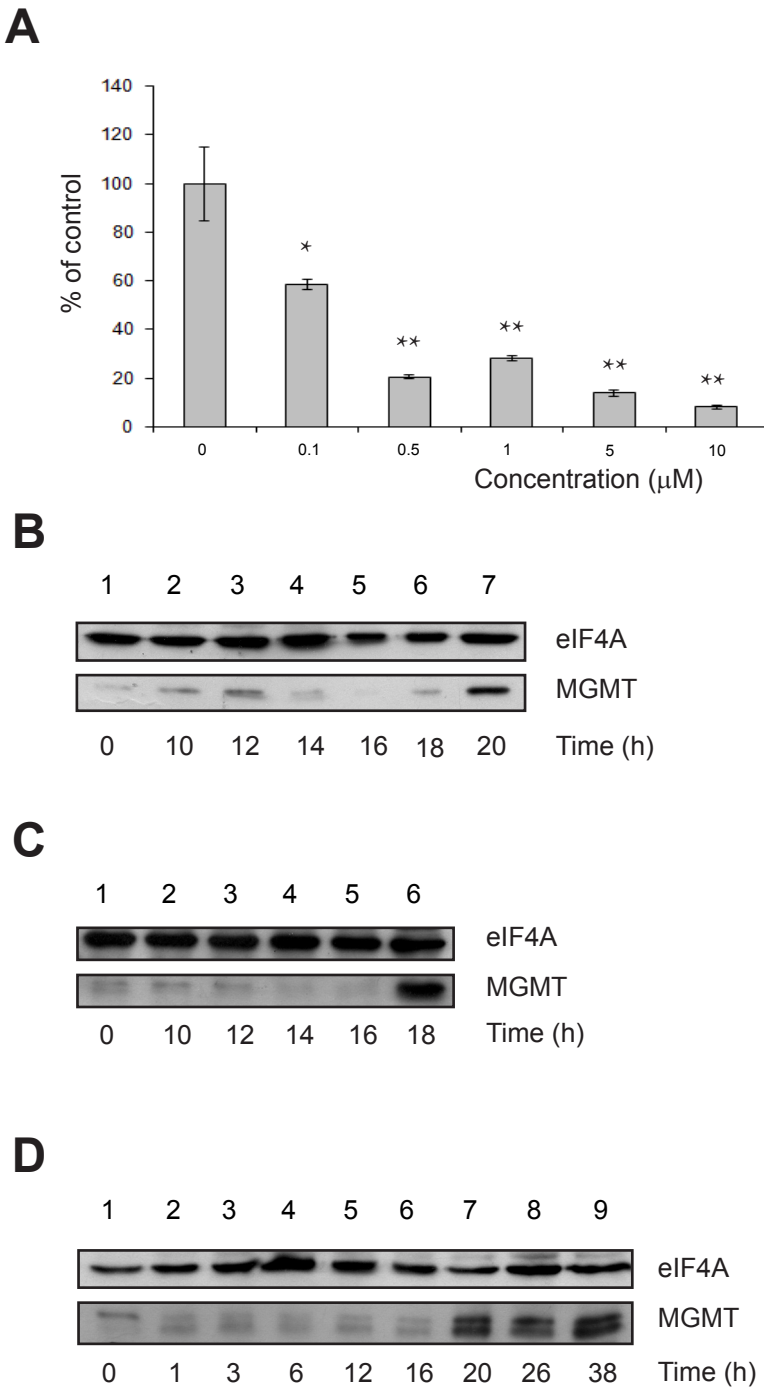

Figure 6.1 Cycloheximide inhibits protein synthesis in T98G cells

Panel A. T98G cells were treated with different concentrations of cycloheximide for 24 hours and one hour prior to harvesting, cells were incubated with 10μCi/ml [^{35}S] methionine, as described in Materials and Methods. Extracts were prepared and incorporation of radioactive methionine into protein determined as cpm/μg protein; results are presented as a % of the rate obtained in cells incubated in the absence of cycloheximide. Error bars are the S.D (n=3). A standard T Test was performed and p values were assigned limits where *<0.05, **<0.005 and ***<0.001. **Panel B.** Cells were incubated in the absence (lane 1) or presence of 10μM cycloheximide (lanes 2-7) for 24 hours. Extracts were prepared and aliquots containing 10μg of protein were resolved by SDS-PAGE and proteins visualised by Western blotting using the antisera indicated. **Panel C, D.** Cells were treated as in **(B)** and incubated for the times indicated.

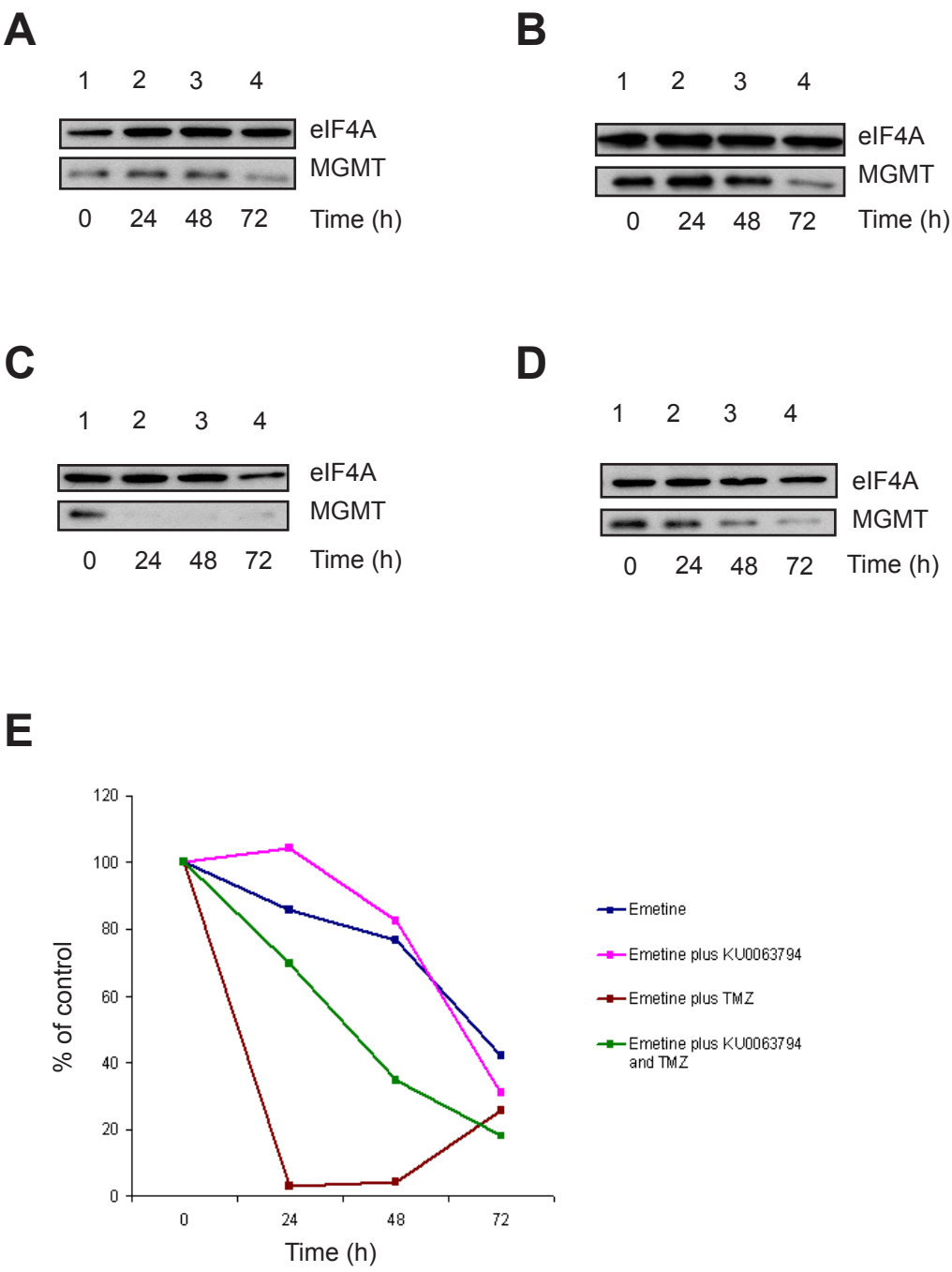

Figure 6.2 Inhibition of mTOR signalling does not affect the half life of MGMT protein in T98G cells but stabilises MGMT in the presence of TMZ

Panel A. T98G cells were incubated in the absence (lane 1) or presence of 10μM emetine alone for up to 72 hours (lanes 2-4) Cells were also incubated in the absence or presence of 10μM KU0063794 and 10μM emetine **(Panel B)**,10μM TMZ and 10μM emetine **(Panel C)** or 10μM KU0063794 and10μM TMZ and 10μM emetine **(Panel D)**. Extracts were prepared and aliquots containing 10μg of protein were resolved by SDS-PAGE and proteins visualised by Western blotting using the antiserum indicated (n=2). **Panel E.** Data shown in Panels A-D was quantified using Image J software and the steady state level of MGMT protein expressed relative to eIF4A, with levels in untreated cells set at 100%.

- KU0063794 is having a stabilising effect on the MGMT protein when used to treat cells in combination with TMZ

6.5 Conclusions

These experiments clearly show that MGMT protein is relatively stable in T98G cells, with a half-life of approximately 60 hours (quantified in Fig.6.2E). In contrast to findings with TMZ, rates of MGMT turnover were unchanged when cells were incubated in the presence of KU0063794. However, when used in combination with TMZ, KU0063794 had a negative effect on MGMT protein levels and inhibited the turnover of the protein. How this stabilisation occurs remains unclear and should be the focus of more research, as MGMT can prevent successful chemotherapy. Ideally, I would also liked to have measured the synthesis rates of MGMT under these assays conditions as well. However, the titre of the commercial antisera was insufficient to allow for immunoprecipitation of the MGMT protein following pulse labelling of cells with [^{35}S] methionine (data not shown).

Chapter VII

Discussion

7 Discussion

7.1 The chemicals derived from connectivity mapping effected the T98G cells in different ways

The initial aim of my research was to use compounds to temporarily down-regulate MGMT protein synthesis in T98G cells, whilst remaining non-toxic to the cells. This down-regulation of MGMT protein would then create a window of opportunity to treat the cells with the DNA methylating agent, TMZ. The cells lacking MGMT would not be able to repair the damage caused by TMZ and so the cells should acquire double-strand DNA breaks, arrest in the G2 phase of the cell cycle and undergo apoptosis.

T98G cells were used as they over-express MGMT relative to other GBM cell lines [258,259]. This was important as it gave me a good platform to study MGMT protein levels and how they differed under a variety of treatment regimes. It is important to take in to account that the some characteristics of high grade glioma cells are unusual, due to genetic aberrations such as loss of p53 and PTEN function, as well as EGFR amplifications [65–67], which could cause compounds to have unusual effects in these cells, that may not have been observed in other cell types.

It was important before beginning treatments, to ensure complete cell lysis was effective, so as to get results during Western blotting that reflected protein levels in the whole cell. When using an additional detergent in the lysis buffer, there was not an increase in the recovery of MGMT protein (Fig.3.4). This may be due to the T98G cells having weak nuclear membranes, causing the nuclei to leak or rupture easily during the lysis procedure, even without detergent.

The initial drug treatments that I trialled were; direct inhibitors of mTOR kinase activity (Torin1), mTORC1 complex inhibitors (rapamycin), or upstream regulators of mTORC1 signalling (PI103, LY294002). Rapamycin inhibits mTORC1 by forming a complex with FKBP12 which then binds to mTORC1 and interacts with DEPTOR. Rapamycin inhibited protein synthesis in T98G cells at 10μM levels (Fig.3.5B) and inhibited cell growth compared to untreated cells over a 24 hour period (Fig.3.5C). However, Western blotting showed no effect of

rapamycin on the phosphorylation status of 4E-BP1 and so the observed effect of cell growth was unlikely to be a result of efficient inhibition of cap-dependent translation initiation. It is possible that rapamycin was also inhibiting protein synthesis via the phosphorylation of eIF2α, as an increase was seen during incubation of cells with rapamycin (Fig.3.2A). It has also been suggested that mTORC1 interacts with GCN2, and inhibition of mTORC1 results in the activation of GCN2, which in turn phosphorylates eIF2α [263,264], thereby inhibiting protein synthesis.

Torin 1 is a small molecule kinase inhibitor that directly inhibits mTOR function [245]. It is therefore not surprising that a dephosphorylation of 4E-BP1 was observed after a 24 hour incubation of cells with Torin 1 and that protein synthesis was decreased by 80% (Student's t-test, $p<0.001$), indicating a definite inhibition of signalling through mTORC1. Although both LY294002 and PI103 are PI3K inhibitors, they differ in their relative selectivity. LY294002 is specific for PI3K [242] but it will inhibit mTOR at high concentrations; PI103 is not as specific as LY294002, in addition to mTOR, it also inhibits DNAPK [243]. Due to the hyperactivity of PI3K signalling in T98G cells occurring from the loss of PTEN function [265,266], high doses of LY294002 were needed to inhibit signalling through mTORC1 (Fig.3.6A) and reduce levels of protein synthesis (Fig.3.9B). The broad inhibition of kinases in T98G cells incubated with PI103 was not desirable, as high concentrations were needed to inhibit mTORC1 signalling (Fig.3.7 A), and this resulted in cell cytotoxicity (Fig.3.9C).

The initial drug treatments outlined that an effective compound for inhibiting the mTOR pathway would need to inhibit PI3K signalling. With this in mind, the connectivity mapping algorithm was employed to find compounds that could inhibit this pathways, without affecting non-specific targets. I used gene signatures derived from rapamycin, LY294002 and custom gene list expression profiles to find similar compounds. Interestingly, as well as producing positive 'connections' to PI3K and RTK inhibitors (Fig.4.1), positive 'connections' were also found for dopamine (D_2) receptor antagonists, sodium channel blockers and corticosteroids. These classes of drugs recurred with the searches using

the KU0063794 and A769662 gene signatures (Fig.4.2), and using the patient-derived TMZ-resistant glioma data (Table 3.1). The dopamine receptor antagonists revealed by the connectivity mapping mostly consisted of the phenothiazene group of compounds. Although usually used as antipsychotics [255,267], a member of this class of compounds (thioridazine) has recently been re-popularised as a treatment for ovarian cancer [256]. It has been suggested that dopamine antagonists influence Akt/mTOR signalling through the inhibition of phosphorylation of both Akt and GSK3, effectively inhibiting mTORC1 signalling [268]. Corticosteroids have also been implicated in influencing mTOR signalling [269], but only in a positive manner, suggesting that steroid signalling/mTOR interactions have not been fully elucidated.

Each of the compounds that were identified from the connectivity mapping experiments had previously been implicated in interacting with proteins upstream of mTORC1. Resveratrol is a phytoalexin found in red grape skins and the roots of Japanese knotweed, that can activate AMPK in some cell types [270–272]. Even when T98G cells were incubated with resveratrol at high concentrations, no effect was observed on mTOR signalling (Fig.4.3Band C). However, a decrease in the number of cells in G1 phase of the cell cycle and an increase in cells in S phase was observed in cells incubated with resveratrol for 24 hours (Fig.4.3D). This S phase arrest has also been observed in SW480 cells [273], but the cause remains unclear.

Beta escin (also known as escin or aescin) is a triterpenoid saponin that has been isolated from the seed of the horse chestnut (*Aesculus hippocastanum*). It has been shown to exhibit anti-edematous, anti-inflammatory, and anti-carcinogenic properties in various disease models [274]. It has previously been shown to inhibit Jak/Stat signalling in hepatocellular carcinoma cells through the inhibition of Jak 1/2 and Stat3 [247]. This is interesting as the activation of Jak can phosphorylate PI3K, therefore propagating signalling through the PI3K/mTOR signalling pathway. However, during incubation with T98G cells, beta escin was observed to be extremely toxic, even at low doses (Fig.4.4), making it unsuitable for use in this circumstance, due to its cytotoxic and non

specific effects. Thalidomide is a derivative of glutamic acid that is a well characterised anti-emetic that caused undesirable and unpredicted teratogenic effects in unborn babies during the 1970's and was therefore withdrawn from pharmaceutical use. This compound has recently been re-discovered as an effective treatment for multiple myeloma [275], and also displays anti-angiogenic and anti-inflammatory properties [276]. The anti-angiogenic properties of thalidomide are thought to result from an inhibition of VEGF and FGF receptors [277]; it is for this reason that this compound was of interest. Interestingly, although inhibition of specific types of RTK has been demonstrated by thalidomide in other cell types, thalidomide seemed to have little or no effect on the T98G cells, even at high concentrations. This was not only true for MGMT levels in the T98G cells, but also 4E-BP1 phosphorylation but also for the methionine incorporation assays; when compared to untreated controls, the rate of methionine incorporation into protein did not vary in cells incubated with thalidomide (Fig.4.8B). These results could be reflecting that the main RTK mutations in T98G cells are in EGFR and PDGFR (Fig.1.4), and that it is these receptors that need to be inhibited specifically.

Thioridazine is a phenothiazene that has been widely used as an anti-psychotic for many years [255]. In endometrial and cervical cell lines, new research suggests that thioridazine effectively inhibits the PI3K/Akt/mTOR signalling pathways [256], introducing the possibility that it could be used as a novel anticancer agent. Thioridazine could be affecting the PI3K/Akt/mTOR signalling pathway in these cells through the inhibition of the $D_{2/3}$ dopamine receptors. As mentioned before, mTOR signalling can be inhibited by $D_{2/3}$ antagonists by preventing the phosphorylation of both Akt and GSK3, therefore inhibiting mTORC1 signalling [268]. However, in contrast with the results observed in other cell lines, T98G cells incubated with thioridazine showed no inhibition of PI3K/mTOR signalling at a variety of times of incubation and concentrations. There was a decrease in methionine incorporation into protein compared to untreated controls, suggesting an inhibition of protein synthesis. This could be accounted for by the increase in eIF2α phosphorylation that was

observed in parallel to the inhibition of protein synthesis (Fig.4.9). The phosphorylation of eIF2α may have been a resultant factor of ER stress brought about by thioridazine, which has also been recently observed in other cell lines [278]. ER stress can activate PERK, by the sequestering of the regulatory chaperone GRP78 (BiP), which is usually bound to the ER lumen domain of the eIF2 kinase, PERK. During cell stress, GRP78 binds preferentially to misfolded proteins over the PERK ER domain. This allows PERK to homo-dimerise, resulting in the phosphorylation and activation of the PERK cytoplasmic kinase domain. This is then capable of phosphorylating the alpha subunit of eIF2, resulting in the stabilisation of the eIF2α-GDP-eIF2B complex, therefore inhibiting formation of the initiation ternary complex, and the ribosomal recruitment to mRNA which follows.

Each of the compounds derived from the connectivity mapping database either directly or indirectly were incubated with T98G cells in different concentrations for different amounts of time. This allowed me to monitor the cells in different contexts, which gave me a broad overview of how the compounds were affecting the cells. Based on these initial observations I had to narrow down the compounds to a manageable amount. I used KU0063794 as a positive control throughout my work as this was useful as a reference, but it also produced some very interesting results. Figure 7.2 summarises how each of the four final compounds could be affecting the mTOR signalling pathway.

The connectivity mapping database showed positive connections to a lot of AMPK activators, such as resveratrol, so I also used a direct AMPK activator as this fulfilled the criteria of affecting both PI3K signalling and mTOR signalling through activation of TSC1/2 (Fig.7.2). DAPH was the only compound which was directly predicted through the connectivity mapping technique, which I chose to continue. This was due to it being a receptor tyrosine kinase inhibitor, specific for EGFR, a truncated form of which is known to be specifically over-expressed in GBM. The inhibition of EGFR also inhibits signalling through the PI3K/mTOR and ERK1/2 signalling pathways. TMZ was also used in

combination with these compounds, and alone, to identify if the compounds were in fact sensitising the cells to TMZ through inhibition of MGMT.

A769662 is a compound in the thienopyridone family of drugs, that has been shown to activate AMPK both via allosteric binding to the γ subunit, and through phosphorylation of the β subunit [279]. Contrary to the expected inhibitory effect of A769662 on protein synthesis, I observed an increase in p70S6K Th389 and Akt Thr308 phosphorylation accompanied with a lack of 4E-BP1 dephosphorylation. These data suggested that no inhibition of the mTOR signalling pathway was taking place (Fig.4.5E). The protein synthesis data, polysome profiles and m^7GTP-Sepharose assays all supported this observation further and actually suggested an increase in cellular protein synthesis in the presence of A769662. These observations were also seen in U87-MG cells which lack MGMT protein, making it unlikely that the mechanism of action is entirely cell line specific. The most interesting effect that A769662 displayed in my work was its ability to inhibit eIF2α phosphorylation in nutrient deprived cells (Fig.5.8). During a 72 hour incubation of cells with both TMZ and γ ray exposure, all cells, including untreated controls, displayed an elevated phosphorylation of eIF2α. This increase in phosphorylation could have been caused by amino acid deprivation, as the cells were incubated in the same media for an extended amount of time. However, the cells that were also incubated with A769662 did not show this increased level of phosphorylation. This leads me to speculate that A769662 causes an increase in mitochondrial function and therefore ATP production. This would account for the positive effect observed in mTOR signalling, and the increased rates of methionine incorporation into protein. The unexpected effect on protein synthesis could be due to phosphorylated AMPK simultaneously triggering mitophagy and the biogenesis of new mitochondria, via the activation of PGC1α, which is then responsible for the transcription of mitochondrial genes [280].

DAPH is an RTK inhibitor that shows specificity for EGFR. It has also been shown to effectively reverse fibril formation and therefore reduce the neurotoxic effects often associated with Alzheimer's disease [281]. Incubation of T98G and

U87-MG cells with DAPH resulted in a slight, yet definite decrease in mTOR signalling, and increased levels of 4E-BP1 dephosphorylation. Interestingly there was also an 80% (Student's t-test, $p<0.005$) decrease in methionine incorporation into protein in T98G cells compared to untreated T98G cells. However, the polysome analysis of cells incubated with DAPH for 24 hours indicated a minimal loss of polysomes and a slight increase in 80S monosomes. The presence of polysomes even with the massive decrease in translation rates could possibly indicate ribosome stalling. Eukaryotic elongation factor 2 (eEF2) has been shown to catalyse the translocation of peptidyl-tRNA from the A site to the P site on the ribosome. It has been shown that phosphorylation of eEF2 at Thr56 by eEF2 kinase inhibits its activity [282–285] and therefore causes ribosome stalling. eEF2 can be dephosphorylated by mTORC1 signalling through eEF2 kinase. Therefore the inhibition of mTORC1 could allow for eEF2 phosphorylation and promote ribosome stalling. In addition to an elongation block, the increase in 80S monosomes is also indicative of a slight initiation block, which is supported by the dephosphorylation of 4E-BP1.

TMZ is a methylating agent that creates methyl adducts on DNA, eventually leading to replication fork collapse and double-strand DNA breaks. The halting of the cell cycle in response to TMZ is primarily through p53 signalling, which prevents CDK1/cyclin b complex formation and progression through the cell cycle. However, cell cycle arrest was not observed in T98G cells incubated with TMZ. This could be due to the lack of p53 in T98G cells due to a deletion mutation, which is found in 38% of GBM tumours (Fig.1.4). Overall incubation with TMZ alone had little effect on the T98G cells or the U87-MG cells, clearly indicating that alone, this is not an effective treatment.

7.2 MGMT protein stability

KU0063794 directly inhibits the kinase activity of mTOR and therefore inhibits the activity of both the mTORC1 and mTORC2 complexes (Fig.7.2). The effect of KU0063794 on the mTOR signalling pathway is noticeable by both its dramatic reduction in translation rates and the massive dephosphorylation of

4E-BP1 that it causes. However, it was of significant interest that during long incubation periods with KU0063794, levels of MGMT protein did not decrease. This prompted questions about the half-life of the MGMT protein (and its stability) in T98G cells. To determine the half-life of the protein, cells were incubated with both the compound and the antibiotic, cycloheximide, which inhibits translation elongation. When MGMT protein levels were measured by Western blotting, there was an apparent dramatic rise in MGMT protein levels at around 20 hours of incubation with the compound. The cell cycle of T98G cells is also around 20 hours long, suggesting that the increase in MGMT could have been due to the proliferation of cells as a result of lack of inhibition by cycloheximide. During the incubation of T98G cells with cycloheximide, a shift in MGMT protein size was also seen. Phosphorylation of MGMT at the Ser204 position has been observed in liver cells and this phosphorylation has been shown to protect the protein from proteolytic digestion [286]. It is possible therefore, that the shift seen in the Western blotting experiments may be due to the phosphorylation and hence stabilisation of this protein. Further work would be needed to investigate whether this was the case here.

7.3 MGMT translational regulation

In line with effects on translation initiation, polysome profile analysis of cells treated with KU0063794 showed a stark reduction in actively translating polysomes. Although some ribosomes were still actively involved in translation, it was a massive reduction compared to untreated cells. This could indicate that MGMT protein is being preferentially translated in the remaining polysomes, a suggestion that becomes more interesting when looking at the structure of the MGMT mRNA. MGMT mRNA has a very long 3' UTR, which contains 3 possible stem loop structures (Fig.7.1). It has been shown previously that some mRNAs are translationally controlled by 3' stem loop structures [287], so it is possible that this is also the case for MGMT mRNA. To investigate if this could be the case, quantitative RT-PCR was carried out on the fractions obtained from the polysome profile analysis. The fractions were pooled into 4 categories, free

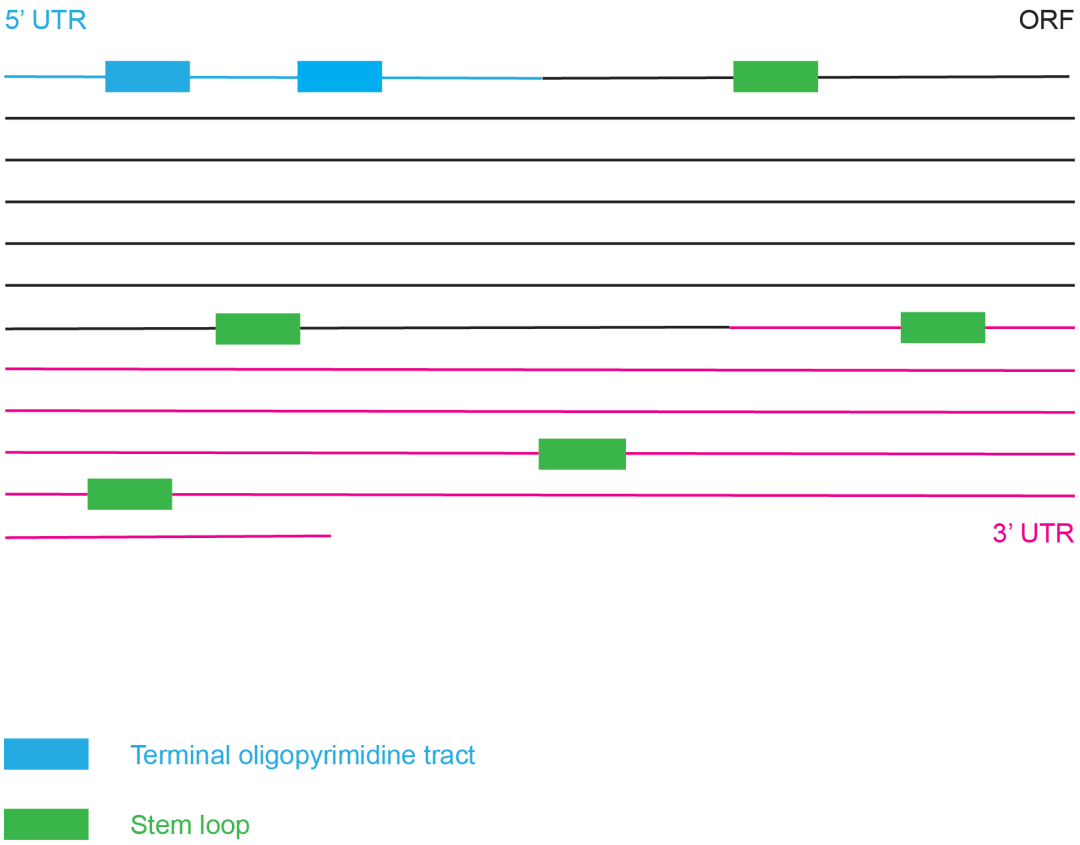

Figure 7.1 Diagram representing putative MGMT mRNA structural and regulatory elements

The mature mRNA sequence for MGMT was entered in to RegRNA, a regulatory RNA motif and elements finder (developed by *Huang et al.*, 2006). Possible structures were then identified by the program. The diagram illustrates secondary structures and motifs that may be of interest in future work.

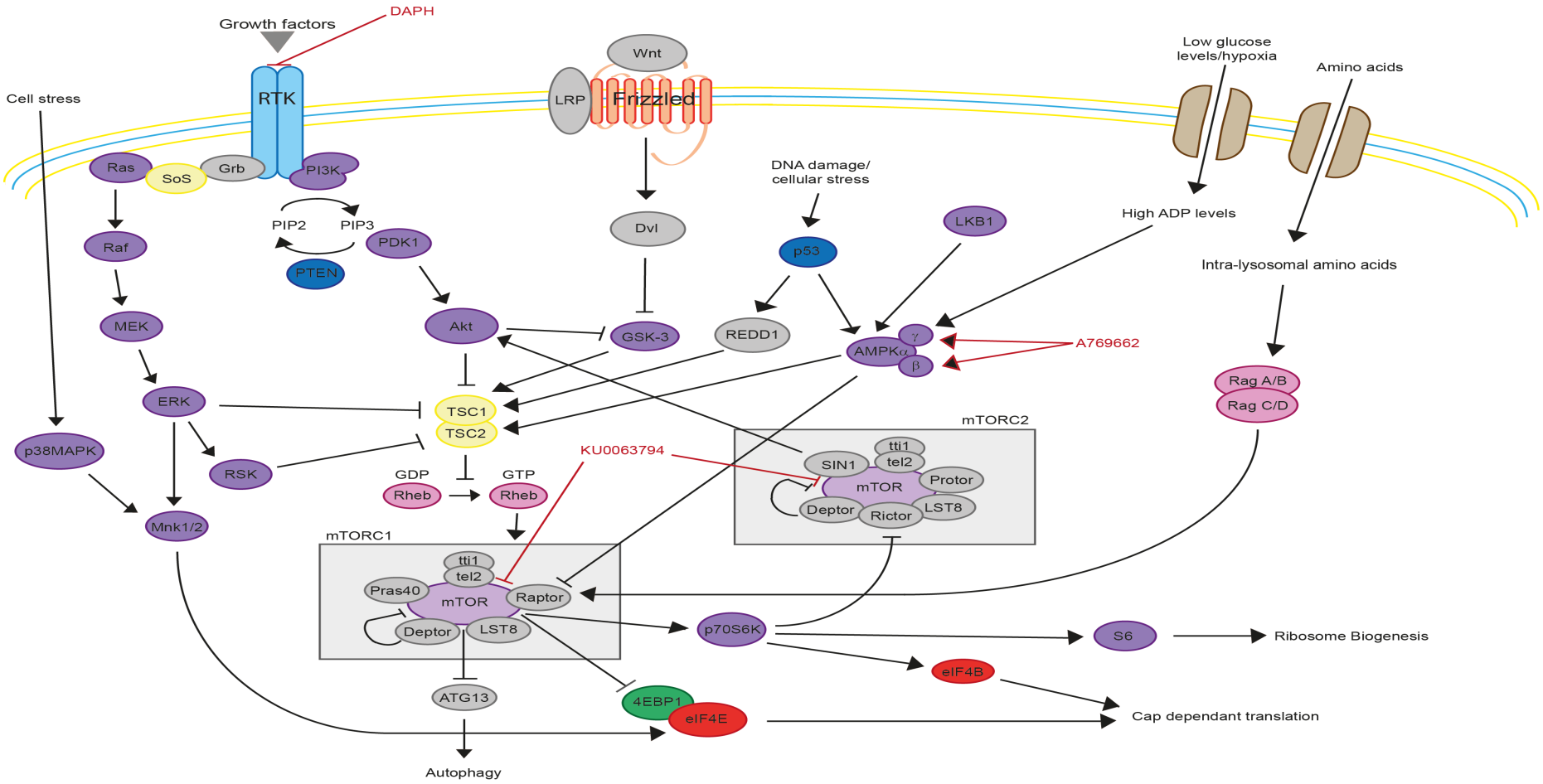

Figure 7.2 Schematic representation of mTOR signalling pathway and associated proteins

How the different compounds are possibly interacting with the mTOR signalling pathway in T98G cells.

material, subunits, light polysomes and heavy polysomes. As there are large variations in the amount of RNA in each of these fractions, a standard normalisation technique involving the expression of an abundant mRNA was not possible (as was previously performed). Instead, I wanted to measure the shift in MGMT mRNA between fractions, and compare that to the shift of a common and abundant mRNA, GAPDH. It is important to note that although the amount of RNA in each fraction changed between treatments, the total amount of RNA across each gradient was similar, except for the amount of RNA in the cells incubated with A769662, which showed an increase in total RNA concentration. The qRT-PCR results displayed extremely interesting results, showing that MGMT mRNA was present in heavy polysomes during incubation with each compound. This observation was especially interesting for T98G cells incubated with KU0063794 for 24 hours, as the amount of translating ribosomes were greatly reduced compared to untreated cells, and GAPDH mRNA was present in reduced amounts in both polysome fractions, and an increase was seen in the subunit fractions. This shift in mRNA reinforces the suspected reduction in actively translating ribosomes due to a block in initiation; secondary effects could also reflect a possible reduction in ribosome biogenesis. However, during these reduced translation rates in KU0063794 treated cells, MGMT mRNA was still present at similar amounts to untreated cells in both heavy and light polysomes, suggesting that it is in fact still being translated. An alternative possibility if that the mRNA is present in stalled complexes or that it is present in a protected form, such as a stress granule or a P body. As well as translational regulation of the MGMT mRNA, protein expression could also be influenced by transcription factor expression, miRNAs and methylation or acetylation of the MGMT promoter.

7.4 Future work

This work highlights the importance of understanding the stability and regulation of DNA repair proteins when considering approaches to cancer

therapy. Understanding types of regulation is the only way a multifaceted approach can be developed to modulate such proteins in the future.

The methylation of the MGMT promoter is by far the most commonly mentioned type of regulation of MGMT protein expression [55,56,58,65,288–290], yet this is not the only form. As mentioned in the section on protein expression, alternative splicing of the pre-mRNA may also play a part in the post-transcriptional regulation of MGMT. However, although alternative predicted mRNA isoforms exist, regulation of MGMT at this level has not been fully explored and generally lacks support in the scientific community [57]. I explored the possibility that during reduced cap dependent translation, MGMT mRNA is preferentially translated. Although I showed that MGMT mRNA remains in polysomes during translation inhibition, these experiments need to be further repeated. An EDTA control would also need to be performed to ensure that the MGMT mRNA quantified was indeed in polysomes and not in a protected form, such as an intracellular vesicle, P body or associated with a high molecular weight protein complex.

The stability of a protein is also a very important factor to consider when attempting to regulate its expression and/or degradation. During my research I observed a shift in the size of MGMT protein during Western blot analysis. Previous research suggests that this shift in size could be the result of cleavage of the C-terminus of the MGMT protein [286]. Both cleavage and phosphorylation of the MGMT protein have been suggested to increase its resistance to proteolytic digestion [286]. However, this research is poorly documented, and experiments directed at investigating this phenomenon should be carried out. This could be investigated further using an antibody that is raised against the C-terminus of the MGMT protein, and also by creating a specific antibody for MGMT to study phosphorylation of the protein. Another way of investigating the cleavage of the protein and ascertaining if this cleaved form is present natively in cells would be to examine both an uncleaved MGMT protein, and an artificially created MGMT protein lacking a C-terminus using X-ray crystallography. Anan antibody could then be created that can only bind the

MGMT isoform that lacks a C-terminus. This antibody could then be used to study the stability of the protein, and if this changes during cell treatments outlined in this thesis.

During my research, I used immortalised cell lines to study MGMT levels and signalling pathways in GBM cells. However, there are marked differences in the control of MGMT protein expression observed between clinical specimens and cell lines, and this highlights the pitfalls of translating a cell line phenomenon into a clinical procedure. As GBM cells are so heterogeneous, it would be extremely interesting to ascertain the effect that chemical compounds, including PI3K/mTOR signalling inhibitors had on primary cells derived from brain tumours. Considering each cell in the GBM population could theoretically express a different level of MGMT protein and have different underlying mutations, this could be of considerable value to determine the percentage of cells that could be sensitised to treatment, or not. The use of the compounds *in vivo* would also be useful to determine their efficacy in sensitising cells to TMZ. However, this would be complicated as obtaining ethics for experimental studies involving human subjects, especially those that could be seen to be physically and/or emotionally vulnerable is difficult.

When screening different chemical compounds for their effect on specific proteins, high throughput methods could be extremely helpful. Antibody conjugated fluorescent assays are now available that can quantify the amount of many proteins in one sample in parallel. This minimises the need for the quantification of Western blots, and the need for carrying out multiple identical experiments with cell treatments to measure different protein phosphorylation states and levels.

These are just some of the avenues that could be explored to clarify the role of MGMT outside of its direct mechanism of action, which would be necessary to fully understand its regulation, and hence modulate it for therapeutic applications.

7.5 Conclusions

The research presented here shows that regulating MGMT protein levels through the inhibition of cap dependent translation using mTOR inhibitors is not as effective as hypothesised. Signalling pathways, MGMT stability and genetic mutations, all vary from one cell type to another. Therefore when tackling a heterogeneous disease such as GBM, the treatments need to be carefully tailored to the cell type, and the specific mutations most commonly seen in that disease state need to be taken in to account. It is because of this that the only way to tackle a disease that shows a plethora of aberrations is through a combination of therapies, including ionising radiation, TMZ chemotherapy, inhibition of hyperactive PI3K/Akt/mTOR signalling and inhibition of amplified RTKs. This research also shows how important it is to identify how DNA repair enzymes are transcribed and translated, as only then can they be manipulated to aid in cancer treatment, instead of creating a barrier between treatment and successful cancer elimination. This research also highlights the importance of genetic profiling of tumours, to identify the most abundant cell types and mutations within a tumour, to have the best chance of finding an effective treatment.

8 Bibliography

1 Rachet, B., Mitry, E., Quinn, M. J., Cooper, N. and Coleman, M. P. (2008) Survival from brain tumours in England and Wales up to 2001. Br. J. Cancer **99 Suppl 1**, S98–101.

2 Louis, D. N., Ohgaki, H., Wiestler, O. D., Cavenee, W. K., Burger, P. C., Jouvet, A., Scheithauer, B. W. and Kleihues, P. (2007) The 2007 WHO classification of tumours of the central nervous system. Acta Neuropathol. **114**, 97–109.

3 Dohrmann, G. J., Farwell, J. R. and Flannery, J. T. (1976) Glioblastoma multiforme in children. J. Neurosurg., Journal of Neurosurgery Publishing Group **44**, 442–448.

4 Bonavia, R., Inda, M.-M., Cavenee, W. K. and Furnari, F. B. (2011) Heterogeneity maintenance in glioblastoma: a social network. Cancer Res. **71**, 4055–60.

5 (2008) Comprehensive genomic characterization defines human glioblastoma genes and core pathways. Nature **455**, 1061–8.

6 Scottish Government, S. A. H. R. R. E. E. 3DG T. 556 8400 ceu@scotland. gsi. gov. u. (2002, May 30) Scottish Referral Guidelines for Suspected Cancer , Scottish Government, St. Andrew's House, Regent Road, Edinburgh EH1 3DG Tel:0131 556 8400 ceu@scotland.gsi.gov.uk.

7 Batchelor, T. T., Sorensen, A. G., di Tomaso, E., Zhang, W.-T., Duda, D. G., Cohen, K. S., Kozak, K. R., Cahill, D. P., Chen, P.-J., Zhu, M., et al. (2007) AZD2171, a Pan-VEGF Receptor Tyrosine Kinase Inhibitor, Normalizes Tumor Vasculature and Alleviates Edema in Glioblastoma Patients. Cancer Cell **11**, 83–95.

8 Selby, R. (1994) The surgical treatment of cerebral glioblastoma multiforme: an historical review. J. Neurooncol. **18**, 175–182.

9 Kirk, E. A., Howard, V. C. and Scott, C. A. (1995) Description of Posterior Fossa Syndrome in Children After Posterior Fossa Brain Tumor Surgery. J. Pediatr. Oncol. Nurs. **12**, 181–187.

10 KERNOHAN, J. W. and MABON, R. F. (1949) A simplified classification of the gliomas. Proc. Staff Meet. Mayo Clin. **24**, 71–5.

11 Wallace, C., Forsyth, P. and Edwards, D. (1996) Lymph node metastases from glioblastoma multiforme. AJNR Am. J. Neuroradiol. **17**, 1929–1931.

12 Adamson, C., Kanu, O. O., Mehta, A. I., Di, C., Lin, N., Mattox, A. K. and Bigner, D. D. (2009) Glioblastoma multiforme: a review of where we have been and where we are going. Expert Opin. Investig. Drugs **18**, 1061–83.

13 Stupp, R., Mason, W. P., van den Bent, M. J., Weller, M., Fisher, B., Taphoorn, M. J. B., Belanger, K., Brandes, A. A., Marosi, C., Bogdahn, U., et al. (2005) Radiotherapy plus Concomitant and Adjuvant Temozolomide for Glioblastoma. N. Engl. J. Med., Massachusetts Medical Society **352**, 987–996.

14 Duffau, H. (2006) New concepts in surgery of WHO grade II gliomas: functional brain mapping, connectionism and plasticity--a review. J. Neurooncol. **79**, 77–115.

15 Duffau, H. (2005) Lessons from brain mapping in surgery for low-grade glioma: insights into associations between tumour and brain plasticity. Lancet Neurol. **4**, 476–486.

16 Newlands, E. S., Blackledge, G. R., Slack, J. a, Rustin, G. J., Smith, D. B., Stuart, N. S., Quarterman, C. P., Hoffman, R., Stevens, M. F. and

Brampton, M. H. (1992) Phase I trial of temozolomide (CCRG 81045: M&B 39831: NSC 362856). Br. J. Cancer **65**, 287–91.

17 Rottenberg, D. A., Ginos, J. Z., Kearfott, K. J., Junck, L., Dhawan, V. and Jarden, J. O. (1985) In vivo measurement of brain tumor pH using [11C]DMO and positron emission tomography. Ann. Neurol. **17**, 70–9.

18 Marchesi, F., Turriziani, M., Tortorelli, G., Avvisati, G., Torino, F. and De Vecchis, L. (2007) Triazene compounds: mechanism of action and related DNA repair systems. Pharmacol. Res. **56**, 275–87.

19 Ogawa, K., Hiraku, Y., Oikawa, S., Murata, M., Sugimura, Y., Kawamura, J. and Kawanishi, S. (2003) Molecular mechanisms of DNA damage induced by procarbazine in the presence of Cu(II). Mutat. Res. Toxicol. Environ. Mutagen. **539**, 145–155.

20 Wang, L. G., Liu, X. M., Kreis, W. and Budman, D. R. (1999) The effect of antimicrotubule agents on signal transduction pathways of apoptosis: a review. Cancer Chemother. Pharmacol. **44**, 355–61.

21 Westphal, M., Hilt, D. C., Bortey, E., Delavault, P., Olivares, R., Warnke, P. C., Whittle, I. R., Jääskeläinen, J. and Ram, Z. (2003) A phase 3 trial of local chemotherapy with biodegradable carmustine (BCNU) wafers (Gliadel wafers) in patients with primary malignant glioma. Neuro. Oncol. **5**, 79–88.

22 Ferguson, S. D., Foster, K. and Yamini, B. (2007) Convection-enhanced delivery for treatment of brain tumors. Expert Rev. Anticancer Ther. **7**, S79–85.

23 Kyrtopoulos, S. A., Anderson, L. M., Chhabra, S. K., Souliotis, V. L., Pletsa, V., Valavanis, C. and Georgiadis, P. (1997) DNA adducts and the mechanism of carcinogenesis and cytotoxicity of methylating agents of

environmental and clinical significance. Cancer Detect. Prev. **21**, 391–405.

24 Margison, G. P. and Santibáñez-Koref, M. F. (2002) O6-alkylguanine-DNA alkyltransferase: Role in carcinogenesis and chemotherapy. BioEssays, Wiley Subscription Services, Inc., A Wiley Company **24**, 255–266.

25 Li, G.-M. (2008) Mechanisms and functions of DNA mismatch repair. Cell Res. **18**, 85–98.

26 Mojas, N., Lopes, M. and Jiricny, J. (2007) Mismatch repair-dependent processing of methylation damage gives rise to persistent single-stranded gaps in newly replicated DNA. Genes Dev. **21**, 3342–55.

27 Chapman, J. R., Taylor, M. R. G. and Boulton, S. J. (2012) Playing the end game: DNA double-strand break repair pathway choice. Mol. Cell, Elsevier **47**, 497–510.

28 Lieber, M. R., Gu, J., Lu, H., Shimazaki, N. and Tsai, A. G. (2010) Nonhomologous DNA end joining (NHEJ) and chromosomal translocations in humans. Subcell. Biochem. **50**, 279–96.

29 Bachrati, C. Z. and Hickson, I. D. (2009) Dissolution of double Holliday junctions by the concerted action of BLM and topoisomerase IIIalpha. Methods Mol. Biol. **582**, 91–102.

30 Shiloh, Y. and Ziv, Y. (2013) The ATM protein kinase: regulating the cellular response to genotoxic stress, and more. Nat. Rev. Mol. Cell Biol., Nature Publishing Group **14**, 197–210.

31 Yang, J., Yu, Y., Hamrick, H. E. and Duerksen-Hughes, P. J. (2003) ATM, ATR and DNA-PK: initiators of the cellular genotoxic stress responses. Carcinogenesis **24**, 1571–80.

32 Sultana, R., Abdel-Fatah, T., Perry, C., Moseley, P., Albarakti, N., Mohan, V., Seedhouse, C., Chan, S. and Madhusudan, S. (2013) Ataxia telangiectasia mutated and Rad3 related (ATR) protein kinase inhibition is synthetically lethal in XRCC1 deficient ovarian cancer cells. PLoS One **8**, e57098.

33 Walker, J. R., Corpina, R. A. and Goldberg, J. (2001) Structure of the Ku heterodimer bound to DNA and its implications for double-strand break repair. Nature **412**, 607–14.

34 Hammarsten, O. (1998) DNA-dependent protein kinase: DNA binding and activation in the absence of Ku. Proc. Natl. Acad. Sci. **95**, 525–530.

35 Yaneva, M. (1997) Interaction of DNA-dependent protein kinase with DNA and with Ku: biochemical and atomic-force microscopy studies. EMBO J., European Molecular Biology Organization **16**, 5098–5112.

36 Momand, J., Zambetti, G. P., Olson, D. C., George, D. and Levine, A. J. (1992) The mdm-2 oncogene product forms a complex with the p53 protein and inhibits p53-mediated transactivation. Cell **69**, 1237–45.

37 Oliner, J. D., Pietenpol, J. A., Thiagalingam, S., Gyuris, J., Kinzler, K. W. and Vogelstein, B. (1993) Oncoprotein MDM2 conceals the activation domain of tumour suppressor p53. Nature **362**, 857–60.

38 Haupt, Y., Maya, R., Kazaz, A. and Oren, M. (1997) Mdm2 promotes the rapid degradation of p53. Nature **387**, 296–9.

39 Honda, R., Tanaka, H. and Yasuda, H. (1997) Oncoprotein MDM2 is a ubiquitin ligase E3 for tumor suppressor p53. FEBS Lett. **420**, 25–7.

40 Kubbutat, M. H., Jones, S. N. and Vousden, K. H. (1997) Regulation of p53 stability by Mdm2. Nature **387**, 299–303.

41 Giles, J. (2004) Chemistry Nobel for trio who revealed molecular death-tag. Nature **431**, 729.

42 Pickart, C. M. (2001) Mechanisms underlying ubiquitination. Annu. Rev. Biochem. **70**, 503–33.

43 Dye, B. T. and Schulman, B. A. (2007) Structural mechanisms underlying posttranslational modification by ubiquitin-like proteins. Annu. Rev. Biophys. Biomol. Struct. **36**, 131–50.

44 Xu, P., Duong, D. M., Seyfried, N. T., Cheng, D., Xie, Y., Robert, J., Rush, J., Hochstrasser, M., Finley, D. and Peng, J. (2009) Quantitative proteomics reveals the function of unconventional ubiquitin chains in proteasomal degradation. Cell **137**, 133–45.

45 D, K. (2009) The emerging complexity of protein ubiquitination, Portland Press Ltd.

46 Shieh, S. Y., Ikeda, M., Taya, Y. and Prives, C. (1997) DNA damage-induced phosphorylation of p53 alleviates inhibition by MDM2. Cell **91**, 325–34.

47 Jin, P., Gu, Y. and Morgan, D. O. (1996) Role of inhibitory CDC2 phosphorylation in radiation-induced G2 arrest in human cells. J. Cell Biol. **134**, 963–70.

48 Christmann, M., Verbeek, B., Roos, W. P. and Kaina, B. (2011) O(6)-Methylguanine-DNA methyltransferase (MGMT) in normal tissues and tumors: enzyme activity, promoter methylation and immunohistochemistry. Biochim. Biophys. Acta **1816**, 179–90.

49 Ludlum, D. B. (1990) DNA alkylation by the haloethylnitrosoureas: Nature of modifications produced and their enzymatic repair or removal. Mutat. Res. Mol. Mech. Mutagen. **233**, 117–126.

50 Kitange, G. J., Carlson, B. L., Mladek, A. C., Decker, P. A., Mark, A., Wu, W., Grogan, P. T., Giannini, C., Ballman, K. V, Jan, C., et al. (2010) Evaluation of MGMT Promoter Methylation Status and Correlation with Temozolomide Response in Orthotopic Glioblastoma Xenograft Model **92**, 23–31.

51 Esteller, M., Hamilton, S. R., Burger, P. C., Baylin, S. B. and Herman, J. G. (1999) Inactivation of the DNA repair gene O6-methylguanine-DNA methyltransferase by promoter hypermethylation is a common event in primary human neoplasia. Cancer Res. **59**, 793–7.

52 Paz, M. F., Yaya-Tur, R., Rojas-Marcos, I., Reynes, G., Pollan, M., Aguirre-Cruz, L., García-Lopez, J. L., Piquer, J., Safont, M.-J., Balaña, C., et al. (2004) CpG Island Hypermethylation of the DNA Repair Enzyme Methyltransferase Predicts Response to Temozolomide in Primary Gliomas. Clin. Cancer Res. **10** , 4933–4938.

53 Lavon, I., Fuchs, D., Zrihan, D., Efroni, G., Zelikovitch, B., Fellig, Y. and Siegal, T. (2007) Novel mechanism whereby nuclear factor kappaB mediates DNA damage repair through regulation of O(6)-methylguanine-DNA-methyltransferase. Cancer Res. **67**, 8952–9.

54 BOCANGEL, D., SENGUPTA, S., MITRA, S. and BHAKAT, K. K. (2009) p53-Mediated Down-regulation of the Human DNA Repair Gene O6-Methylguanine-DNA Methyltransferase (MGMT) via Interaction with Sp1 Transcription Factor. Anticancer Res **29**, 3741–3750.

55 Everhard, S., Tost, J., El Abdalaoui, H., Crinière, E., Busato, F., Marie, Y., Gut, I. G., Sanson, M., Mokhtari, K., Laigle-Donadey, F., et al. (2009)

Identification of regions correlating MGMT promoter methylation and gene expression in glioblastomas. Neuro. Oncol. **11**, 348–56.

56 Van Nifterik, K. a, van den Berg, J., van der Meide, W. F., Ameziane, N., Wedekind, L. E., Steenbergen, R. D. M., Leenstra, S., Lafleur, M. V. M., Slotman, B. J., Stalpers, L. J. a, et al. (2010) Absence of the MGMT protein as well as methylation of the MGMT promoter predict the sensitivity for temozolomide. Br. J. Cancer, Nature Publishing Group **103**, 29–35.

57 Iatsyshyna, a. (2013) MGMT expression: insights into its regulation. 1. Epigenetic factors. Biopolym. Cell **29**, 99–106.

58 Ramakrishnan, V., Kushwaha, D., Koay, D. C., Reddy, H., Mao, Y., Zhou, L., Ng, K., Zinn, P., Carter, B. and Chen, C. C. Post-transcriptional regulation of O(6)-methylguanine-DNA methyltransferase MGMT in glioblastomas. Cancer Biomark. **10**, 185–93.

59 Alonso, M. M., Gomez-Manzano, C., Bekele, B. N., Yung, W. K. A. and Fueyo, J. (2007) Adenovirus-Based Strategies Overcome Temozolomide Resistance by Silencing the O6-Methylguanine-DNA Methyltransferase Promoter. Cancer Res. **67**, 11499–11504.

60 Assi, H., Candolfi, M., Baker, G., Mineharu, Y., Lowenstein, P. R. and Castro, M. G. (2012) Gene therapy for brain tumors: basic developments and clinical implementation. Neurosci. Lett., Elsevier Ireland Ltd **527**, 71–7.

61 Stewart, L. A. (2002) Chemotherapy in adult high-grade glioma: a systematic review and meta-analysis of individual patient data from 12 randomised trials. Lancet **359**, 1011–8.

62 Catlin, S. N., Busque, L., Gale, R. E., Guttorp, P. and Abkowitz, J. L. (2011) The replication rate of human hematopoietic stem cells in vivo. Blood **117**, 4460–6.

63 Batts, E. D., Maisel, C., Kane, D., Liu, L., Fu, P., O'Brien, T., Remick, S., Bahlis, N. and Gerson, S. L. (2007) O6-benzylguanine and BCNU in multiple myeloma: a phase II trial. Cancer Chemother. Pharmacol. **60**, 415–21.

64 Koch, D., Hundsberger, T., Boor, S. and Kaina, B. (2007) Local intracerebral administration of O(6)-benzylguanine combined with systemic chemotherapy with temozolomide of a patient suffering from a recurrent glioblastoma. J. Neurooncol. **82**, 85–9.

65 Lotfi, M., Afsharnezhad, S., Raziee, H. R., Ghaffarzadegan, K., Sharif, S., Shamsara, J., Lary, S. and Behravan, J. Immunohistochemical assessment of MGMT expression and p53 mutation in glioblastoma multiforme. Tumori **97**, 104–8.

66 Ruano, Y., Ribalta, T., de Lope, A. R., Campos-Martín, Y., Fiaño, C., Pérez-Magán, E., Hernández-Moneo, J.-L., Mollejo, M. and Meléndez, B. (2009) Worse outcome in primary glioblastoma multiforme with concurrent epidermal growth factor receptor and p53 alteration. Am. J. Clin. Pathol. **131**, 257–63.

67 Koul, D. (2008) PTEN signaling pathways in glioblastoma. Cancer Biol. Ther. **7**, 1321–5.

68 Shinji Kohsaka and Shinya Tanaka. (2013) Chemotherapeutic Agent for Glioma, Clinical Management and Evolving Novel Therapeutic Strategies for Patients with Brain Tumors. In Chemotherapeutic Agent for Glioma, Clinical Management and Evolving Novel Therapeutic Strategies for Patients with Brain Tumors (Dr. Terry Lichtor, ed.).

69 Christensen, J. G., Burrows, J. and Salgia, R. (2005) c-Met as a target for human cancer and characterization of inhibitors for therapeutic intervention. Cancer Lett. **225**, 1–26.

70 Fu, Z. and Tindall, D. J. (2008) FOXOs, cancer and regulation of apoptosis. Oncogene, Nature Publishing Group **27**, 2312–9.

71 Torti, D. and Trusolino, L. (2011) Oncogene addiction as a foundational rationale for targeted anti-cancer therapy: promises and perils. EMBO Mol. Med. **3**, 623–36.

72 Brown, E. J., Albers, M. W., Shin, T. B., Ichikawa, K., Keith, C. T., Lane, W. S. and Schreiber, S. L. (1994) A mammalian protein targeted by G1-arresting rapamycin-receptor complex. Nature **369**, 756–8.

73 Vézina, C., Kudelski, A. and Sehgal, S. N. (1975) Rapamycin (AY-22,989), a new antifungal antibiotic. I. Taxonomy of the producing streptomycete and isolation of the active principle. J. Antibiot. (Tokyo). **28**, 721–6.

74 Sehgal, S. N., Baker, H. and Vézina, C. (1975) Rapamycin (AY-22,989), a new antifungal antibiotic. II. Fermentation, isolation and characterization. J. Antibiot. (Tokyo). **28**, 727–32.

75 Laplante, M. and Sabatini, D. M. (2012) mTOR Signaling in Growth Control and Disease. Cell **149**, 274–293.

76 Kim, D.-H., Sarbassov, D. D., Ali, S. M., Latek, R. R., Guntur, K. V. P., Erdjument-Bromage, H., Tempst, P. and Sabatini, D. M. (2003) GbetaL, a positive regulator of the rapamycin-sensitive pathway required for the nutrient-sensitive interaction between raptor and mTOR. Mol. Cell **11**, 895–904.

77 Jacinto, E., Loewith, R., Schmidt, A., Lin, S., Rüegg, M. A., Hall, A. and Hall, M. N. (2004) Mammalian TOR complex 2 controls the actin cytoskeleton and is rapamycin insensitive. Nat. Cell Biol. **6**, 1122–8.

78 Peterson, T. R., Laplante, M., Thoreen, C. C., Sancak, Y., Kang, S. A., Kuehl, W. M., Gray, N. S. and Sabatini, D. M. (2009) DEPTOR is an mTOR inhibitor frequently overexpressed in multiple myeloma cells and required for their survival. Cell **137**, 873–86.

79 Kaizuka, T., Hara, T., Oshiro, N., Kikkawa, U., Yonezawa, K., Takehana, K., Iemura, S.-I., Natsume, T. and Mizushima, N. (2010) Tti1 and Tel2 are critical factors in mammalian target of rapamycin complex assembly. J. Biol. Chem. **285**, 20109–16.

80 Hara, K., Maruki, Y., Long, X., Yoshino, K., Oshiro, N., Hidayat, S., Tokunaga, C., Avruch, J. and Yonezawa, K. (2002) Raptor, a binding partner of target of rapamycin (TOR), mediates TOR action. Cell **110**, 177–89.

81 Kim, D.-H., Sarbassov, D. D., Ali, S. M., King, J. E., Latek, R. R., Erdjument-Bromage, H., Tempst, P. and Sabatini, D. M. (2002) mTOR interacts with raptor to form a nutrient-sensitive complex that signals to the cell growth machinery. Cell **110**, 163–75.

82 Vander Haar, E., Lee, S.-I., Bandhakavi, S., Griffin, T. J. and Kim, D.-H. (2007) Insulin signalling to mTOR mediated by the Akt/PKB substrate PRAS40. Nat. Cell Biol. **9**, 316–23.

83 Pearson, G., Robinson, F., Beers Gibson, T., Xu, B. E., Karandikar, M., Berman, K. and Cobb, M. H. (2001) Mitogen-activated protein (MAP) kinase pathways: regulation and physiological functions. Endocr. Rev. **22**, 153–83.

84 Seger, R. and Krebs, E. G. (1995) The MAPK signaling cascade. FASEB J. **9**, 726–35.

85 Ullrich, A. and Schlessinger, J. (1990) Signal transduction by receptors with tyrosine kinase activity. Cell **61**, 203–12.

86 Lemmon, M. A. and Schlessinger, J. (2010) Cell signaling by receptor tyrosine kinases. Cell **141**, 1117–34.

87 Lodish H, Berk A, Z. S. (2000) Receptor Tyrosine Kinases and Ras, W. H. Freeman.

88 Boulton, T. G., Nye, S. H., Robbins, D. J., Ip, N. Y., Radziejewska, E., Morgenbesser, S. D., DePinho, R. A., Panayotatos, N., Cobb, M. H. and Yancopoulos, G. D. (1991) ERKs: a family of protein-serine/threonine kinases that are activated and tyrosine phosphorylated in response to insulin and NGF. Cell **65**, 663–75.

89 Proud, C. G. (2007) Signalling to translation: how signal transduction pathways control the protein synthetic machinery. Biochem J **403**, 217–234.

90 Marais, R., Wynne, J. and Treisman, R. (1993) The SRF accessory protein Elk-1 contains a growth factor-regulated transcriptional activation domain. Cell **73**, 381–93.

91 Chen, R. H., Abate, C. and Blenis, J. (1993) Phosphorylation of the c-Fos transrepression domain by mitogen-activated protein kinase and 90-kDa ribosomal S6 kinase. Proc. Natl. Acad. Sci. U. S. A. **90**, 10952–6.

92 Morton, S., Davis, R. J., Mclaren, A. and Cohen, P. (2003) A reinvestigation of the multisite phosphorylation of the transcription factor c-Jun **22**.

93 Dalby, K. N., Morrice, N., Caudwell, F. B., Avruch, J. and Cohen, P. (1998) Identification of regulatory phosphorylation sites in mitogen-activated protein kinase (MAPK)-activated protein kinase-1a/p90rsk that are inducible by MAPK. J. Biol. Chem. **273**, 1496–505.

94 Fukunaga, R. and Hunter, T. (1997) MNK1, a new MAP kinase-activated protein kinase, isolated by a novel expression screening method for identifying protein kinase substrates. EMBO J. **16**, 1921–33.

95 Waskiewicz, A. J. (1997) Mitogen-activated protein kinases activate the serine/threonine kinases Mnk1 and Mnk2. EMBO J. **16**, 1909–1920.

96 Deak, M., Clifton, A. D., Lucocq, L. M. and Alessi, D. R. (1998) Mitogen- and stress-activated protein kinase-1 (MSK1) is directly activated by MAPK and SAPK2/p38, and may mediate activation of CREB. EMBO J. **17**, 4426–41.

97 Wortzel, I. and Seger, R. (2011) The ERK Cascade: Distinct Functions within Various Subcellular Organelles . Genes & Cancer **2** , 195–209.

98 Bamford, S., Dawson, E., Forbes, S., Clements, J., Pettett, R., Dogan, A., Flanagan, A., Teague, J., Futreal, P. A., Stratton, M. R., et al. (2004) The COSMIC (Catalogue of Somatic Mutations in Cancer) database and website. Br J Cancer **91**, 355–358.

99 Schubbert, S., Shannon, K. and Bollag, G. (2007) Hyperactive Ras in developmental disorders and cancer. Nat Rev Cancer, Nature Publishing Group **7**, 295–308.

100 Dong, C., Davis, R. J. and Flavell, R. A. (2002) MAP kinases in the immune response. Annu. Rev. Immunol. **20**, 55–72.

101 Raman, M. and Cobb, M. H. (2003) MAP Kinase Modules: Many Roads Home. Curr. Biol. **13**, R886–R888.

102 Shi, Y. and Gaestel, M. (2002) In the cellular garden of forking paths: how p38 MAPKs signal for downstream assistance. Biol. Chem. **383**, 1519–36.

103 Vanhaesebroeck, B., Leevers, S. J., Panayotou, G. and Waterfield, M. D. (1997) Phosphoinositide 3-kinases: a conserved family of signal transducers. Trends Biochem. Sci. **22**, 267–72.

104 Didichenko, S. A. and Thelen, M. (2001) Phosphatidylinositol 3-kinase c2alpha contains a nuclear localization sequence and associates with nuclear speckles. J. Biol. Chem. **276**, 48135–42.

105 Zhou, X., Wang, L., Hasegawa, H., Amin, P., Han, B.-X., Kaneko, S., He, Y. and Wang, F. (2010) Deletion of PIK3C3/Vps34 in sensory neurons causes rapid neurodegeneration by disrupting the endosomal but not the autophagic pathway. Proc. Natl. Acad. Sci. **107**, 9424–9429.

106 Skolnik, E. Y., Margolis, B., Mohammadi, M., Lowenstein, E., Fischer, R., Drepps, A., Ullrich, A. and Schlessinger, J. (1991) Cloning of PI3 kinase-associated p85 utilizing a novel method for expression/cloning of target proteins for receptor tyrosine kinases. Cell **65**, 83–90.

107 Wang, S. I., Puc, J., Li, J., Bruce, J. N., Cairns, P., Sidransky, D. and Parsons, R. (1997) Somatic Mutations of PTEN in Glioblastoma Multiforme Advances in Brief Somatic Mutations of PTEN in Glioblastoma Multiforme 4183–4186.

108 Toker, A. and Newton, A. C. (2000) Cellular signaling: pivoting around PDK-1. Cell **103**, 185–8.

109 Alessi, D. R., James, S. R., Downes, C. P., Holmes, A. B., Gaffney, P. R., Reese, C. B. and Cohen, P. (1997) Characterization of a 3-phosphoinositide-dependent protein kinase which phosphorylates and activates protein kinase Balpha. Curr. Biol. **7**, 261–9.

110 Stokoe, D., Stephens, L. R., Copeland, T., Gaffney, P. R., Reese, C. B., Painter, G. F., Holmes, A. B., McCormick, F. and Hawkins, P. T. (1997) Dual role of phosphatidylinositol-3,4,5-trisphosphate in the activation of protein kinase B. Science **277**, 567–70.

111 Sarbassov, D. D., Guertin, D. A., Ali, S. M. and Sabatini, D. M. (2005) Phosphorylation and Regulation of Akt/PKB by the Rictor-mTOR Complex. Science (80-.). **307**, 1098–1101.

112 Jacinto, E., Facchinetti, V., Liu, D., Soto, N., Wei, S., Jung, S. Y., Huang, Q., Qin, J. and Su, B. (2006) SIN1/MIP1 maintains rictor-mTOR complex integrity and regulates Akt phosphorylation and substrate specificity. Cell **127**, 125–37.

113 Fang, X. (2000) Phosphorylation and inactivation of glycogen synthase kinase 3 by protein kinase A. Proc. Natl. Acad. Sci. **97**, 11960–11965.

114 Dillon, R. L. and Muller, W. J. Distinct biological roles for the akt family in mammary tumor progression. Cancer Res **70**, 4260–4264.

115 Datta, S. R., Brunet, A. and Greenberg, M. E. (1999) Cellular survival: a play in three Akts. Genes Dev. **13**, 2905–2927.

116 Rao, T. P. and Kühl, M. (2010) An Updated Overview on Wnt Signaling Pathways: A Prelude for More . Circ. Res. **106** , 1798–1806.

117 Inoki, K., Ouyang, H., Zhu, T., Lindvall, C., Wang, Y., Zhang, X., Yang, Q., Bennett, C., Harada, Y., Stankunas, K., et al. (2006) TSC2 integrates Wnt

and energy signals via a coordinated phosphorylation by AMPK and GSK3 to regulate cell growth. Cell **126**, 955–68.

118 Xiao, B., Sanders, M. J., Underwood, E., Heath, R., Mayer, F. V, Carmena, D., Jing, C., Walker, P. A., Eccleston, J. F., Haire, L. F., et al. (2011) Structure of mammalian AMPK and its regulation by ADP. Nature **472**, 230–3.

119 Oakhill, J. S., Steel, R., Chen, Z.-P., Scott, J. W., Ling, N., Tam, S. and Kemp, B. E. (2011) AMPK is a direct adenylate charge-regulated protein kinase. Science **332**, 1433–5.

120 Salt, I. P., Johnson, G., Ashcroft, S. J. and Hardie, D. G. (1998) AMP-activated protein kinase is activated by low glucose in cell lines derived from pancreatic beta cells, and may regulate insulin release. Biochem. J. **335 (Pt 3**, 533–9.

121 Marsin, A. S., Bertrand, L., Rider, M. H., Deprez, J., Beauloye, C., Vincent, M. F., Van den Berghe, G., Carling, D. and Hue, L. (2000) Phosphorylation and activation of heart PFK-2 by AMPK has a role in the stimulation of glycolysis during ischaemia. Curr. Biol. **10**, 1247–55.

122 Inoki, K., Zhu, T. and Guan, K.-L. (2003) TSC2 Mediates Cellular Energy Response to Control Cell Growth and Survival. Cell **115**, 577–590.

123 Brugarolas, J., Lei, K., Hurley, R. L., Manning, B. D., Reiling, J. H., Hafen, E., Witters, L. A., Ellisen, L. W. and Kaelin, W. G. (2004) Regulation of mTOR function in response to hypoxia by REDD1 and the TSC1/TSC2 tumor suppressor complex. Genes Dev. **18**, 2893–904.

124 Budanov, A. V and Karin, M. (2008) p53 target genes sestrin1 and sestrin2 connect genotoxic stress and mTOR signaling. Cell **134**, 451–60.

125 Blommaart, E. F., Luiken, J. J., Blommaart, P. J., van Woerkom, G. M. and Meijer, A. J. (1995) Phosphorylation of ribosomal protein S6 is inhibitory for autophagy in isolated rat hepatocytes. J. Biol. Chem. **270**, 2320–6.

126 Smith, E. M., Finn, S. G., Tee, A. R., Browne, G. J. and Proud, C. G. (2005) The tuberous sclerosis protein TSC2 is not required for the regulation of the mammalian target of rapamycin by amino acids and certain cellular stresses. J. Biol. Chem. **280**, 18717–27.

127 Kim, E., Goraksha-Hicks, P., Li, L., Neufeld, T. P. and Guan, K.-L. (2008) Regulation of TORC1 by Rag GTPases in nutrient response. Nat. Cell Biol. **10**, 935–45.

128 Sancak, Y., Peterson, T. R., Shaul, Y. D., Lindquist, R. A., Thoreen, C. C., Bar-Peled, L. and Sabatini, D. M. (2008) The Rag GTPases bind raptor and mediate amino acid signaling to mTORC1. Science **320**, 1496–501.

129 Zoncu, R., Bar-Peled, L., Efeyan, A., Wang, S., Sancak, Y. and Sabatini, D. M. (2011) mTORC1 senses lysosomal amino acids through an inside-out mechanism that requires the vacuolar H(+)-ATPase. Science **334**, 678–83.

130 Pullen, N. and Thomas, G. (1997) The modular phosphorylation and activation of p70s6k. FEBS Lett. **410**, 78–82.

131 Yang, Z. and Klionsky, D. J. (2010) Mammalian autophagy: core molecular machinery and signaling regulation. Curr. Opin. Cell Biol. **22**, 124–31.

132 He, C. and Klionsky, D. J. (2009) Regulation mechanisms and signaling pathways of autophagy. Annu. Rev. Genet. **43**, 67–93.

133 Pende, M., Um, S. H., Mieulet, V., Sticker, M., Goss, V. L., Mestan, J., Mueller, M., Fumagalli, S., Kozma, S. C. and Thomas, G. (2004) S6K1(-/-)/S6K2(-/-) mice exhibit perinatal lethality and rapamycin-sensitive 5'-terminal oligopyrimidine mRNA translation and reveal a mitogen-activated protein kinase-dependent S6 kinase pathway. Mol. Cell. Biol. **24**, 3112–24.

134 Hosokawa, N., Hara, T., Kaizuka, T., Kishi, C., Takamura, A., Miura, Y., Iemura, S., Natsume, T., Takehana, K., Yamada, N., et al. (2009) Nutrient-dependent mTORC1 association with the ULK1-Atg13-FIP200 complex required for autophagy. Mol. Biol. Cell **20**, 1981–91.

135 Kim, J., Kundu, M., Viollet, B. and Guan, K.-L. (2011) AMPK and mTOR regulate autophagy through direct phosphorylation of Ulk1. Nat. Cell Biol. **13**, 132–41.

136 Liang, J., Shao, S. H., Xu, Z.-X., Hennessy, B., Ding, Z., Larrea, M., Kondo, S., Dumont, D. J., Gutterman, J. U., Walker, C. L., et al. (2007) The energy sensing LKB1-AMPK pathway regulates p27(kip1) phosphorylation mediating the decision to enter autophagy or apoptosis. Nat. Cell Biol. **9**, 218–24.

137 Crighton, D., Wilkinson, S., O'Prey, J., Syed, N., Smith, P., Harrison, P. R., Gasco, M., Garrone, O., Crook, T. and Ryan, K. M. (2006) DRAM, a p53-Induced Modulator of Autophagy, Is Critical for Apoptosis. Cell **126**, 121–134.

138 Tasdemir, E., Maiuri, M. C., Galluzzi, L., Vitale, I., Djavaheri-Mergny, M., D'Amelio, M., Criollo, A., Morselli, E., Zhu, C., Harper, F., et al. (2008) Regulation of autophagy by cytoplasmic p53. Nat. Cell Biol. **10**, 676–87.

139 Rubinsztein, D. C., Codogno, P. and Levine, B. (2012) Autophagy modulation as a potential therapeutic target for diverse diseases. Nat.

Rev. Drug Discov., Nature Publishing Group, a division of Macmillan Publishers Limited. All Rights Reserved. **11**, 709–30.

140 Sonenberg, N. and Hinnebusch, A. G. (2009) Regulation of Translation Initiation in Eukaryotes: Mechanisms and Biological Targets. Cell **136**, 731–745.

141 Morley, S. J., Coldwell, M. J. and Clemens, M. J. (2005) Initiation factor modifications in the preapoptotic phase. Cell Death Differ. **12**, 571–84.

142 Proud, C. G. (2008) mTOR signalling and human disease. J. Med. Genet. s33–s35.

143 Jackson, R. J., Hellen, C. U. T. and Pestova, T. V. (2010) The mechanism of eukaryotic translation initiation and principles of its regulation. Nat. Rev. Mol. Cell Biol., Nature Publishing Group **11**, 113–27.

144 Gingras, A. C., Raught, B. and Sonenberg, N. (1999) eIF4 initiation factors: effectors of mRNA recruitment to ribosomes and regulators of translation. Annu. Rev. Biochem. **68**, 913–63.

145 Hershey JW, M. W. (2000) Pathways and mechanism of initiation of protein synthesis. In Translational control of gene expression, pp p33–88, Cold Spring Habor Lab Press, New York.

146 Dever, T. E. (2002) Gene-specific regulation by general translation factors. Cell **108**, 545–56.

147 Preiss, T. and W Hentze, M. (2003) Starting the protein synthesis machine: eukaryotic translation initiation. Bioessays **25**, 1201–11.

148 Harashima, S. and Hinnebusch, A. G. (1986) Multiple GCD genes required for repression of GCN4, a transcriptional activator of amino acid

biosynthetic genes in Saccharomyces cerevisiae. Mol. Cell. Biol. **6**, 3990–8.

149 Erickson, F. L. and Hannig, E. M. (1996) Ligand interactions with eukaryotic translation initiation factor 2: role of the gamma-subunit. EMBO J. **15**, 6311–20.

150 Pain, V. M. (1996) Initiation of protein synthesis in eukaryotic cells. Eur. J. Biochem. **236**, 747–71.

151 Asano, K., Clayton, J., Shalev, A. and Hinnebusch, A. G. (2000) A multifactor complex of eukaryotic initiation factors, eIF1, eIF2, eIF3, eIF5, and initiator tRNA(Met) is an important translation initiation intermediate in vivo. Genes Dev. **14**, 2534–46.

152 Asano, K., Krishnamoorthy, T., Phan, L., Pavitt, G. D. and Hinnebusch, A. G. (1999) Conserved bipartite motifs in yeast eIF5 and eIF2Bepsilon, GTPase-activating and GDP-GTP exchange factors in translation initiation, mediate binding to their common substrate eIF2. EMBO J. **18**, 1673–88.

153 Price, N. and Proud, C. (1994) The guanine nucleotide-exchange factor, eIF-2B. Biochimie **76**, 748–60.

154 Pavitt, G. D., Ramaiah, K. V, Kimball, S. R. and Hinnebusch, A. G. (1998) eIF2 independently binds two distinct eIF2B subcomplexes that catalyze and regulate guanine-nucleotide exchange. Genes Dev. **12**, 514–26.

155 Kimball, S. R., Mellor, H., Flowers, K. M. and Jefferson, L. S. (1996) Role of translation initiation factor eIF-2B in the regulation of protein synthesis in mammalian cells. Prog. Nucleic Acid Res. Mol. Biol. **54**, 165–96.

156 Jennings, M. D. and Pavitt, G. D. (2010) eIF5 has GDI activity necessary for translational control by eIF2 phosphorylation. Nature **465**, 378–81.

157 R, W., H, J., T, A., Wek, R. C., Jiang, H.-Y. and Anthony, T. G. (2006) Coping with stress: eIF2 kinases and translational control. Biochem. Soc. Trans., Portland Press Ltd. **34**, 7–11.

158 Kumar, A., Haque, J., Lacoste, J., Hiscott, J. and Williams, B. R. (1994) Double-stranded RNA-dependent protein kinase activates transcription factor NF-kappa B by phosphorylating I kappa B. Proc. Natl. Acad. Sci. U. S. A., National Academy of Sciences **91**, 6288–92.

159 Offermann, M. K., Zimring, J., Mellits, K. H., Hagan, M. K., Shaw, R., Medford, R. M., Mathews, M. B., Goodbourn, S. and Jagus, R. (1995) Activation of the double-stranded-RNA-activated protein kinase and induction of vascular cell adhesion molecule-1 by poly (I).poly (C) in endothelial cells. Eur. J. Biochem. **232**, 28–36.

160 Gil, J., Alcamí, J. and Esteban, M. (1999) Induction of apoptosis by double-stranded-RNA-dependent protein kinase (PKR) involves the alpha subunit of eukaryotic translation initiation factor 2 and NF-kappaB. Mol. Cell. Biol. **19**, 4653–63.

161 Balachandran, S., Kim, C. N., Yeh, W. C., Mak, T. W., Bhalla, K. and Barber, G. N. (1998) Activation of the dsRNA-dependent protein kinase, PKR, induces apoptosis through FADD-mediated death signaling. EMBO J. **17**, 6888–902.

162 Donzé, O., Dostie, J. and Sonenberg, N. (1999) Regulatable expression of the interferon-induced double-stranded RNA dependent protein kinase PKR induces apoptosis and fas receptor expression. Virology **256**, 322–9.

163 Hinnebusch, A. G. and Natarajan, K. (2002) Gcn4p, a master regulator of gene expression, is controlled at multiple levels by diverse signals of starvation and stress. Eukaryot. Cell **1**, 22–32.

164 Jiang, H.-Y. and Wek, R. C. (2005) Phosphorylation of the alpha-subunit of the eukaryotic initiation factor-2 (eIF2alpha) reduces protein synthesis and enhances apoptosis in response to proteasome inhibition. J. Biol. Chem. **280**, 14189–202.

165 Harding, H. P., Zhang, Y. and Ron, D. (1999) Protein translation and folding are coupled by an endoplasmic-reticulum-resident kinase. Nature **397**, 271–4.

166 Shi, Y., Vattem, K. M., Sood, R., An, J., Liang, J., Stramm, L. and Wek, R. C. (1998) Identification and characterization of pancreatic eukaryotic initiation factor 2 alpha-subunit kinase, PEK, involved in translational control. Mol. Cell. Biol. **18**, 7499–509.

167 Moore, C. E., Omikorede, O., Gomez, E., Willars, G. B. and Herbert, T. P. (2011) PERK activation at low glucose concentration is mediated by SERCA pump inhibition and confers preemptive cytoprotection to pancreatic β-cells. Mol. Endocrinol. **25**, 315–26.

168 Chaudhuri, J., Chowdhury, D. and Maitra, U. (1999) Distinct functions of eukaryotic translation initiation factors eIF1A and eIF3 in the formation of the 40 S ribosomal preinitiation complex. J. Biol. Chem. **274**, 17975–80.

169 Olsen, D. S., Savner, E. M., Mathew, A., Zhang, F., Krishnamoorthy, T., Phan, L. and Hinnebusch, A. G. (2003) Domains of eIF1A that mediate binding to eIF2, eIF3 and eIF5B and promote ternary complex recruitment in vivo. EMBO J. **22**, 193–204.

170 Kolupaeva, V. G., Unbehaun, A., Lomakin, I. B., Hellen, C. U. T. and Pestova, T. V. (2005) Binding of eukaryotic initiation factor 3 to ribosomal 40S subunits and its role in ribosomal dissociation and anti-association. RNA **11**, 470–86.

171 Masutani, M., Sonenberg, N., Yokoyama, S. and Imataka, H. (2007) Reconstitution reveals the functional core of mammalian eIF3. EMBO J. **26**, 3373–83.

172 Hershey, J. W. B. (2010) Regulation of protein synthesis and the role of eIF3 in cancer. Braz. J. Med. Biol. Res. **43**, 920–30.

173 Ray, B. K., Lawson, T. G., Kramer, J. C., Cladaras, M. H., Grifo, J. A., Abramson, R. D., Merrick, W. C. and Thach, R. E. (1985) ATP-dependent unwinding of messenger RNA structure by eukaryotic initiation factors. J. Biol. Chem. **260**, 7651–8.

174 Pause, A. and Sonenberg, N. (1992) Mutational analysis of a DEAD box RNA helicase: the mammalian translation initiation factor eIF-4A. EMBO J. **11**, 2643–54.

175 Pause, A., Méthot, N., Svitkin, Y., Merrick, W. C. and Sonenberg, N. (1994) Dominant negative mutants of mammalian translation initiation factor eIF-4A define a critical role for eIF-4F in cap-dependent and cap-independent initiation of translation. EMBO J. **13**, 1205–15.

176 Li, Q., Imataka, H., Morino, S., Rogers, G. W., Richter-Cook, N. J., Merrick, W. C. and Sonenberg, N. (1999) Eukaryotic translation initiation factor 4AIII (eIF4AIII) is functionally distinct from eIF4AI and eIF4AII. Mol. Cell. Biol. **19**, 7336–46.

177 Yang, H.-S., Jansen, A. P., Komar, A. A., Zheng, X., Merrick, W. C., Costes, S., Lockett, S. J., Sonenberg, N. and Colburn, N. H. (2003) The

transformation suppressor Pdcd4 is a novel eukaryotic translation initiation factor 4A binding protein that inhibits translation. Mol. Cell. Biol. **23**, 26–37.

178 Dorrello, N. V., Peschiaroli, A., Guardavaccaro, D., Colburn, N. H., Sherman, N. E. and Pagano, M. (2006) S6K1- and betaTRCP-mediated degradation of PDCD4 promotes protein translation and cell growth. Science **314**, 467–71.

179 Dennis, M. D., Jefferson, L. S. and Kimball, S. R. (2012) Role of p70S6K1-mediated phosphorylation of eIF4B and PDCD4 proteins in the regulation of protein synthesis. J. Biol. Chem. **287**, 42890–9.

180 Richter-Cook, N. J., Dever, T. E., Hensold, J. O. and Merrick, W. C. (1998) Purification and characterization of a new eukaryotic protein translation factor. Eukaryotic initiation factor 4H. J. Biol. Chem. **273**, 7579–87.

181 Shahbazian, D., Roux, P. P., Mieulet, V., Cohen, M. S., Raught, B., Taunton, J., Hershey, J. W. B., Blenis, J., Pende, M. and Sonenberg, N. (2006) The mTOR/PI3K and MAPK pathways converge on eIF4B to control its phosphorylation and activity. EMBO J., European Molecular Biology Organization **25**, 2781–91.

182 Nielsen, P. J. and Trachsel, H. (1988) The mouse protein synthesis initiation factor 4A gene family includes two related functional genes which are differentially expressed. EMBO J. **7**, 2097–105.

183 Weinstein, D. C., Honoré, E. and Hemmati-Brivanlou, A. (1997) Epidermal induction and inhibition of neural fate by translation initiation factor 4AIII. Development **124**, 4235–42.

184 CHAN, C. C. (2004) eIF4A3 is a novel component of the exon junction complex. RNA **10**, 200–209.

185 Nevins, T. A., Harder, Z. M., Korneluk, R. G. and Holcík, M. (2003) Distinct regulation of internal ribosome entry site-mediated translation following cellular stress is mediated by apoptotic fragments of eIF4G translation initiation factor family members eIF4GI and p97/DAP5/NAT1. J. Biol. Chem. **278**, 3572–9.

186 Henis-Korenblit, S., Shani, G., Sines, T., Marash, L., Shohat, G. and Kimchi, A. (2002) The caspase-cleaved DAP5 protein supports internal ribosome entry site-mediated translation of death proteins. Proc. Natl. Acad. Sci. U. S. A. **99**, 5400–5.

187 Mader, S., Lee, H., Pause, A. and Sonenberg, N. (1995) The translation initiation factor eIF-4E binds to a common motif shared by the translation factor eIF-4 gamma and the translational repressors 4E-binding proteins. Mol. Cell. Biol. **15**, 4990–7.

188 Imataka, H., Gradi, A. and Sonenberg, N. (1998) A newly identified N-terminal amino acid sequence of human eIF4G binds poly(A)-binding protein and functions in poly(A)-dependent translation. EMBO J. **17**, 7480–9.

189 Gradi, A., Imataka, H., Svitkin, Y. V, Rom, E., Raught, B., Morino, S. and Sonenberg, N. (1998) A novel functional human eukaryotic translation initiation factor 4G. Mol. Cell. Biol. **18**, 334–42.

190 Tarun, S. Z., Wells, S. E., Deardorff, J. A. and Sachs, A. B. (1997) Translation initiation factor eIF4G mediates in vitro poly(A) tail-dependent translation. Proc. Natl. Acad. Sci. U. S. A. **94**, 9046–51.

191 Tarun, S. Z. and Sachs, A. B. (1996) Association of the yeast poly(A) tail binding protein with translation initiation factor eIF-4G. EMBO J. **15**, 7168–77.

192 Piron, M., Vende, P., Cohen, J. and Poncet, D. (1998) Rotavirus RNA-binding protein NSP3 interacts with eIF4GI and evicts the poly(A) binding protein from eIF4F. EMBO J. **17**, 5811–21.

193 Imataka, H. and Sonenberg, N. (1997) Human eukaryotic translation initiation factor 4G (eIF4G) possesses two separate and independent binding sites for eIF4A. Mol. Cell. Biol. **17**, 6940–7.

194 Morino, S., Imataka, H., Svitkin, Y. V, Pestova, T. V and Sonenberg, N. (2000) Eukaryotic translation initiation factor 4E (eIF4E) binding site and the middle one-third of eIF4GI constitute the core domain for cap-dependent translation, and the C-terminal one-third functions as a modulatory region. Mol. Cell. Biol. **20**, 468–77.

195 Goyer, C., Altmann, M., Lee, H. S., Blanc, A., Deshmukh, M., Woolford, J. L., Trachsel, H. and Sonenberg, N. (1993) TIF4631 and TIF4632: two yeast genes encoding the high-molecular-weight subunits of the cap-binding protein complex (eukaryotic initiation factor 4F) contain an RNA recognition motif-like sequence and carry out an essential function. Mol. Cell. Biol. **13**, 4860–74.

196 Aravind, L. and Koonin, E. V. (2000) Eukaryote-specific domains in translation initiation factors: implications for translation regulation and evolution of the translation system. Genome Res. **10**, 1172–84.

197 Raught, B., Gingras, A. C., Gygi, S. P., Imataka, H., Morino, S., Gradi, A., Aebersold, R. and Sonenberg, N. (2000) Serum-stimulated, rapamycin-sensitive phosphorylation sites in the eukaryotic translation initiation factor 4GI. EMBO J. **19**, 434–44.

198 Dobrikov, M., Dobrikova, E., Shveygert, M. and Gromeier, M. (2011) Phosphorylation of eukaryotic translation initiation factor 4G1 (eIF4G1) by protein kinase C{alpha} regulates eIF4G1 binding to Mnk1. Mol. Cell. Biol. **31**, 2947–59.

199 Haghighat, A. and Sonenberg, N. (1997) eIF4G dramatically enhances the binding of eIF4E to the mRNA 5'-cap structure. J. Biol. Chem. **272**, 21677–80.

200 Hilbert, M., Kebbel, F., Gubaev, A. and Klostermeier, D. (2011) eIF4G stimulates the activity of the DEAD box protein eIF4A by a conformational guidance mechanism. Nucleic Acids Res. **39**, 2260–70.

201 Marcotrigiano, J., Lomakin, I. B., Sonenberg, N., Pestova, T. V, Hellen, C. U. and Burley, S. K. (2001) A conserved HEAT domain within eIF4G directs assembly of the translation initiation machinery. Mol. Cell **7**, 193–203.

202 Willcocks, M. M., Carter, M. J. and Roberts, L. O. (2004) Cleavage of eukaryotic initiation factor eIF4G and inhibition of host-cell protein synthesis during feline calicivirus infection. J. Gen. Virol. **85**, 1125–30.

203 Tomoo, K., Shen, X., Okabe, K., Nozoe, Y., Fukuhara, S., Morino, S., Ishida, T., Taniguchi, T., Hasegawa, H., Terashima, A., et al. (2002) Crystal structures of 7-methylguanosine 5'-triphosphate (m(7)GTP)- and P(1)-7-methylguanosine-P(3)-adenosine-5',5'-triphosphate (m(7)GpppA)-bound human full-length eukaryotic initiation factor 4E: biological importance of the C-terminal flexible region. Biochem. J. **362**, 539–44.

204 Marcotrigiano, J., Gingras, A. C., Sonenberg, N. and Burley, S. K. (1997) Cocrystal structure of the messenger RNA 5' cap-binding protein (eIF4E) bound to 7-methyl-GDP. Cell **89**, 951–61.

205 Joshi, B., Cai, A. L., Keiper, B. D., Minich, W. B., Mendez, R., Beach, C. M., Stepinski, J., Stolarski, R., Darzynkiewicz, E. and Rhoads, R. E. (1995) Phosphorylation of eukaryotic protein synthesis initiation factor 4E at Ser-209. J. Biol. Chem. **270**, 14597–603.

206 Scheper, G. C. and Proud, C. G. (2002) Does phosphorylation of the cap-binding protein eIF4E play a role in translation initiation? Eur. J. Biochem. **269**, 5350–9.

207 Flynn, A. and Proud, C. G. (1995) Serine 209, not serine 53, is the major site of phosphorylation in initiation factor eIF-4E in serum-treated Chinese hamster ovary cells. J. Biol. Chem. **270**, 21684–8.

208 Whalen, S. G., Gingras, A. C., Amankwa, L., Mader, S., Branton, P. E., Aebersold, R. and Sonenberg, N. (1996) Phosphorylation of eIF-4E on serine 209 by protein kinase C is inhibited by the translational repressors, 4E-binding proteins. J. Biol. Chem. **271**, 11831–7.

209 Morley, S. J. (2001) The regulation of eIF4F during cell growth and cell death. Prog. Mol. Subcell. Biol. **27**, 1–37.

210 Pyronnet, S., Imataka, H., Gingras, A. C., Fukunaga, R., Hunter, T. and Sonenberg, N. (1999) Human eukaryotic translation initiation factor 4G (eIF4G) recruits mnk1 to phosphorylate eIF4E. EMBO J. **18**, 270–9.

211 Waskiewicz, A. J., Johnson, J. C., Penn, B., Mahalingam, M., Kimball, S. R. and Cooper, J. A. (1999) Phosphorylation of the cap-binding protein eukaryotic translation initiation factor 4E by protein kinase Mnk1 in vivo. Mol. Cell. Biol. **19**, 1871–80.

212 Knauf, U., Tschopp, C. and Gram, H. (2001) Negative regulation of protein translation by mitogen-activated protein kinase-interacting kinases 1 and 2. Mol. Cell. Biol. **21**, 5500–11.

213 Scheper, G. C., Morrice, N. A., Kleijn, M. and Proud, C. G. (2001) The mitogen-activated protein kinase signal-integrating kinase Mnk2 is a eukaryotic initiation factor 4E kinase with high levels of basal activity in mammalian cells. Mol. Cell. Biol. **21**, 743–54.

214 Ueda, T., Watanabe-Fukunaga, R., Fukuyama, H., Nagata, S. and Fukunaga, R. (2004) Mnk2 and Mnk1 are essential for constitutive and inducible phosphorylation of eukaryotic initiation factor 4E but not for cell growth or development. Mol. Cell. Biol. **24**, 6539–49.

215 Topisirovic, I., Ruiz-Gutierrez, M. and Borden, K. L. B. (2004) Phosphorylation of the eukaryotic translation initiation factor eIF4E contributes to its transformation and mRNA transport activities. Cancer Res. **64**, 8639–42.

216 Marcotrigiano, J., Gingras, A. C., Sonenberg, N. and Burley, S. K. (1999) Cap-dependent translation initiation in eukaryotes is regulated by a molecular mimic of eIF4G. Mol. Cell **3**, 707–16.

217 Lin, T. A., Kong, X., Haystead, T. A., Pause, A., Belsham, G., Sonenberg, N. and Lawrence, J. C. (1994) PHAS-I as a link between mitogen-activated protein kinase and translation initiation. Science **266**, 653–6.

218 Pause, A., Belsham, G. J., Gingras, A. C., Donzé, O., Lin, T. A., Lawrence, J. C. and Sonenberg, N. (1994) Insulin-dependent stimulation of protein synthesis by phosphorylation of a regulator of 5'-cap function. Nature **371**, 762–7.

219 Poulin, F., Gingras, A. C., Olsen, H., Chevalier, S. and Sonenberg, N. (1998) 4E-BP3, a new member of the eukaryotic initiation factor 4E-binding protein family. J. Biol. Chem. **273**, 14002–7.

220 Beugnet, A., Wang, X. and Proud, C. G. (2003) Target of rapamycin (TOR)-signaling and RAIP motifs play distinct roles in the mammalian TOR-dependent phosphorylation of initiation factor 4E-binding protein 1. J. Biol. Chem. **278**, 40717–22.

221 Ma, X. M. and Blenis, J. (2009) Molecular mechanisms of mTOR-mediated translational control. Nat. Rev. Mol. Cell Biol. **10**, 307–18.

222 Kozak, M. and Shatkin, A. J. (1978) Migration of 40 S ribosomal subunits on messenger RNA in the presence of edeine. J. Biol. Chem. **253**, 6568–77.

223 Pestova, T. V and Kolupaeva, V. G. (2002) The roles of individual eukaryotic translation initiation factors in ribosomal scanning and initiation codon selection. Genes Dev. **16**, 2906–22.

224 Passmore, L. A., Schmeing, T. M., Maag, D., Applefield, D. J., Acker, M. G., Algire, M. A., Lorsch, J. R. and Ramakrishnan, V. (2007) The eukaryotic translation initiation factors eIF1 and eIF1A induce an open conformation of the 40S ribosome. Mol. Cell **26**, 41–50.

225 Unbehaun, A., Borukhov, S. I., Hellen, C. U. T. and Pestova, T. V. (2004) Release of initiation factors from 48S complexes during ribosomal subunit joining and the link between establishment of codon-anticodon base-pairing and hydrolysis of eIF2-bound GTP. Genes Dev. **18**, 3078–93.

226 Algire, M. A., Maag, D. and Lorsch, J. R. (2005) Pi release from eIF2, not GTP hydrolysis, is the step controlled by start-site selection during eukaryotic translation initiation. Mol. Cell **20**, 251–62.

227 Pestova, T. V, Lomakin, I. B., Lee, J. H., Choi, S. K., Dever, T. E. and Hellen, C. U. (2000) The joining of ribosomal subunits in eukaryotes requires eIF5B. Nature **403**, 332–5.

228 Marintchev, A., Kolupaeva, V. G., Pestova, T. V and Wagner, G. (2003) Mapping the binding interface between human eukaryotic initiation factors 1A and 5B: a new interaction between old partners. Proc. Natl. Acad. Sci. U. S. A. **100**, 1535–40.

229 Coldwell, M. J. and Morley, S. J. (2006) Specific isoforms of translation initiation factor 4GI show differences in translational activity. Mol. Cell. Biol. **26**, 8448–60.

230 Coldwell, M. J., Sack, U., Cowan, J. L., Barrett, R. M., Vlasak, M., Sivakumaran, K. and Morley, S. J. (2012) Multiple isoforms of the translation initiation factor eIF4GII are generated via use of alternative promoters, splice sites and a non-canonical initiation codon. Biochem. J. **448**, 1–11.

231 Mueller, O., Lightfoot, S. and Schroder, A. (2004) RNA Integrity Number (RIN) Standardization of RNA Quality Control. Tech. Rep. 5989-1165EN, Agil. Technol. Appl. Note.

232 Fang, H., Harris, S., Su, Z., Chen, M., Qian, F., Shi, L., Perkins, R. and Tong, W. (2009) ArrayTrack: An FDA and Public Genomic Tool. In Protein Networks and Pathway Analysis SE - 20 (Nikolsky, Y., and Bryant, J., eds.), pp 379–398, Humana Press.

233 Bottley, A., Phillips, N. M., Webb, T. E., Willis, A. E. and Spriggs, K. A. (2010) eIF4A Inhibition Allows Translational Regulation of mRNAs Encoding Proteins Involved in Alzheimer's Disease. PLoS One, Public Library of Science **5**, e13030.

234 Lamb, J., Crawford, E. D., Peck, D., Modell, J. W., Blat, I. C., Wrobel, M. J., Lerner, J., Brunet, J. P., Subramanian, A., Ross, K. N., et al. (2006) The Connectivity Map: Using Gene-Expression Signatures to Connect Small Molecules, Genes, and Disease. Science (80-.). **313**, 1929–1935.

235 Zhang, S. D. and Gant, T. W. (2008) A simple and robust method for connecting small-molecule drugs using gene-expression signatures. BMC Bioinformatics **9**.

236 Lamb, J., Crawford, E. D., Peck, D., Modell, J. W., Blat, I. C., Wrobel, M. J., Lerner, J., Brunet, J.-P., Subramanian, A., Ross, K. N., et al. (2006) The Connectivity Map: using gene-expression signatures to connect small molecules, genes, and disease. Science **313**, 1929–35.

237 Zimmer, M., Lamb, J., Ebert, B. L., Lynch, M., Neil, C., Schmidt, E., Golub, T. R. and Iliopoulos, O. (2010) The connectivity map links iron regulatory protein-1-mediated inhibition of hypoxia-inducible factor-2a translation to the anti-inflammatory 15-deoxy-delta12,14-prostaglandin J2. Cancer Res. **70**, 3071–9.

238 Wei, G., Twomey, D., Lamb, J., Schlis, K., Agarwal, J., Stam, R. W., Opferman, J. T., Sallan, S. E., den Boer, M. L., Pieters, R., et al. (2006) Gene expression-based chemical genomics identifies rapamycin as a modulator of MCL1 and glucocorticoid resistance. Cancer Cell **10**, 331–342.

239 Lambiv, W. L., Vassallo, I., Delorenzi, M., Shay, T., Diserens, A.-C., Misra, A., Feuerstein, B., Murat, A., Migliavacca, E., Hamou, M.-F., et al. (2011) The Wnt inhibitory factor 1 (WIF1) is targeted in glioblastoma and has a tumor suppressing function potentially by induction of senescence. Neuro. Oncol. **13**, 736–47.

240 Parsons, D. W., Jones, S., Zhang, X., Lin, J. C.-H., Leary, R. J., Angenendt, P., Mankoo, P., Carter, H., Siu, I.-M., Gallia, G. L., et al. (2008) An Integrated Genomic Analysis of Human Glioblastoma Multiforme. Sci. **321** , 1807–1812.

241 Kimball, S. R. (1999) Eukaryotic initiation factor eIF2. Int. J. Biochem. Cell Biol. **31**, 25–9.

242 Mahoss, C. J., William, F., Kwan, Y. and Raymond, F. (1994) A Specific Inhibitor of Phosphatidylinositol 3 = Kinase , **269**, 5241–5248.

243 Fan, Q.-W., Knight, Z. A., Goldenberg, D. D., Yu, W., Mostov, K. E., Stokoe, D., Shokat, K. M. and Weiss, W. A. (2006) A dual PI3 kinase/mTOR inhibitor reveals emergent efficacy in glioma. Cancer Cell **9**, 341–349.

244 Fan, Q.-W., Cheng, C., Hackett, C., Feldman, M., Houseman, B. T., Nicolaides, T., Haas-Kogan, D., James, C. D., Oakes, S. A., Debnath, J., et al. (2010) Akt and autophagy cooperate to promote survival of drug-resistant glioma. Sci. Signal. **3**, ra81.

245 Guertin, D. A. and Sabatini, D. M. (2009) The Pharmacology of mTOR Inhibition. Sci. Signal. **2**, pe24.

246 Buchdunger, E., Trinks, U., Mett, H., Regenass, U., Müller, M., Meyer, T., McGlynn, E., Pinna, L. a, Traxler, P. and Lydon, N. B. (1994) 4,5-Dianilinophthalimide: a protein-tyrosine kinase inhibitor with selectivity for the epidermal growth factor receptor signal transduction pathway and potent in vivo antitumor activity. Proc. Natl. Acad. Sci. U. S. A. **91**, 2334–8.

247 Tan, S. M.-L., Li, F., Rajendran, P., Kumar, A. P., Hui, K. M. and Sethi, G. (2010) Identification of Î²-Escin as a Novel Inhibitor of Signal Transducer and Activator of Transcription 3/Janus-Activated Kinase 2 Signaling Pathway that Suppresses Proliferation and Induces Apoptosis in Human Hepatocellular Carcinoma Cells. J. Pharmacol. Exp. Ther. **334**, 285–293.

248 Price, N. L., Gomes, A. P., Ling, A. J. Y., Duarte, F. V., Martin-Montalvo, A., North, B. J., Agarwal, B., Ye, L., Ramadori, G., Teodoro, J. S., et al. (2012) SIRT1 Is Required for AMPK Activation and the Beneficial Effects of Resveratrol on Mitochondrial Function. Cell Metab. **15**, 675–690.

249 Bowers, J. L., Tyulmenkov, V. V, Jernigan, S. C. and Klinge, C. M. (2000) Resveratrol Acts as a Mixed Agonist/Antagonist for Estrogen Receptors α and β. Endocrinol. **141** , 3657–3667.

250 Joe, A. K., Liu, H., Suzui, M., Vural, M. E., Xiao, D. and Weinstein, I. B. (2002) Resveratrol Induces Growth Inhibition, S-phase Arrest, Apoptosis, and Changes in Biomarker Expression in Several Human Cancer Cell Lines. Clin. Cancer Res. **8** , 893–903.

251 Göransson, O., Mcbride, A., Hawley, S. A., Ross, F. A., Shpiro, N., Foretz, M., Viollet, B., Hardie, D. G. and Sakamoto, K. (2007) UKPMC Funders Group Author Manuscript UKPMC Funders Group Author Manuscript MECHANISM OF ACTION OF A-769662 , A VALUABLE TOOL FOR ACTIVATION OF AMP-ACTIVATED PROTEIN KINASE. J. Biol. Chem. **282**, 32549–32560.

252 García-Martínez, J. M., Moran, J., Clarke, R. G., Gray, A., Cosulich, S. C., Chresta, C. M. and Alessi, D. R. (2009) Ku-0063794 is a specific inhibitor of the mammalian target of rapamycin (mTOR) . Biochem. J. **421**, 29–42.

253 D'Amato, R. J., Loughnan, M. S., Flynn, E. and Folkman, J. (1994) Thalidomide is an inhibitor of angiogenesis. Proc. Natl. Acad. Sci. U. S. A. **91**, 4082–5.

254 Singhal, S., Mehta, J., Desikan, R., Ayers, D., Roberson, P., Eddlemon, P., Munshi, N., Anaissie, E., Wilson, C., Dhodapkar, M., et al. (1999) Antitumor Activity of Thalidomide in Refractory Multiple Myeloma. N. Engl. J. Med., Massachusetts Medical Society **341**, 1565–1571.

255 Meltzer, H. Y., Sachar, E. J. and Frantz, A. G. (1975) Dopamine antagonism by thioridazine in schizophrenia. Biol. Psychiatry **10**, 53–7.

256 Kang, S., Dong, S. M., Kim, B.-R., Park, M. S., Trink, B., Byun, H.-J. and Rho, S. B. (2012) Thioridazine induces apoptosis by targeting the PI3K/Akt/mTOR pathway in cervical and endometrial cancer cells. Apoptosis **17**, 989–97.

257 Shi, Y., Yan, H., Frost, P., Gera, J. and Lichtenstein, A. (2005) Mammalian target of rapamycin inhibitors activate the AKT kinase in multiple myeloma cells by up-regulating the insulin-like growth factor receptor/insulin receptor substrate-1/phosphatidylinositol 3-kinase cascade. Mol. Cancer Ther. **4** , 1533–1540.

258 Ueda, S., Mineta, T., Nakahara, Y., Okamoto, H., Shiraishi, T. and Tabuchi, K. (2004) Induction of the DNA repair gene O6-methylguanine—DNA methyltransferase by dexamethasone in glioblastomas. J. Neurosurg., Journal of Neurosurgery Publishing Group **101**, 659–663.

259 Stein, G. H. (1979) T98G: an anchorage-independent human tumor cell line that exhibits stationary phase G1 arrest in vitro. J. Cell. Physiol. **99**, 43–54.

260 Quiros, S., Roos, W. P. and Kaina, B. (2011) Rad51 and BRCA2 - New Molecular Targets for Sensitizing Glioma Cells to Alkylating Anticancer Drugs. PLoS One, Public Library of Science **6**, e27183.

261 Pegg, A. E., Dolan, M. E. and Moschel, R. C. (1995) Structure, function, and inhibition of O6-alkylguanine-DNA alkyltransferase. Prog. Nucleic Acid Res. Mol. Biol. **51**, 167–223.

262 Grollman, A. P. and Huang, M. T. (1973) Inhibitors of protein synthesis in eukaryotes: tools in cell research. Fed. Proc. **32**, 1673–8.

263 Cherkasova, V. a and Hinnebusch, A. G. (2003) Translational control by TOR and TAP42 through dephosphorylation of eIF2alpha kinase GCN2. Genes Dev. **17**, 859–72.

264 Chotechuang, N., Azzout-Marniche, D., Bos, C., Chaumontet, C., Gausserès, N., Steiler, T., Gaudichon, C. and Tomé, D. (2009) mTOR, AMPK, and GCN2 coordinate the adaptation of hepatic energy metabolic pathways in response to protein intake in the rat. Am. J. Physiol. Endocrinol. Metab. **297**, E1313–23.

265 Frei, K., Ambar, B., Adachi, N., Yonekawa, Y. and Fontana, A. (1998) Ex vivo malignant glioma cells are sensitive to Fas (CD95/APO-1) ligand-mediated apoptosis. J. Neuroimmunol. **87**, 105–13.

266 Furnari, F. B., Lin, H., Huang, H. S. and Cavenee, W. K. (1997) Growth suppression of glioma cells by PTEN requires a functional phosphatase catalytic domain. Proc. Natl. Acad. Sci. U. S. A. **94**, 12479–84.

267 Amaral, L., Kristiansen, J. E., Viveiros, M. and Atouguia, J. (2001) Activity of phenothiazines against antibiotic-resistant Mycobacterium tuberculosis: a review supporting further studies that may elucidate the potential use of thioridazine as anti-tuberculosis therapy. J. Antimicrob. Chemother. **47**, 505–11.

268 Salles, M.-J., Hervé, D., Rivet, J.-M., Longueville, S., Millan, M. J., Girault, J.-A. and Mannoury la Cour, C. (2013) Transient and rapid activation of Akt/GSK-3β and mTORC1 signaling by D3 dopamine receptor stimulation in dorsal striatum and nucleus accumbens. J. Neurochem. **125**, 532–44.

269 White, J. P., Gao, S., Puppa, M. J., Sato, S., Welle, S. L. and Carson, J. A. (2013) Testosterone regulation of Akt/mTORC1/FoxO3a signaling in skeletal muscle. Mol. Cell. Endocrinol. **365**, 174–86.

270 Baur, J. A., Pearson, K. J., Price, N. L., Jamieson, H. A., Lerin, C., Kalra, A., Prabhu, V. V, Allard, J. S., Lopez-Lluch, G., Lewis, K., et al. (2006) Resveratrol improves health and survival of mice on a high-calorie diet. Nature **444**, 337–42.

271 Zang, M., Xu, S., Maitland-Toolan, K. A., Zuccollo, A., Hou, X., Jiang, B., Wierzbicki, M., Verbeuren, T. J. and Cohen, R. A. (2006) Polyphenols stimulate AMP-activated protein kinase, lower lipids, and inhibit accelerated atherosclerosis in diabetic LDL receptor-deficient mice. Diabetes **55**, 2180–91.

272 Park, C. E., Kim, M.-J., Lee, J. H., Min, B.-I., Bae, H., Choe, W., Kim, S.-S. and Ha, J. (2007) Resveratrol stimulates glucose transport in C2C12 myotubes by activating AMP-activated protein kinase. Exp. Mol. Med. **39**, 222–9.

273 Zhou, R., Fukui, M., Choi, H. J. and Zhu, B. T. (2009) Induction of a reversible, non-cytotoxic S-phase delay by resveratrol: implications for a mechanism of lifespan prolongation and cancer protection. Br. J. Pharmacol. **158**, 462–74.

274 Sirtori, C. R. (2001) Aescin: pharmacology, pharmacokinetics and therapeutic profile. Pharmacol. Res. **44**, 183–93.

275 Moehler, T. (2012) Clinical experience with thalidomide and lenalidomide in multiple myeloma. Curr. Cancer Drug Targets **12**, 372–90.

276 Kumar, V. and Chhibber, S. (2011) Thalidomide: an old drug with new action. J. Chemother. **23**, 326–34.

277 Shortt, J., Hsu, A. K. and Johnstone, R. W. (2013) Thalidomide-analogue biology: immunological, molecular and epigenetic targets in cancer therapy. Oncogene.

278 Varadarajan, S., Bampton, E. T. W., Smalley, J. L., Tanaka, K., Caves, R. E., Butterworth, M., Wei, J., Pellecchia, M., Mitcheson, J., Gant, T. W., et al. (2012) A novel cellular stress response characterised by a rapid reorganisation of membranes of the endoplasmic reticulum. Cell Death Differ. **19**, 1896–907.

279 Sanders, M. J., Ali, Z. S., Hegarty, B. D., Heath, R., Snowden, M. A. and Carling, D. (2007) Defining the mechanism of activation of AMP-activated protein kinase by the small molecule A-769662, a member of the thienopyridone family. J. Biol. Chem. **282**, 32539–48.

280 Mihaylova, M. M. and Shaw, R. J. (2012) The AMP-activated protein kinase (AMPK) signaling pathway coordinates cell growth, autophagy, & metabolism. Nat. Cell Biol. **13**, 1016–1023.

281 Blanchard, B. J., Chen, A., Rozeboom, L. M., Stafford, K. A., Weigele, P. and Ingram, V. M. (2004) Efficient reversal of Alzheimer's disease fibril formation and elimination of neurotoxicity by a small molecule. Proc. Natl. Acad. Sci. U. S. A. **101**, 14326–14332.

282 Nairn, A. C. and Palfrey, H. C. (1987) Identification of the major Mr 100,000 substrate for calmodulin-dependent protein kinase III in mammalian cells as elongation factor-2. J. Biol. Chem. **262**, 17299–303.

283 Carlberg, U., Nilsson, A. and Nygård, O. (1990) Functional properties of phosphorylated elongation factor 2. Eur. J. Biochem. **191**, 639–45.

284 Ryazanov, A. G., Shestakova, E. A. and Natapov, P. G. (1988) Phosphorylation of elongation factor 2 by EF-2 kinase affects rate of translation. Nature **334**, 170–3.

285 Redpath, N. T., Price, N. T., Severinov, K. V and Proud, C. G. (1993) Regulation of elongation factor-2 by multisite phosphorylation. Eur. J. Biochem. **213**, 689–99.

286 Lim, I. K., Park, T. J. and Paik, W. K. (2000) Phosphorylation of methylated-DNA-protein-cysteine S-methyltransferase at serine-204 significantly increases its resistance to proteolytic digestion. Biochem. J. **352**, 801–808.

287 Ling, J., Morley, S. J., Pain, V. M., Marzluff, W. F. and Gallie, D. R. (2002) The histone 3'-terminal stem-loop-binding protein enhances translation through a functional and physical interaction with eukaryotic initiation factor 4G (eIF4G) and eIF3. Mol. Cell. Biol. **22**, 7853–67.

288 Costa, B. M., Caeiro, C., Guimaraes, I., Martinho, O., Jaraquemada, T., Augusto, I., Castro, L., Osorio, L., Linhares, P., Honavar, M., et al. Prognostic value of MGMT promoter methylation in glioblastoma patients treated with temozolomide-based chemoradiation: a Portuguese multicentre study. Oncol Rep **23**, 1655–1662.

289 Liu, L. and Gerson, S. L. (2006) Targeted Modulation of MGMT: Clinical Implications. Clin. Cancer Res. **12** , 328–331.

290 Shah, N., Lin, B., Sibenaller, Z., Ryken, T., Lee, H., Yoon, J.-G., Rostad, S. and Foltz, G. (2011) Comprehensive Analysis of MGMT Promoter Methylation: Correlation with MGMT Expression and Clinical Response in GBM. PLoS One, Public Library of Science **6**, e16146.

9 Appendices

Table A1. KU0063794 top 30 most changed genes

Gene Name	log2 Fold Change	Fold Change
ACPP	0.981268152	1.9742
ANKRA2	0.986884171	1.9819
ARHGAP15	1.023255352	2.0325
BCL6	1.009848767	2.013699999
BTG1	1.196166363	2.2913
C6orf66	-0.965784285	0.512
CABC1	0.968053878	1.956200001
CCNG2	2.062432604	4.1769
CDC25A	-1.124062704	0.4588
CDR2L	-1.012169823	0.4958
CYP1A1	1.509594508	2.847300001
EDN1	1.022261272	2.031100001
FZD9	-1.17722907	0.4422
HBP1	1.522909459	2.873699999
IFRD1	-0.958476638	0.5146
IRS2	1.353153885	2.554700001
KIAA0430	1.027861775	2.038999999
KLF9	1.011996488	2.0167
KLHL24	2.130799111	4.3796
MAP6D1	-1.025030237	0.4914
MRPS12	-1.143054137	0.4528
MYC	0.978634962	1.9706
P2RY2	-1.236843416	0.4243

PHLDA2	-1.09819665	0.4671
PUS1	-0.966066089	0.5119
SLC38A2	1.004393523	2.0061
SOCS2	1.210949873	2.3149
SRPK2	1.443606651	2.719999999
TXNIP	1.066881379	2.094900001
YPEL5	0.992695932	1.9899

Table A2. A769662 top 30 most changed genes

Gene Name	log2 Fold Change	Fold Change
CYP1A1	0.804714436	1.7468
C1orf25	0.547844628	1.4619
IFI6	0.540324906	1.4543
S100P	0.520749097	1.4347
CCNG2	0.456806149	1.3725
PTGER4	0.439250781	1.3559
SAT1	0.418135964	1.3362
ALDH1A3	0.412076939	1.3306
ACACB	0.40729836	1.3262
TAF1C	0.401958066	1.3213
VPS13A	0.3950628	1.315
BNIP3	0.379620962	1.301
HERC5	0.377512488	1.2991
FGD1	0.377068206	1.2987
PRR3	-0.382513434	0.7671
PKN1	-0.382701517	0.767
HMOX1	-0.384018789	0.7663

CIAO1	-0.384772056	0.7659
SPG21	-0.385714194	0.7654
SAPS1	-0.397448103	0.7592
MRPS12	-0.402969476	0.7563
TRIM16	-0.407937702	0.7537
NSUN5	-0.411003598	0.7521
WDR43	-0.411195433	0.752
GNA11	-0.425462479	0.7446
COQ6	-0.465141549	0.7244
MOCS2	-0.47252925	0.7207
SCRIB	-0.49228146	0.7109
OGFRL1	-0.50021788	0.707
RPL39L	-0.531156057	0.692

Table A3. Top 40 raw connections for KU0063794

Reference set name	Reference set score
sirolimus_0.1muM_6h_MCF7_human_Affy	13.92258
LY-294002_10muM_6h_MCF7_human_Affy	11.10976
trifluoperazine_10muM_6h_MCF7_human_Affy	9.775658
LY-294002_10muM_6h_PC3_human_Affy	9.453888
sirolimus_0.1muM_6h_PC3_human_Affy	9.2613

	07
wortmannin_10nM_6h_MCF7_human_Affy	8.946853
fluphenazine_10muM_6h_MCF7_human_Affy	8.863023
wortmannin_1muM_6h_MCF7_human_Affy	8.691507
benzamil_11.2muM_6h_PC3_human_Affy	7.178659
quinostatin_10muM_6h_MCF7_human_Affy	7.111233
thioridazine_9.8muM_6h_MCF7_human_Affy	7.013487
perhexiline_10.2muM_6h_MCF7_human_Affy	7.011583
mefloquine_9.6muM_6h_MCF7_human_Affy	6.912848
valinomycin_0.1muM_6h_PC3_human_Affy	6.830011
5707885_50muM_6h_PC3_human_Affy	6.735766
benzamil_11.2muM_6h_MCF7_human_Affy	6.688961
prochlorperazine_10muM_6h_MCF7_human_Affy	6.676652
methylbenzethonium chloride_8.6muM_6h_MCF7_human_Affy	6.644783
latamoxef_7muM_6h_MCF7_human_Affy	6.59585
tetrandrine_6.4muM_6h_MCF7_human_Affy	6.5400

	84
pyrvinium_3.4muM_6h_MCF7_human_Affy	6.452494
wortmannin_10nM_6h_PC3_human_Affy	6.34037
fluphenazine_10muM_6h_PC3_human_Affy	6.312909
colforsin_50muM_6h_MCF7_human_Affy	6.31133
tribenoside_8.4muM_6h_MCF7_human_Affy	6.307069
thioridazine_10muM_6h_MCF7_human_Affy	6.169052
ticlopidine_13.4muM_6h_MCF7_human_Affy	6.019736
rottlerin_10muM_6h_MCF7_human_Affy	5.844306
meclozine_8.6muM_6h_MCF7_human_Affy	5.838759
prenylamine_9.6muM_6h_MCF7_human_Affy	5.807941
valinomycin_0.1muM_6h_MCF7_human_Affy	5.783689
chlorcyclizine_11.8muM_6h_MCF7_human_Affy	5.745349
resveratrol_10muM_6h_MCF7_human_Affy	5.73307
troglitazone_10muM_6h_MCF7_human_Affy	5.723215
trifluoperazine_10muM_6h_PC3_human_Affy	5.6245

	48
phenazopyridine_16muM_6h_MCF7_human_Affy	5.622387
cloperastine_11muM_6h_MCF7_human_Affy	5.60801
wortmannin_10nM_6h_HL60_human_Affy	5.445246
thioridazine_10muM_6h_HL60_human_Affy	5.371287
calmidazolium_5muM_6h_MCF7_human_Affy	5.369066

Table A4. Top 40 raw connections for A769662

Reference set name	Reference set score
sirolimus_0.1muM_6h_MCF7_human_Affy	5.361376
thioridazine_10muM_6h_HL60_human_Affy	4.909457
colforsin_50muM_6h_MCF7_human_Affy	4.871303
LY-294002_10muM_6h_MCF7_human_Affy	4.715455
corynanthine_10.2muM_6h_MCF7_human_Aff	4.5539

y	68
mepacrine_7.8muM_6h_MCF7_human_Affy	4.506069
prochlorperazine_10muM_6h_MCF7_human_Affy	4.386518
benserazide_13.6muM_6h_PC3_human_Affy	4.37901
thioridazine_10muM_6h_MCF7_human_Affy	4.343961
antimycin A_7.2muM_6h_MCF7_human_Affy	4.225799
deferoxamine_0.1mM_6h_MCF7_human_Affy	4.215092
lanatoside C_4muM_6h_MCF7_human_Affy	4.166614
LY-294002_10muM_6h_PC3_human_Affy	4.159472
scriptaid_10muM_6h_PC3_human_Affy	4.152782
ambroxol_9.6muM_6h_PC3_human_Affy	4.134336
rescinnamine_6.4muM_6h_MCF7_human_Affy	4.128798
5707885_50muM_6h_MCF7_human_Affy	4.107751
acepromazine_9muM_6h_PC3_human_Affy	4.097582
fluphenazine_10muM_6h_MCF7_human_Affy	4.066056
fusaric acid_22.4muM_6h_MCF7_human_Affy	3.9281

	46
protriptyline_13.4muM_6h_MCF7_human_Affy	3.884098
trifluoperazine_10muM_6h_MCF7_human_Affy	3.875845
cloperastine_11muM_6h_MCF7_human_Affy	3.791321
latamoxef_7muM_6h_MCF7_human_Affy	3.722222
orciprenaline_7.6muM_6h_HL60_human_Affy	3.71879
desipramine_13.2muM_6h_MCF7_human_Affy	3.681111
cisapride_8.6muM_6h_PC3_human_Affy	3.668551
remoxipride_9.8muM_6h_HL60_human_Affy	3.635593
helveticoside_7.4muM_6h_MCF7_human_Affy	3.631192
sirolimus_0.1muM_6h_PC3_human_Affy	3.630254
dimethadione_31muM_6h_PC3_human_Affy	3.629435
cefoperazone_5.8muM_6h_HL60_human_Affy	3.578197
AG-013608_10muM_6h_MCF7_human_Affy	3.555638
liothyronine_6.2muM_6h_PC3_human_Affy	3.550181
tetryzoline_16.8muM_6h_HL60_human_Affy	3.5376

	94
0175029-0000_1muM_6h_MCF7_human_Affy	3.526779
prenylamine_9.6muM_6h_MCF7_human_Affy	3.511628
fulvestrant_1muM_6h_MCF7_human_Affy	3.500392
alprostadil_11.2muM_6h_HL60_human_Affy	3.486287
dl-alpha tocopherol_9.2muM_6h_PC3_human_Affy	3.417329

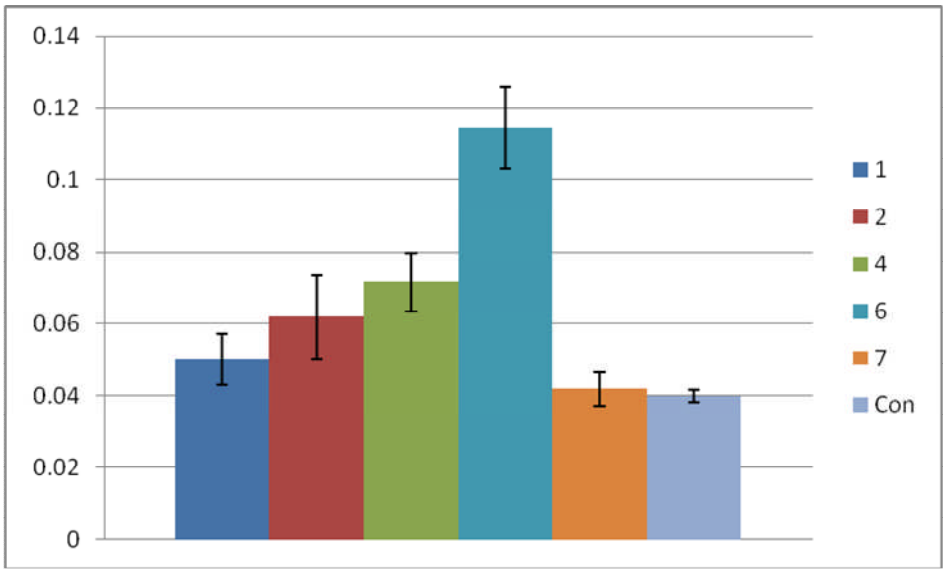

Figure A5. Helicase assay

1.Resveratrol, 2.Thalidomide, 3.Beta escin, 4.Spiperone, 5.DAPH, 6.KU0063794, 7.A769662.

CTCGGCCCCGCCCCCGCGCCCCGGATATGCTGGGACAGCCCGCGCCCCTAGAACGCTTTGCGTCCCGACG
CCCGCAGGTCCTCGCGGTGCGCACCGTTTGCGACTTGGTACTTGGAAAAATGGACAAGGATTGTGAAATG
AAACGCACCACACTGGACAGCCCTTTGGGGAAGCTGGAGCTGTCTGGTTGTGAGCAGGGTCTGCACGAAA
TAAAGCTCCTGGGCAAGGGGACGTCTGCAGCTGATGCCGTGGAGGTCCCAGCCCCCGCTGCGGTTCTCGG
AGGTCCGGAGCCCCTGATGCAGTGCACAGCCTGGCTGAATGCCTATTTCCACCAGCCCGAGGCTATCGAA
GAGTTCCCCGTGCCGGCTCTTCACCATCCCGTTTTCCAGCAAGAGTCGTTCACCAGACAGGTGTTATGGA
AGCTGCTGAAGGTTGTGAAATTCGGAGAAGTGATTTCTTACCAGCAATTAGCAGCCCTGGCAGGCAACCC
CAAAGCCGCGCGAGCAGTGGGAGGAGCAATGAGAGGCAATCCTGTCCCCATCCTCATCCCGTGCCACAGA
GTGGTCTGCAGCAGCGGAGCCGTGGGCAACTACTCCGGAGGACTGGCCGTGAAGGAATGGCTTCTGGCCC
ATGAAGGCCACCGGTTGGGGAAGCCAGGCTTGGGAGGGAGCTCAGGTCTGGCAGGGGCCTGGCTCAAGGG
AGCGGGAGCTACCTCGGGCTCCCCGCCTGCTGGCCGAAACTGAGTATGTGCAGTAGGATGGATGTTTGAG
CGACACACACGTGTAACACTGCATCGGATGCGGGGCGTGGAGGCACCGCTGTATTAAAGGAAGTGGCAGT
GTCCTGGGAACAAGCGTGTCTGCCCTTTCTGTTTCCATATTTTACAGCAGGATGAGTTCAGACGCCCGCG
GTCCTGCACACATTTGTTTCCTTCTCTAACGCTGCCCTTGCTCTATTTTTCATGTCCATTAAAACAGGCC
AAGTGAGTGTGGAAGGCCTGGCTCATGTTGGGCCACAGCCCAGGATGGGGCAGTCTGGCACCCTCAGGCC
ACAGACGGCTGCCATAGCCGCTGTCCAGGGCCAGCTAAGGCCCATCCCAGGCCGTCCACACTAGAAAGCT
GGCCCTGCCCCATCCCCACCATGCCTCCCTTCCTGGCTGTGTCCATGGCTGTGATGGCATTCTCCACTCA
GCAGTTCCTAGCATCCCACACCCAGGTCTCACTGAAAGAAAGGGGAACAGGCCATGGCAGTCAGTGCTTA
CAGAG

Figure A6. MGMT mRNA sequence